University of Milano - Bicocca Department of Biotechnology and Biosciences

2010

Cristiano Zona

Design and Synthesis of Nanoparticles for Therapy and Imaging of Alzheimer's Disease

Thesis Supervisor

Prof. Francesco Nicotra
Full Professor of Organic Chemistry
University of Milano-Bicocca
Department of Bioscience and Biotechnology
Italy

Thesis Co-Supervisor

Barbara La Ferla, PhD
Researcher
University of Milano-Bicocca
Department of Bioscience and Biotechnology
Italy

Ph.D. School Coordinator

Prof. Franca Morazzoni
Full Professor of General and Inorganic Chemistry
University of Milano-Bicocca
Department of Material Science
Italy

keywords

Nanoparticles (NPs), Amyloid-beta peptide (Aβ), Alzheimer's disease (AD), Small Molecules, Curcumin, Click Chemistry, Stability, Affinity

abstract

Various types of nanoparticles (NPs), such as Liposomes, Solid Lipid NPs and Polymeric NPs, are being extensively explored for their potentialities in the medical field. NPs are attractive tools in biomedical applications thanks to their biocompatibility, non-immunogenicity, non-toxicity, biodegradability, high physical stability, possibility of drug loading and releasing, and higher probability for surface functionalization.

The project is devoted to the synthesis of NPs functionalized with amyloid-beta ligands (Aβ-ligands), imaging tools and/or blood brain barrier-transporters (BBB-transporters) for the cure and the diagnosis of Alzheimer's disease (AD).

Amyloid β (Aβ) aggregates are considered as possible targets for therapy and/or diagnosis of Alzheimer disease (AD). It has been previously shown that some small molecules targets Aβ plaques and, among them, curcumin interacts with their precursors, suggesting a potential role for the prevention or the treatment of AD. Herein, a chemoselective ligation procedure was used to generate NPs decorated with a curcumin derivative, designed to maintain all the features required for interaction with Aβ. In summary, this thesis describes the preparation and characterization of new curcumin derivatives and NPs, with affinity for Aβ peptide. They could be exploited as ligands and/or vectors for the targeted delivery of new diagnostic and therapeutic molecules for AD.

The NPs preparations and the biological results were obtained in collaboration with scientists involved in a joint European project:

NAD - Nanoparticles for therapy and diagnosis of Alzheimer's Disease - 2008-2012, FP7-NMP-2007-LARGE-1-Large-scale integrating project NMP-2007-4.0-4 Substantial innovation in the European medical industry: development of nanotechnology-based systems for in-vivo diagnosis and therapy.

CONTENTS

FIGURES LIST

TABLES LIST

ABBREVIATIONS

In the list below, there are the main abbreviations; the others are presented in the text.

Aβ	Amyloid beta
AD	Alzheimer's Disease
ADD	Amyloid beta-derived diffusible ligands
AICD	APP intracellular domain
APP	Amyloid β precursor protein
BACE1	β-secretase 1
BBB	Blood brain barrier
Bd	Broad doublet
Bt	Broad triplet
CaMKII	Calcium-calmodulin protein kinase
Cdk5	Cyclin-dependent Kinase 5
CG	Chrysamine G
ChEIs	Cholinesterase inhibitors
CNS	Central nervous system
COSY	Two dimensional $^{1}H/^{1}H$ Correlation spectroscopy
COX	Cytochrome-c-oxidase
CR	Congo Red
CSF	Cerebrospinal fluid
CUR	Curcumin
D	Doublet
Dd	Double doublet
DMAP	Dimethylaminopyridine
DMF	*N*,*N*-Dimethylformamide
DMSO	Dimethyl sulfoxide
Fc	Fragment crystallisable region
GAG	Glycosaminoglycan
GSH	Glutathione
GSK-3β	Glycogen synthase kinase 3
HFIP	Hexafluoroisopropanol
HSQC	Two dimensional $^{1}H/^{13}C$ Heteronuclear single quantum coherence spectroscopy
IDE	Insulin degrading enzyme
J	Coupling constant

LMW	Low molecular weight
LRP	Receptor-related protein
LTP	Long-term potentiation
m	Multiplet
MAO-B	Monoamine oxidase B
MAPK	Mitogen-activated protein kinase
MARK	Microtubule affinity-regulating kinase
MDB	Microtubule-binding main domain
MPL	Mass-per-length
Myr	Myricetin
NEP	Neprilysin
NFT	Neurofibrillary tangle
NGDA	Nordihydroguaiaretic acid
NMR	Nuclear magnetic resonance
NPs	Nanoparticles
NSAID	Nonsteroidal anti-inflammatory drug
PBS	Phosphate buffered saline
PET	Positron emission tomography
PHF	Paired helical filament
PKA	Protein kinase A
ppm	Part per million
PS1	Protein preselin 1
PS2	Protein preselin 2
Py	Pyridine
r.t.	Room temperature
RAGE	Receptor for advanced glycation end products
RIF	Rifapicin
ROS	Reactive oxygen species
RMT	Receptor-mediated transcytosis
s	Singlet
SPECT	Single photon emission computerized tomography
STD	Saturation transfer difference
TA	Tannic acid
TC	Tetracycline
TFA	Trifluoroacetic acid
TFE	Trifluoroethanol
TfR	Transferrin receptor
THF	Tetrahydrofuran
ThS	Thioflavin S
ThT	Thioflavin T
δ	Chemical Shift

State of the art

It was in 1906 that Alois Alzheimer first presented at a scientific meeting a case of progressive dementia in a 51 years old patient. Postmortem analysis revealed two pathologies, namely, senile plaques and neurofibrillary tangles. In 1910 Emil Kraeplin, Alzheimer's mentor, named this disease after its discover. [1]

Alzheimer's disease (AD) is the most common cause of dementia among neurodegenerative diseases in the elderly population, affecting about 25 million people worldwide (2005). In Western countries it is the fourth common cause of death after heart disease, cancer and stroke. Its incidence and costs are predicted to raise because of the increasing of the life expectancy and the average age.[2,3] Hence, it was estimated that the number of affected people will double every 20 years;[4] this emphasizes the role of AD as a major health problem, that would gain even more ethical and economical relevance in near future.

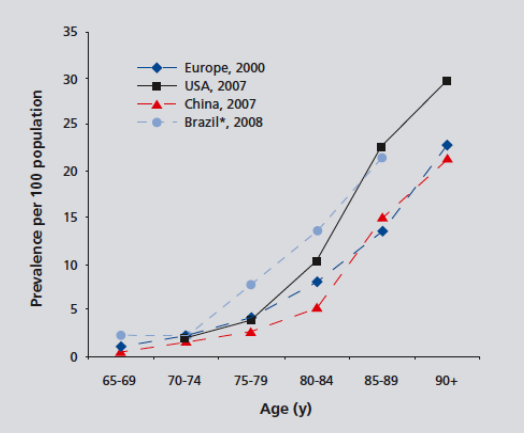

Figure 1: Worldwide prevalence of dementia.

The progression of symptoms varies from patient to patient, but can be divided into seven stages: i) stage 1 is characterized by the absence of cognitive decline, individuals in this stage exhibit no problems in daily living. ii) stage 2 is characterized by very mild cognitive decline, individuals in this stage forget names and locations of objects and may have trouble finding words – all behaviours that are dependent on the functions of the entorhinal cortex hippocampus and part of the prefrontal cortex. iii) stage 3 is characterized by mild

cognitive decline, individuals in this stage face difficulties in travelling to new locations and in handling problems at work. These behaviours also depend on the entorhinal cortex and hippocampus and part of the prefrontal cortex.[5] iv) Stage 4 is characterized by moderate cognitive decline, individuals in this stage have difficulty completing complex tasks, that depends on intact prefrontal cortex function. v-vii) stages 5 to 7 are characterized by moderately severe cognitive decline to very severe cognitive decline. In addition to manifesting behaviours typical of entorhinal cortical, hippocampal, and prefrontal cortical disfunction, individuals in these later stages of AD require help in daily living.[5]

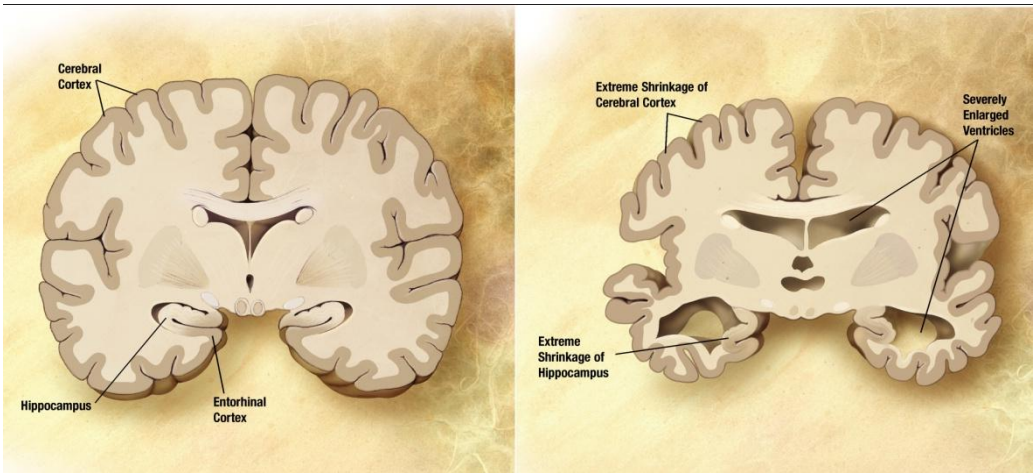

Figure 2: Difference between an healthy brain and an Alzheimer's disease brain.

Thus, memory formation and recall, abilities that depend on entorhinal cortical, hippocampal, and prefrontal cortical function, are the first to show impairment during the early stages of cognitive decline in AD. Death occurs on average 9 years after diagnosis.[6,7] At the microscopic level, the characteristic lesions in Alzheimer's disease are extracellular senile or neuritic plaques; they are constituted by deposits of β-amyloid (Aβ) peptide, by intraneuronal fibrillary tangles (NFTs) in the medial temporal lobe structures and cortical areas of the brain, as well as the selective loss of neurons and synaptic connections. NFTs are composed of paired helical filaments (PHFs) that consist of aggregation of hyperphosphorylated tau protein, associated with the microtubule protein, whereas senile neuritic plaques are rich in Aβ. The causes that induce the above pathological characteristics are poorly known at present,[8] but genetic, pathological and biochemical clues suggest that the progressive production and subsequent accumulation of Aβ (a

proteolytic fragment of the membrane-associated Amyloid Precursor Protein - APP), play a central role. Aβ peptide is formed in abnormal amounts by an aberrant cleavage of Amyloid Precursor Protein (APP), a transmembrane glycoprotein (100–130 kDa) whose primary function is not known, although it is implicated in neural plasticity and synapse formation of neurons.

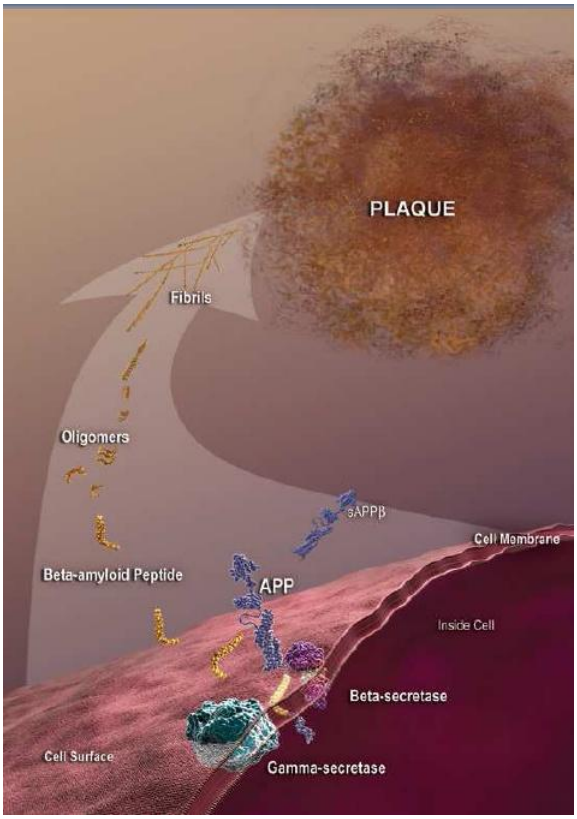

Figure 3: Misfolding of amyloid precursor protein (APP).

The major physiological route of APP processing in neurons is carried out by α-secretase and γ-secretase to produce P3 protein. Instead, in AD an amyloidogenic pathway is boosted with the cleavage of APP by β-secretase followed by γ-secretase, to produce Aβ peptides with a number of amino acid residues ranging between 39 and 42. The predominant ones are $A\beta_{1\text{-}40}$ (90%) and $A\beta_{1\text{-}42}$ (10%) as determined by biochemical studies on cell lysates and brains. In the brain, cells release this peptide in a soluble form that, under normal circumstances, is cleared. However, under abnormal conditions rendering more APP prone to β-secretase cleavage, the Aβ clearance mechanism in the process is overloaded. This eventually leads to the accumulation of Aβ that progressively forms oligomeric, multimeric and fibrillar aggregates. This phenomenon is known as "misfolding of protein" (Figure 3)[9]

and it is a characteristic feature of different neurodegenerative diseases.[10] The aggregation and accumulation of Aβ culminates with the formation of extracellular plaques, one of the morphological hallmarks of the disease, detectable post-mortem in AD brains. These plaques are correlated with the extent of cognitive loss.[10]

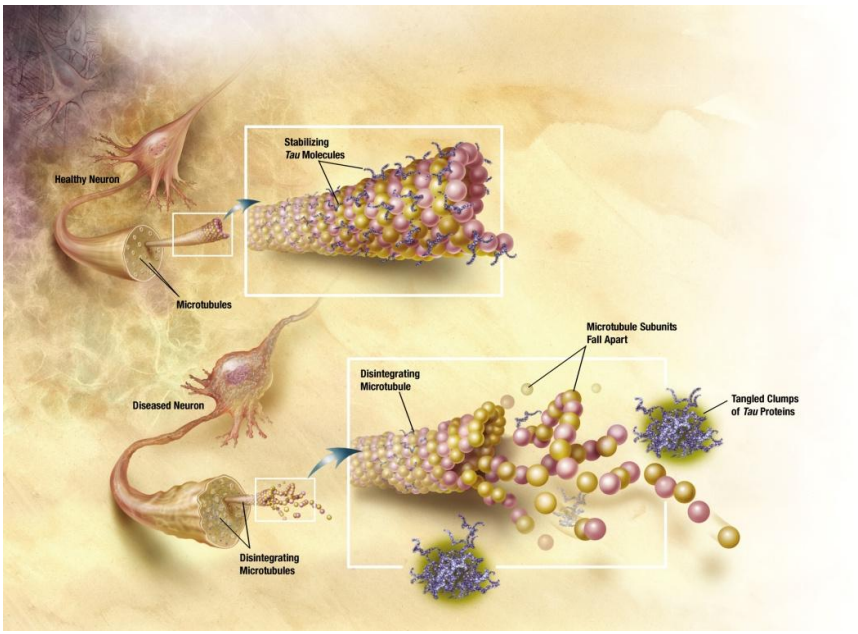

Figure 4: Example of an healthy neuron and a diseased neuron.

While the aetiology of AD remains unclear, there is an increase of the genetic evidence that altered cellular processing of APP is a causative factor in many cases. However, citoxicity of Aβ is not only caused by the ability to form fibrillar aggregates in the extracellular environment, but also by the presence of soluble Aβ oligomers into the intracellular environment. All the forms or their intermediates produce different damages to cell membrane and different organelles, inducing alterations of physiological biochemical pathways and leading to oxidative stress, inflammation and, at the end, to cell death.[10]

1.1. Amyloid β

The production and accumulation of Aβ in the central nervous system (CNS) are key events in the development of AD. The levels of Aβ in the brain are regulated by the activity of enzymes involved in its production, degradation and clearance.[11]

Aβ peptide is present in the brain of healthy humans throughout life and the mere presence of Aβ does not mean neuropathy. In contrast, when neuronal injury appears, the aggregation of physiologically secreted soluble Aβ into oligomers and large Aβ fibrils is currently considered to be a crucial event in AD onset. Of course, the main question (not yet answered) remains the reason why the Aβ peptide - which normally circulates in soluble form in the cerebrospinal fluid (CSF) and in plasma - becomes prone to aggregate, forming highly toxic oligomers, protofibrils and mature fibrils finally accumulating in plaques.[10]

Aβ peptides derive from proteolysis of the large transmembrane protein APP, which is a type I integral membrane glycoprotein (abundantly expressed in the brain) produced in three predominant forms: 695, 751 or 770 amino acids.[11]

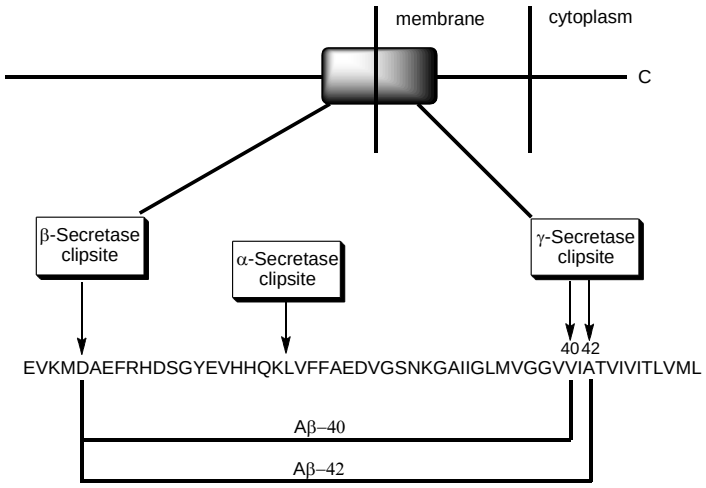

Figure 5: Principal metabolic derivates of amyloid precursor protein.

The Aβ peptide is derived through endoproteolytic processing of APP by sequential enzymatic actions of: (i) alpha-site amyloid precursor protein cleaving enzyme α-secretase,

denominated the non-amyloidogenic pathway, and (ii) beta-site amyloid precursor protein-cleaving enzyme (BACE-1) (a β-secretase, and γ-secretase protein complex with presenilin 1 at its catalytic core) corresponding to the amyloidogenic process (Figure 6).[12]

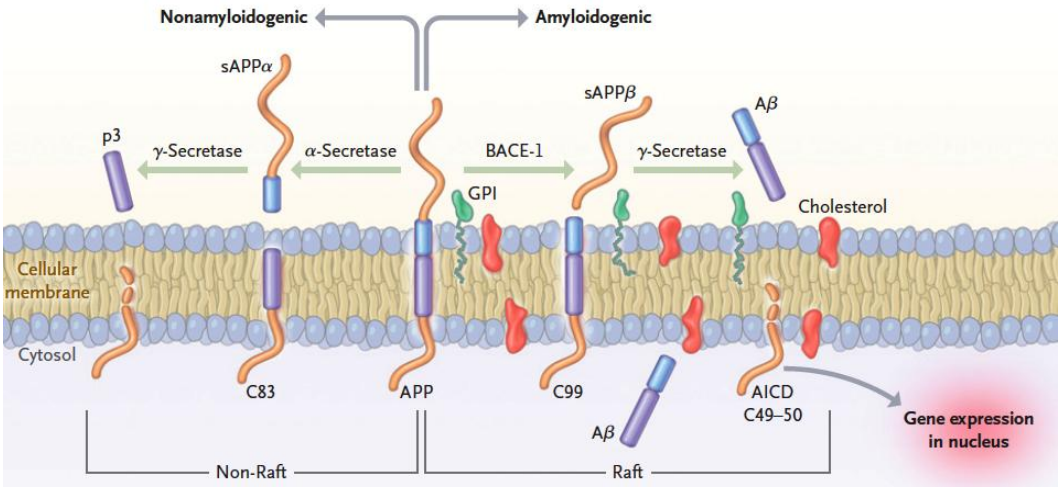

Figure 6: Processing of Amyloid Precursor Protein.

In the α-secretase pathway, α-secretase cleaves in the middle of the amyloid-β region to release a large soluble APP-fragment, sAPPα. The carboxy (C)- terminal C83 peptide is metabolized to p3 by γ-secretase. In the amyloid-forming β-secretase pathway, β-secretase releases a large soluble fragment, sAPPβ. The C-terminal C99 peptide is then cleaved by γ-secretase at several positions, leading to the formation of amyloid-$\beta_{1\text{-}40}$ ($A\beta_{1\text{-}40}$) and the pathogenic amyloid-$\beta_{1\text{-}42}$ ($A\beta_{1\text{-}42}$) in the extracellular space. γ-Secretase cleavage also releases the APP intracellular domain (AICD), which could have a role in transcriptional regulation. The soluble Aβ is prone to aggregation.[7]

The C-terminal 12 amino acid residues of the Aβ peptide are hydrophobic and confer to the peptide the ability to self aggregate and polymerise into amyloid fibrils. The term β of Aβ indicates its propensity to form partial β-plated sheet structures, once it aggregates into amyloid fibrils.[10]

Depending on the exact point of cleavage by γ-secretase, three principal forms of Aβ are produced and comprise respectively 39, 40, and 42 amino acid residues. The relative amount of $A\beta_{1\text{-}42}$ is particularly important, because it's more prone to oligomerize and form amyloid fibrils with to the shorter peptides.[10]

Production of β-amyloid is a normal process, but in a small number of individuals an imbalance between production, clearance and aggregation of peptides causes Aβ to accumulate; this excess may be the initiating factor in AD. This idea, called the "amyloid cascade hypothesis", is based on studies of genetic forms of AD, and evidence that $A\beta_{1-42}$ is toxic to cells.[12] A number of studies have confirmed that $A\beta_{1-42}$ is the more neurotoxic form of Aβ. It has been shown that $A\beta_{1-40}$ and $A\beta_{1-42}$ possess different biochemical properties; $A\beta_{1-42}$ is considered to be the major etiologic agent in the pathogenesis of AD, because of its more aggressive aggregation or oligomerization properties. The mutations associated with inherited forms of AD provide strong evidence, which show that the aggregation of $A\beta_{1-42}$ is a causative factor in the aetiology of AD, since the mutations increase the relative amount of $A\beta_{1-42}$.[13]

The "amyloid cascade hypothesis" is initiated by the generation of $A\beta_{1-42}$. In familial early onset AD, $A\beta_{1-42}$ is overproduced, owing to pathogenic mutations. In sporadic AD, various factors contribute to an increased load of $A\beta_{1-42}$ oligomers and aggregates. Aβ oligomers might directly injure the synapses and neuritis of brain neurons, and, in addition, activate microglia and astrocytes. Tau pathologies, which contributes substantially to the disease process through hyperphosphorylated tau and tangles, are triggered by $A\beta_{1-42}$ (Figure 7).[7]

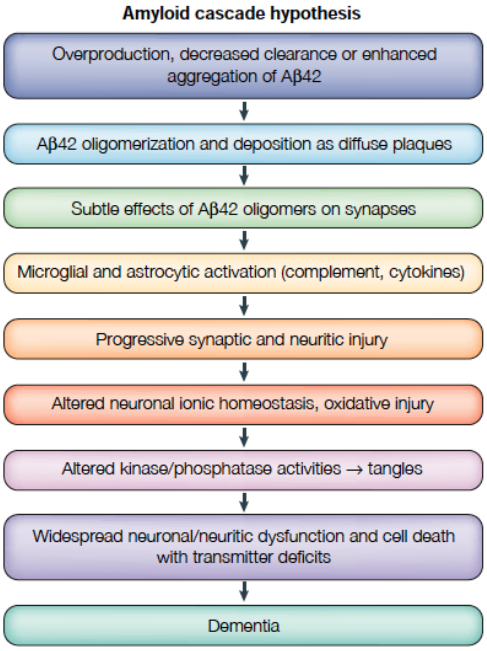

Figure 7: The amyloid cascade hypothesis.

Preventing Aβ aggregation is therapeutically attractive, because this process is believed to be an exclusively pathological event; moreover, the compounds targeting this mechanism are more likely to have a better safety profile, compared to some other approaches currently being pursued. In addition, soluble oligomers can be on a pathway to Aβ fibrils and ultimately amyloid plaque.[13]

A simplified scheme of the Aβ aggregation pathways, that generate toxic assemblies and points of therapeutic intervention is shown in Figure 8.[13] Once Aβ is stabilized as its monomeric form or as non-toxic oligomeric forms, these species might be expected to be cleared by normal pathways.[13]

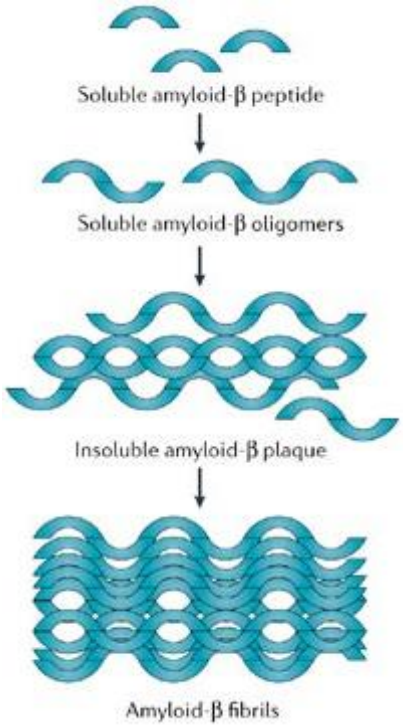

Figure 8: Soluble Aβ peptide aggregation pathways.

1.1.1. Structural features

The toxic effects manifested in AD are thought to arise as a result of conformational changes in Aβ monomers, from predominantly α-helical to a mixture of folding intermediates; they are rich in β-structures, that lead to monomer aggregation and

consequently fibril formation. In the last few years, it has been shown that soluble oligomers might be pathologically more relevant than fibrillar-amyloid deposits.[14-16] This amyloid forming tendency is highly modulated by the amino acid composition.[17]

NH_2-DEAFRHDSGY EVHHQKLVFF AEDVGSNKGA IIGLMVGGVV IA-COOH

Figure 9: The sequence of $A\beta_{1-42}$.

The $A\beta_{1-42}$ sequence is divided into two regions. Residues 1-28 make up a relatively hydrophilic domain, which is extracellular in APP. The C-terminal residue 28-42 represents an hydrophobic domain, associated with the cell membrane in APP. $A\beta_{1-40}$ and $A\beta_{1-42}$ peptides are mainly present as random coil in aqueous solution, but contain some secondary structure elements: a poly-proline II helix (PII) in the N-terminus, and two β-strands in the central part and in the C-terminus.[18,19] The dynamics of monomeric $A\beta_{1–40}$ in aqueous solution was studied by Danielsson *et al.*,[20] by heteronuclear nuclear magnetic resonance experiments.

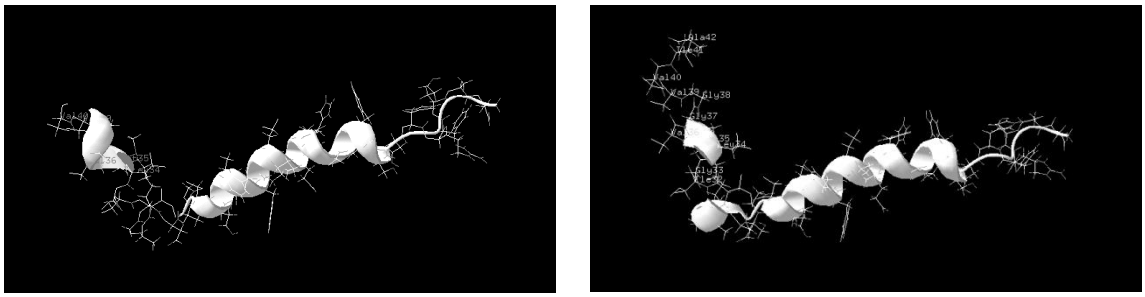

Figure 10: Stereo views of the hydrophobic interactions in the C-terminus of $A\beta_{1-40}$ and $A\beta_{1-42}$ at 1.5 ns of the MD simulations. The residues involved in the hydrophobic interactions are shown in Corey-Pauling-Koltun spheres. (a) $A\beta_{1-40}$; (b) $A\beta_{1-42}$.

The soluble monomeric peptide has a high tendency to form Aβ oligomers, which eventually produce Aβ fibrils.[21] At pH values comprised between 4 and 7, it rapidly precipitates giving rise to an oligomeric β-sheet structure. Although $A\beta_{1–40}$ and $A\beta_{1–42}$ possess identical amino acid sequence, numerous *in vitro* and *in vivo* studies indicate that both peptides have different aggregation and deposition properties. In particular, $A\beta_{1–42}$ aggregates much faster than $A\beta_{1–40}$ *in vitro* and is more toxic than $A\beta_{1–40}$. In 2008, Shen *et al.*[22] performed parallel molecular dynamics (MD) simulations on $A\beta_{1–40}$ and $A\beta_{1–42}$ to

investigate their thermal unfolding processes, with the aim of exploring the physical basis underlying the different dynamic behaviors of both Aβ peptides.

NMR investigations on small Aβ fragments[23-25] and $A\beta_{1-40}$Met35ox suggest that in aqueous solution Aβ peptides can be described as random coils, with only a small population of local non-random structures. Nevertheless, it is suggested a critical role for *in vivo* conformational transitions between soluble α helical and β forms, even if a direct observation of these conformational transitions is difficult, since Aβ peptides have a poor tendency to dissolve in water. For this reason, detailed structural studies are normally performed in mixtures of water and organic fluorinated solvents, such as trifluoroethanol (TFE) or hexafluoroisopropanol (HFIP), and micellar solutions.[26-28] In these media, Aβ peptides are not aggregated and have predominantly α-helical conformations. Mixtures of water and TFE can also induce β structure. This property was exploited by Tommaselli and co-workers,[29] in order to characterize the conformational transitions of Aβ peptides from helical to β forms. Using an integrated approach of experimental (NMR and CD) and theoretical methods (MD simulations), they demonstrated that the 25-35 core sequence is a key-motif in the α-to-β conformational transition. The β conformation is stable in solutions containing 90–99% of water; the addition of appropriate amounts of HFIP turns the peptide conformation from β to α. The current attempts to identify peptide regions driving conformational transitions induced by the surrounding medium, represent a possible approach to understand the molecular basis of AD. In addition, the structural characterization of a partially folded intermediate in the α-to-β transition (and *vice versa*) could allow the rational design of molecules able to interfere with the aggregation process.

The structure of the oligomeric species is not yet known in detail. Recently, a specific Aβ oligomer has been described as a dodecamer able to bind specifically to the dendritic processes of the neuron and block the membrane potentiation.[30,31] From the structural point of view, the oligomer appears to be as a micelle of Aβ-peptides with the hydrophobic C-terminus hidden in the micelle center and a critical 17.6 mM micellar concentration.[14,32] The peptides in the oligomer are mainly unstructured.[33] In 2005, Laurents *et al.* proposed different kinds of Aβ aggregated forms, the so-called β-balls, detected at pH lower than 4.[34]

The product of small oligomers aggregation is the Aβ protofibril. It has a rod-like structure with a length of 8-200 nm, characterized by a core with a high β-sheet content, as

suggested by its resistance to hydrogen exchange and its capacity to bind Congo Red and Thioflavin T. Protofibrils can elongate by the association of smaller protofibrils; their speed depends on Aβ concentration, pH, ionic strength and temperature. In presence of little preformed fibrils They can rapidly convert in Aβ fibrils, even though they seem to be in a prevalent dynamic equilibrium with lower-order oligomers.[35]

The final step in the Aβ aggregation pathway is the protofibril maturation into fibrils. This process may be driven through hydrophobic contact between 3 and 6 protofibrils, that are supposed to form a fibril. Aβ fibrils are composed of multiple protofibrils twisted around each other, resulting in filamentous structures with a diameter of 6-10 nm. $A\beta_{1-40}$ fibrils are constituted of two or three protofibrils arranged to a left-handed superhelix, forming an S-shaped fibril cross section. Amyloid fibrils have been defined as thermodynamically stable, structurally organized, highly insoluble, filamentous protein aggregates; they are composed of repeating units of β-sheets, aligned perpendicular to the fibre axis, with a potential parallel and antiparallel organization. In the amyloid fibrils, this β-sheet structure is limited to an arrangement in which the individual β-strands run transversely to the main fibril axis. This structure is named "cross-β conformation".

The determination of the full molecular structures of amyloid fibrils requires specific experimental approaches,[36,37] because of their non-crystalline, insoluble nature. While monomeric peptides present a prevalent random coil structure, for amyloid fibrils the predominant secondary structural elements are β-strands. Therefore, the study of secondary structure in amyloid fibrils consists on the identification of β-strand and non-β-strand segments (i.e., turns, loops, or bends). Different techniques - such as solid-state NMR,[38-40] hydrogen/deuterium (H/D) exchange,[41,42] proline-scanning mutagenesis,[43] electron paramagnetic resonance (EPR),[44] infrared and Raman spectroscopies[45,46] - have been applied to the problem of secondary structure determination. Solid-state NMR and EPR[47,48] measurements have been also employed for the characterization of fibrils tertiary structure, that depends on the organization of β-strand segments into parallel or antiparallel β-sheets. The quaternary structure in amyloid fibrils is defined as the positions and orientations of β-sheets relative to one another. The most important techniques applied to these experimental studies are X-ray diffraction[49] and solid-state NMR.[50] The experimental determination of quaternary structure in amyloid fibrils is relatively difficult. The last models for amyloid fibrils structures support the idea that its core contains two or more layers of β-sheets. The

quaternary structure is generated by a specific set of contacts among amino acid side chains, that project from adjacent β-sheets. In fibrils formed by relatively long peptides, the adjacent β-sheets may be formed either by β-strands from the same or from different peptide molecules; it indicates that the side chain contacts from which quaternary structure takes origin can be either intramolecular or intermolecular.

1.1.2. Interaction with ligands

The structural features of the interaction of ligands with Aβ are mainly unknown, even if a great number of different molecules that interact with Aβ peptides have been proposed. There are some sporadic exceptions among these compounds. Three relevant cases are reported below. The first example concerns the interaction of Aβ with cyclodextrins, torus-shaped rings built up by different numbers of glucose residues. As firstly reported by Qin *et al.*,[51] β-cyclodextrin interacts with the Aβ-peptide and this is suggested to inhibit the formation of the soluble oligomers with an IC_{50} of 5mM, as determined with scintillation proximity assay.[52] Camilleri *et al.* demonstrated by mass-spectrometry that the stoichiometry of the Aβ -peptide and β-cyclodextrin is 1:1.[53] The main interaction with amino acid residues has been suggested to involve the aromatic rings of phenylalanines and the hydrophobic cavity of cyclodextrin. In 2004, Danielsson and co-workers characterized the interaction between Aβ-peptide and β-cyclodextrin by NMR.[54] The Aβ-peptide has four putative aromatic binding sites, F4, Y10, F19 and F20. They demonstrated that if the phenylalanines at positions 19 and 20 in the fragment $Aβ_{12-28}$ are replaced with glycines (by removing all aromatic side chains) no interaction occurs. This shows that the phenylalanines are necessary for β-cyclodextrin-peptide interaction. For the central fragment $Aβ_{12-28}$, where the phenylalanines are present, the interaction occurs and K_D = 3.8 mM. Induced chemical shift changes suggested that the interaction mainly involves phenylalanine 19. This binding is not strong, but it suites the fibril reducing activity of β-cyclodextrin determined earlier. In the case of the full-length peptide, the combined results from induced chemical shift changes and diffusion data were consistent; they had a two-site binding, involving F19 and Y10, with a total apparent dissociation constant of K_D = 4 mM. The individual K_D for the two sites was determined to be respectively $K_D F$ = 4.7 mM and $K_D Y$ = 6.6 mM, if the sites are assumed to be

independent. The outermost N-terminal aromatic amino acid F4 did not seem to bind β-cyclodextrin with any measurable affinity. This was tested by showing that the fragment $A\beta_{1-9}$ does not bind β-cyclodextrin. Other types of cyclodextrins were studied and showed no binding. This may be caused by the hydrophobic pocket of β-cyclodextrin, that has optimal dimensions for interaction with the aromatic side chains. The α- and γ-cyclodextrins have too small or too large cavities for the interaction to take place.

The second example concerns the study of the interaction between gangliosides and A β_{1-40} peptide. This interaction was characterized in 2004 by Mandal *et al*.[55] in a membrane-mimicking environment, dissolving asialo-GM1 and ganglioside GT1b in a sodium dodecyl sulphate (SDS) solution. As previously reported,[56,57] Aβ peptides associate with gangliosides in Alzheimer's brains and form specific complexes with gangliosides *in vitro*. Different experimental evidences show that ganglioside binding induces Aβ peptide oligomerization.[58-60] From the structural point of view, gangliosides are sialic acid–containing glycosphingolipids and consist of two main components: a hydrophobic ceramide unit, which anchors the gangliosides to the plasma membrane, and a hydrophilic oligosaccharide chain, to which one or more sialic acid units (*N*-acetylneuraminic acid) are attached. Gangliosides are abundant components of neuronal membranes and are involved in important neurobiological events, such as neurodifferentiation, synaptogenesis, and synaptic transmission. Asialo-GM1 and GT1b ganglioside share four sugar moieties in common; however, GT1b has three additional sialic acids compared to asialo-GM1, that does not contain sialic acid units. Asialo-GM1 and GT1b ganglioside binding to $A\beta_{1-40}$ peptide were analyzed by heteronuclear NMR spectroscopy. Experimental data showed that, while GT1b is unable to bind Aβ, asialo-GM1 addition induces appreciable chemical shift variations in $A\beta_{1-40}$ amide protons. In particular, asialo-GM1 docks between region I (E3–V24) and region II (G29–V40) of Aβ. These evidences explain why GM1 does not bind the shorter $A\beta_{1-28}$ peptide.[58] In fact, in the case of $A\beta_{1-28}$, the absence of the main binding region G29–V40 would prevent GM1 binding. In addition, Matsuzaky and co-workers[61] showed that gangliosides follow the order GT1b > GD1a > GD1b > GM1 to induce β-sheet formation. These NMR data agree with previous reports, suggesting that when the size of the ganglioside headgroup increases with the number of sialic acids (GT1b > GD1a > GD1b > GM1), it becomes difficult to accommodate the bulky saccharides between regions I and II of Aβ and β-sheet formation proceeds. The interaction

of Aβ peptide with the ganglioside GM1 is also currently under study by Bruix and co-workers. It isn't worth that opposite results were obtained by Ariga *et al.* using a membrane-mimicking system composed of dipalmitoylphosphatidylcholine (DPPC), where Aβ had lower affinity for asialo-GM1 than for gangliosides with several sialic acids.[62]

1.1.3. Small molecule ligands that interact with Aβ

Thinking about the conformation/oligomerization hypothesis, molecules able to stabilize the soluble Aβ (sAβ) conformation, to destabilize the altered amyloidogenic conformer and to prevent the required conformational transition could be effective inhibitors of amyloid plaque formation and very potent drug candidates for AD treatment.

1.1.3.1.*Small Peptides*

The intrinsic affinity of Aβ itself suggested that Aβ-specific interactions could be the basis for the development of compounds binding to Aβ and preventing its polymerization. It has been claimed that fibrillogenesis can be inhibited by short synthetic peptides partially homologous to Aβ. Several elegant strategies have been used to design peptidic inhibitors of Aβ aggregation. Many of these approaches rely on the use of fragments of the parent Aβ sequence as recognition elements in a dominant negative way. Typically, fibril-disrupting chemical elements are incorporated into Aβ derived peptides in the form of N- or C-terminal modifications, conformationally constrained amino acids, or modifications to the peptide backbone. These concepts have also been applied to D-amino acid variants of the parent Aβ sequence. Given the hypothesis that aggregation intermediates are responsible for Aβ toxicity, one approach to contrast this problem consist of identifying the Aβ regions that are at the basis of the polymerization into amyloid fibrils. Gazit *et al.*.[63] analyzed a variety of short functional fragments from unrelated amyloid-forming proteins and observed a remarkable occurrence of aromatic residues. They speculated that aromatic residues raise the possibility that π-stacking may play an important role in the molecular recognition and self-assembly process that lead to the amyloid formation.

In Aβ the aromatic residues are the two phenylalanine residues at position 19 and 20. In particular, the short fragment of Aβ QKLVFF was shown to bind specifically to full-length peptide.[64] Other studies have shown that not only QKLVFF, but also LVFFA and its derivatives[65] and LPFFD[66] are all potent inhibitors of amyloid formation from Aβ polypeptide. Another recent study demonstrated that the seven amino acid Aβ fragment, KLVFFAE, form well-ordered amyloid fibrils.[38] These findings indicate the pair of phenylalanine residues as the major structural elements that mediate binding of the QKLVFF peptide to the Aβ polypeptide. As the formation of amyloid fibrils is a process of molecular recognition and self-assembly, the high affinity and selectivity of the FF motif seems to provide the molecular recognition element needed for such process in the context of the full-length Aβ. These candidate binding compounds could theoretically prevent all aggregation, or even cause further association of toxic oligomers into larger nontoxic aggregates. Cairo and co-workers[67] proposed inhibitors designed to contain both the ‘‘recognition domain’’ (LVFF or KLVFF) and a ‘‘disrupting domain’’, a polypeptide chain with the ability of interfering with Aβ aggregation. Series of variant of the KLVFF sequence were synthesized. Truncation of the C-terminal phenylalanine reduced the affinity by approximately 10-fold. The D-amino acid sequence KLVFF binds with similar affinity to the L-amino acid sequence, as reported by Chalifour *et al.*.[68] The substitution of tyrosine at either the 19 or 20 position did not alter the affinity; however, replacement of both phenylalanine residues with tyrosine was detrimental. The substitution with histidine at position 19 - but not at position 20 - led to a substantial loss of binding; nevertheless, a double histidine substitution partially restored the binding. The substitution of phenylalanine with tryptophan residues gave mixed results. Murphy *et al.* also focused their attention on the “disrupting domain”; they demonstrated that KLVFF sequences that possess positively charged residues at the C-terminus bind with higher affinities than the KLVFF alone does. Among these peptides, $KLVFFK_4$ (K_D = 37 μM) and $KLVFFK_6$ (K_D = 40 μM) were the most potent in preventing Aβ-associated toxicity. These results suggested that a peptide domain lacking a direct homology with Aβ can play a significant role in the binding. The increased affinities of sequences bearing lysine residues are not caused by non-specific Coulombic interactions of the peptides with the Aβ-fibrils surfaces. In fact, there was a lack of affinity when three lysine residues were substituted with glutamic acid residues (four different isomers). These substitutions were useful to

demonstrate that the position of the positively charged residues has a critical influence on Aβ affinity. The placement of the positively charged residues close to position 20 gives rise to the most potent ligand of the four isomers. Placing the three residues of lysines apart from the region of residues 16-20, with intervening negatively charged residues, reduces the affinity by 14-fold. The placement of a positive charge at the N-terminus of the sequence of residues 16-20 results in an activity that is lower than that of compounds with a modification at C-terminus. Arginine-containing compounds were tested to determine the potency of compounds that incorporate positively charged residues other than lysine. These compounds possess an activity similar to the one with lysine. Another example of peptide inhibitors containing the Aβ amino acid sequence 16-20 was presented by Austen *et al.*:[69] they designed two peptides with RG-GR residues, added at the N- and C-terminal ends of KLVFF to aid solubility, in particular the two molecules are RGKLVFFGR and RGKLVFFGR-NH_2. On the basis of ThT results and TEM micrographs, both peptides inhibited the formation of Aβ late aggregates, but the results for the inhibition of the oligomerization revealed that the second one had the best inhibitory effect, while the first one has a slight blocking effect at higher concentrations. It is likely that the second one inhibits oligomeric formation by binding to the monomeric Aβ molecule, and blocking the formation of early soluble aggregates, as shown by size exclusion chromatography and oligomeric specific ELISA. It is interesting to underline that only RGKLVFF-NH_2, which completely inhibited the early aggregates of Aβ, was able to protect cells from Aβ toxicity. However, in the case of the first peptide, which showed only inhibition of the late aggregates of Aβ, no neuroprotective effects were demonstrated. The results reported by Austen and co-workers provide clear evidence that the neuroprotective effects were caused by the inhibition of formation of early aggregates, rather than late aggregates of Aβ. The studies reported above are quite significant, as they suggest new approaches for the interference with Aβ assembly and peptides, that may be the lead compounds for the development of molecules preventing Aβ aggregation *in vivo*. The use of multiple simultaneous interactions to enhance the affinity and specificity of binding - known as multivalency - is an important concept in biology. In the past, different types of scaffold molecules have been used to obtain multivalent structure, such as colloidal gold particles and poly(ethyleneglycol) (PEG). These approaches have some disadvantages, in particular the large size of the particles (PEG) and the lack of control over the number of peptides

attached (colloidal gold). These disadvantages are overcome using dendrimers, multivalent macromolecules with regular, highly branched, structures and dimensions resembling those of small proteins. Starting from previous information, Chafekar and co-workers[70] synthesized a first generation KLVFF dendrimer (K4 - four KLVFF on one scaffold), by using native chemical ligation, and investigated the effect of dendritic KLVFF on the aggregation of $A\beta_{1-42}$ as well as on preformed aggregates. Their data show that the linkage of KLVFF to a dendrimeric scaffold potentiates its inhibitory effect on the Aβ aggregation and on the disassembly of pre-existing aggregates. In fact, they used 20-fold lower concentration of K4 (per peptide subunit) to obtain a similar inhibition as KLVFF. In a previous study, a branched hexameric PEG linked to inverse FFVLK[71] sequence was shown to increase the potency of Aβ inhibition, but also in this case the K4 conjugate from the study of Chafekar *et al.* gave stronger multivalent effect.

Looking at the A β_{1-42} sequence, Fülop *et al.*[72] proposed another inhibitor with a structure analogue to the sequence 31-35, which plays important roles in the Aβ aggregation.[73,74] Other types of peptides, containing residues acting as β-sheet breaker, were proposed. In particular Soto and co-workers[66] proposed a β-sheet breaker peptide iAβ5 (LPFFD), designed from the central hydrophobic region of Aβ. A proline residue was added into the sequence, to disrupt β-sheet formation, as incorporation of this amino acid within a β-pleated structure is highly unfavourable. An aspartic acid charged residue was added to the end of the peptide to increase its solubility. It was demonstrated that iAβ5 inhibits in a dose-dependent manner fibrillogenesis of either $A\beta_{1-40}$ or A β_{1-42}, disassembles preformed fibrils *in vitro* and prevents neuronal death induced by fibrils in cell culture. In addition, the peptide significantly reduced amyloid β-protein deposition *in vivo* and completely blocked the formation of amyloid fibrils in a rat brain model of amyloidosis. Looking at these results, they hypothesized that β-sheet breaker peptides probably inhibit amyloid formation by binding to monomeric/dimeric Aβ peptides, while blocking the formation of the oligomeric β-sheet-conformation precursor of the fibrils.

Etienne and co-workers[75] proposed peptides which contain α,α-disubstituited amino acid (ααAA) in the hydrophobic core of Aβ (Figure 11); in particular they utilized an alternating ααAA/L-amino acid design to obtain a peptide that interacts with Aβ by hydrogen bonding as well as by side-chain interactions. The ααAAs, that has side-chain larger than methyl, stabilized extended peptide conformations.

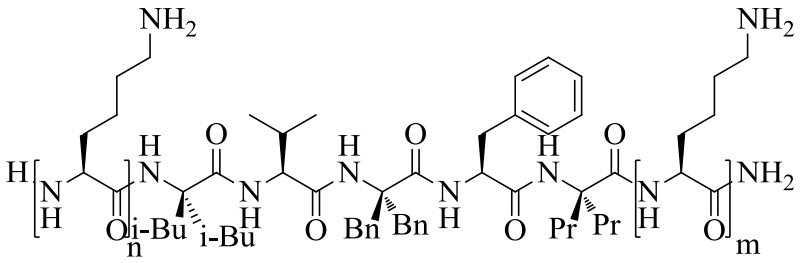

Figure 11: Design of peptides with ααAAs as blockers of assembly; AMY–1: n=1, m=6; AMY–2: n=7, m=0.

The common feature of β-sheet structure in amyloid fibrils, formed by proteins that are otherwise structurally diverse, suggests that peptide backbone hydrogen bonding may be important in the assembly and stability of amyloid fibrils. Starting from this idea, another interesting approach in this area of Aβ mimetics could be the substitution of alternating amide hydrogens with methyl groups. This approach may be useful to prevent the β-sheet propagation necessary for Aβ fibrillization. Furthermore, these N-methylated peptides are more hydrophobic than the unmodified ones; they also have the possibility of increasing blood-brain barrier penetration, resistance to proteolytic degradation and tend to prevent self aggregation. Gordon *et al.*[76] designed inhibitors based on KLVFF motif, containing N-methylated amino acids; in particular the $K_{NMe}LV_{NMe}FF_{NMe}AE$ (Figure 12) was the most potent *in vitro* inhibitor, among the peptides tested. N-methylated derivatives, based on $A\beta_{25\text{-}35}$ sequence GSNKGAIIGLM, were also reported by Hughes *et al.*.[77] They demonstrated that N-methylated derivatives of the Aβ sequence can prevent the aggregation and inhibit the resulting toxicity of the wild type peptide. N-methylation is known to promote β-sheet formation, by locking the residue into a β-conformation; it has been shown to generate soluble monomeric β-sheet peptides. By N-methylating the amide NH groups at the outer edges of the β-sheet and so preventing the intermolecular hydrogen bonding, both aggregation and toxicity should be prevented. Being homologous to $A\beta_{25\text{-}35}$, the NMe derivatives are expected to bind to the peptide and to prevent the further addition of $A\beta_{25\text{-}35}$ monomers. It was shown that these derivatives, which taken individually are soluble and non-toxic, can prevent the aggregation and inhibit the toxicity of the wild type peptide. All the N-methylated peptides had varying effects on prefolded fibrils and fibril assembly, even if the N-methylated glycine peptide(25) had properties similar to the wild

type. In particular, $A\beta_{25-35}$ with N-methylated glycine(33) was shown to completely inhibit fibril formation, disassemble preformed fibrils, and reduce cellular toxicity. Another peptide with the methylation on leucine(34) was able to alter the fibril morphology and to reduce the wild peptide toxicity. These results would imply that the position of N-methylation is crucial for efficacy and that it is linked to a critical region of the growing amyloid fibril.

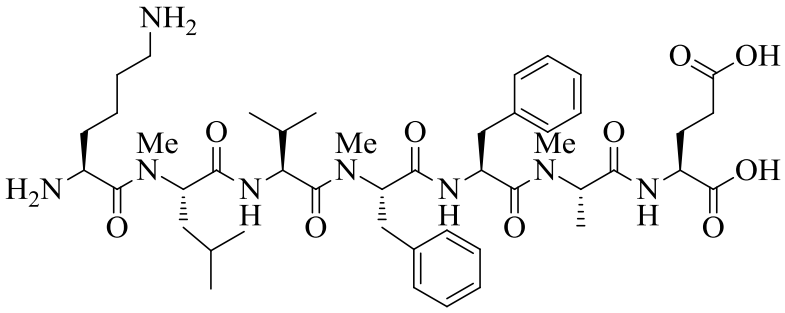

Figure 12: Design of peptides containing N–Methylated amino acid.

Gordon and co-workers[78] investigated the effect of replacing the hydrogen bond donating amide NH backbone with ester bond surrogates at alternating positions, to prevent the hydrogen bonding of the amyloidogenic peptide and to reduce the aggregation. In addition, the ester carbonyl is less basic than the amide carbonyl and, consequently, is a weaker hydrogen bond acceptor. At the same time, the ester bond shares many structural similarities with the amide bond, such as a predominance of the trans conformation and similar bond lengths and angles. Considering this information, they hypothesized that the substitutions would yield peptides with effective fibrillogenesis inhibitor activity and would permit a more direct assessment of the role of hydrogen bonds in stabilizing amyloid fibrils. The synthesized peptides presented two hydrogen bonding faces when arrayed in an extended β-strand conformation; one face had normal hydrogen bonding capabilities, but the other face lacked amide protons and its ability to hydrogen bond was severely limited.

Thus, the incorporation of ester bonds constitutes a more conservative substitution for peptide bonds, than the incorporation of N-methyl amino acids. The incorporation of two ester bonds at alternate residues of the $A\beta_{16-20}$ peptide - similar to the incorporation of N-methyl amino acids - prevents the peptide from forming amyloid fibrils. The incorporation

of ester bonds also results in the formation of an effective inhibitor of $A\beta_{1-40}$ fibrillogenesis. They also analyzed the different behavior of the $A\beta_{16-20}$ ester peptide, the unmodified wild type $A\beta_{16-20}$ and the inhibitor peptide $A\beta_{16-20}$N-methylated. All the three peptides inhibited fibrillogenesis and disassembled preformed fibrils; the efficacy of $A\beta_{16-20}$ ester is similar to that of $A\beta_{16-20}$N-methylated and both are better inhibitors than $A\beta_{16-20}$. The similar inhibitory properties of $A\beta_{16-20}$ ester compared to $A\beta_{16-20}$N-methylated also suggest that interfering with hydrogen bonding is sufficient to prevent $A\beta_{1-40}$ fibrillogenesis and that steric contributions from the N-methyl group are not required. The reported disassembly of pre-existing fibers is also very interesting: it may suggest that many of these peptides can bind at the end of the fibrils and possibly serve to influence the thermodynamic equilibrium between oligomers and fibrils. The considerable efforts in the rational design of Aβ-targeting molecules, based on the parent Aβ sequence, have been quite fruitful in providing a large class of compounds with different activities. These peptidomimetic molecules provide a class of compounds that may help to elucidate the mechanism of amyloid aggregation, perhaps by trapping intermediates, as well as providing inroads to the design of diagnostic and therapeutic reagents.

1.1.3.2.*Non-peptidic small molecule*

Some non-peptidic small molecules are not only able to inhibit the formation and the extension of β-amyloid fibrils (fAβ), but also to destabilize fAβ in vitro. These include naturally occurring or commercially available bioactive compounds, drugs, surfactants,[79] Cu/Zn chelators,[80] phenothiazines[81] and sulfonated dyes such as or Congo red (CR) (Figure 13) and its derivatives[82].

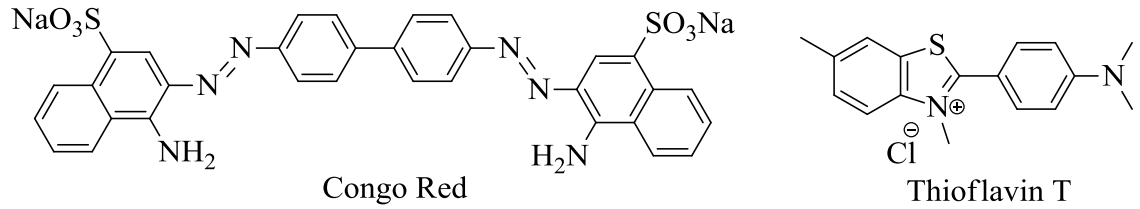

Figure 13: Structure of Congo red and Thioflavin T.

Among them CR was the first small molecule reported to bind to amyloid in tissue sections, exhibiting the characteristic yellow–green birefringence under cross polarized light. Later thioflavin T (ThT) (Figure 13) and thioflavin S (ThS) were also shown to stain amyloid deposits. These two dyes are the classical reagents to detect characteristic β-sheet mediated fibrillization.

CR[83,84] and ThT[85] have also been shown to inhibit fibril formation at higher concentrations. Perhaps, it is not surprising that many reported small molecule inhibitors are similar to CR and ThT, being planar and aromatic. According to Porat *et al*.,[86] who reviewed the possible mode of interaction with Aβ, small molecules with aromatic moieties can intercalate within grooves created by β-sheets, in both the soluble oligomeric forms and in the large fibrils. From this first study, several different types of molecules were found to be active in the inhibition of fAβ aggregation, with a wide range of activity, from less than 100 nM to more than 100 μM. In the table presented below, we resume the IC_{50} values of several compounds for the inhibition of Aβ peptides aggregation. In particular, the compounds are classified for their inhibitory effect and can be roughly divided in two classes: bioactive molecules and drugs not related to Alzheimer diseases. Compounds such as curcumin,[87-89] wine-related polyphenols (myricetin, quercetin, morin, kaempferol, (+)-catechin and (–)-epicatechin),[86] apomorphine,[90] porphyrins,[81,91] omega-3 fatty acid,[91,92] tannic acid,[86,93,94] vitamin A and β-carotene,[95] rifampicin and rifamycin B,[81] tetracycline,[93,94,96] coenzyme Q_{10}[97] belong to the first class. Anti-inflammatory[98-102] and anti-Parkinson agents[103,104] belong to the second class, the latest being the most effective, with particular reference to dopamine and L-DOPA. Analyzing the table presented below, dopamine has the best performance. Dopamine and its precursor L-DOPA are used as drugs acting on the sympathetic nervous system. For example, L-DOPA is used in the treatment of Parkinson's disease and DOPA-responsive dystonia. Despite of its benefits in brain-related disease, dopamine and its precursor have not been used for treatment of Alzheimer diseases yet even though *in vitro* studies were promising. The anti-amyloidogenic and fibril-destabilizing activity of the anti-Parkinsonians drugs, examined in the study of Ono *et al.*[103] (Table 1) was in the order dopamine > Selegiline ~ nordihydroguaiaretic acid (NDGA) > L-Dopa ~ Pergolide > Bromocriptine ~ Rifapicin (RIF). In particular, dopamine exhibited potent anti-amyloidogenic and fibril-destabilizing effects; the effective concentration (EC_{50}), able to inhibit the formation or extension of fAβs, was about

0.01-0.10 μM. This result was in contrast with previous works,[105-107] which identified in NDGA (Figure 14) - that has two ortho-dihydroxyphenyl rings symmetrically bound by a short carbohydrate chain - the most effective molecule. The activity of NDGA could be ascribed to its compact and symmetric structure that might be suitable to specifically bind free Aβ, thus inhibiting the polymerization of Aβ into fAβ.[106] Alternatively, this structure might be suitable for the specific binding to fAβ and the subsequent destabilization of the β-sheet conformation of Aβ rich in fAβ molecules.

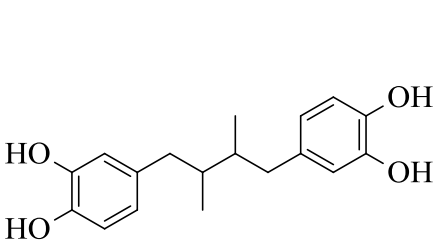

Nordihydroguaiaretic acid

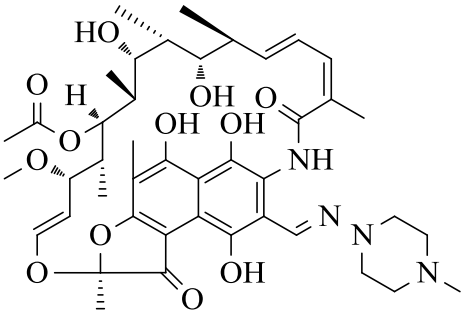

Rifampicin

Figure 14: Structure of Nordihydroguaiaretic acid and Rifampicin.

Table 1: Summary of non-peptidic ligands: anti-amyloidogenic activity and ability to pass the BBB.

Compound	**IC_{50} aggregation μM**		***Information on ability to pass BBB (Ref.)***
	fAβ(1–40)	fAβ(1–42)	
Acetopromazine maleate salt[81]	> 40		
2-(4-Aminophenyl)-methylbenzothiazole[81]	2.0		
Amphotericin B[81]	2.2		
Apigenin[81]	> 40		
Azure A[81]	0.4		
Azure B[81]	0.3		
Azure C[81]	0.2		
Basic blue 41[81]	1.4		
Bromocriptine[103]	14	20	
β-Carotene[95]	2.4	5.2	
Catechin[86,108]	2.9	5.3	X[109-116]
Chlorpromazine hydrochloride[81]	> 40		
Chlorazol black E[81]	0.3		

CoQ_{10}[97]	1.8	5.5	X[117]
Curcumin[87,89]	0.19-0.81	0.63-1.1	X[118-120]
Daunorubicin hydrochloride[81]	1.4		
Dihydrolipoic acid[96]	3.9	20.8	
2,2'-Dihydroxybenzophenone[81]	> 40		
2-[4-(Dimethylamino)phenyl]-6-methylbenzothiazole[81]	2.0		
2, 4-Dinitrophenol[121]	7		X[122]
3,3'-Dipropyl thiodicarbocyanine iodide[81]	0.3		
L-DOPA[103]	5.0	1.7	
Dopamine[103]	0.01	0.04	
(–)-Epicatechin[86,108]	2.8	5.6	X [109-116]
(–)-Epicatechin 3-gallate[81,86]	3.0		X[123]
Exifone[81,86]	0.7		
Ferric dehydroporphyrin IX[81]	0.2		
Ferulic acid[94]	1.8	5.5	
Filipin III[81]	14.6		
Gossypetin[81,86]	1.3		
Haematin (from bovine blood)[81]	0.2		
Hemin[91]	~ 0.4	~ 0.4	
Haemin chloride[81]	0.1		
Hypericin[81,86]	0.9		
Kaempferol[86,108]	1.7	3.2	X[109-115]
Lacmoid[81]	1.4		
α–Lipoic acid[96]	3.2	20	X[124]
Metylene Blue[81,125,126]	2.3	12.5	
Methyl yellow[81]	1.5		
Morin[86,108]	0.24	0.67	X[109-115]
Mycostatin[81]	9.3		
Myricetin[86,93,97,108,127-129]	0.20-0.37	0.34-0.51	X[109-115,121]
NDGA[86,87,93,95-97,103]	0.14-0.21	0.74-1.1	
3-Nitrophenol[121]	80		X[122]
2,3,4,2',4'-Pentahydroxybenzophenone[81,86]	2.8		
Pergolide[103]	0.89	2.0	X[103]
Perphenazine[81]	> 40		

Phthalocyanine[81]	3.2		
Ponceau SS[81]	1.2		
Promazine hydrochloride[81]	> 40		
Propionylpromazine hydrochloride[81]	> 40		
Protoporphyrin IX[91]	~ 65	~ 65	
Pseudohypericin[81]	2.3		
Purpurogallin[81,86]	0.5		
Quercetin[86,108]	0.24	0.72	X[109-115,130]
Quinacrine[81]	8.4		
Quinacrine mustard[81]	1.2		
Retinal[95]	0.18	0.89	
Retinol[95]	0.18	0.76	
Retinoic acid[95]	4.5	20	
Rifampicin[81,93,94,96,103]	4.9-9.7	9.1	X[131]
Rifamycin B[81]	3.1		
Rosmarinic Acid[86,87]	0.29	1.1	
Selegiline[103]	0.68	0.72	X[132]
Tannic acid[86,93]	0.012	0.022	
Tetracycline[93,94,96,129]	10	10	
Thionin[81]	0.3		
2,3,4-Trihydroxybenzophenone[81,86]	3.1		
Zinc protoporphyrin IX[91]	~ 5	~ 5	

Li *et al.*[108] reported that dopamine and L-DOPA were able to inhibit the formation of amyloid fibrils in a solution 1 mg/mL of $A\beta_{1-40}$, in a range from 10 to 100 μM.

Other molecules that present a very high activity against amyloid fibrils and plaque formation are red wine and green tea related polyphenols;[86] these compounds were also analyzed by Ono *et al.*,[121] during their systematic work. The wine-related polyphenols inhibit fAβ formation from both $A\beta_{1-40}$ and $A\beta_{1-42}$, as well as destabilized preformed $fA\beta_{1-40}$ and fA β_{1-40} dose-dependently in vitro. Within this class of compounds, tannic acid showed the best activity.

Tannic acid (TA), a commercial form of tannin, is a polymeric polyphenol with a weak acidity (pK_a around 10) due to its phenol groups. Its structure is based mainly on glucose esters of gallic acid. It is a yellow/light brown amorphous powder, which is highly soluble in water. Ono *et al*. examined the effects of TA on the formation and the extension of $fA\beta_{1-}$

$_{40}$ and fAβ_{1-42}, as well as on the destabilization of fAβs at pH = 7.5 at 37 °C *in vitro*, using fluorescence spectroscopy with ThT, Congo Red and electron microscopy.[93] They also compared the activity of TA with the anti-amyloidogenic and fibril destabilizing effects of Myricetin (Myr) (Figure 15), RIF, Tetracycline (TC) and NDGA. TA exhibited potent anti-amyloidogenic and fibril-destabilizing effects; the EC_{50} values for the formation or the extension of fAβs or for the destabilization of fAβs were about 0.012-0.065 μM for both Aβ_{1-40} and Aβ_{1-42}. They suggested that the anti-amyloidogenic and fibril-destabilizing activity of NDGA and wine-related polyphenols may be classified in the following order: TA > NDGA = Myr = morin = quercetin > kaempferol > (+)-catechin = (–)-epicatechin > TC. It is interesting to see that TA, wine-related polyphenols, NDGA, RIF all possess antioxidant activity. Tomiyama *et al.*[125,126] suggested that RIF binds to Aβ by hydrophobic interactions between its lipophilic ansa chain and the hydrophobic region of Aβ and they could block the association between Aβ molecules that lead to fAβ formation. The anti-amyloidogenic activity of TCs, and of small molecule anionic sulfonates or sulfates is also related to the propensity to bind to Aβ.[107,127]

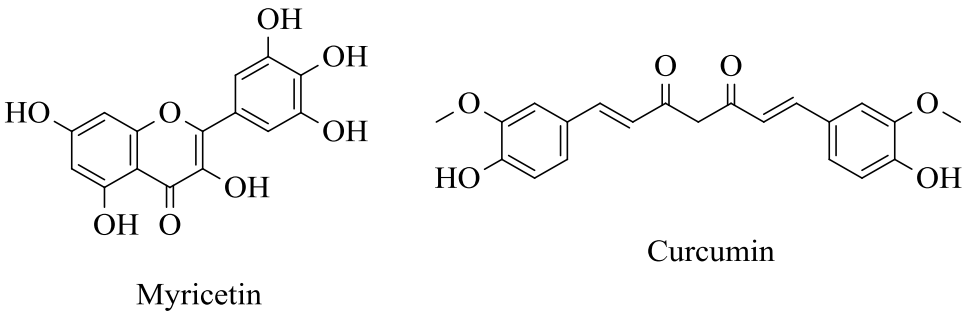

Figure 15: Structure of Myricetin and Curcumin.

Another important Aβ-ligand is the curcumin, a low molecular weight molecule with potent antioxidant and anti-inflammatory activities that has a favorable toxicity profile and is also under development as a potential cancer chemotherapeutic agent. The curcumin (CUR) (Figure 15) is a major component of the yellow curry spice turmeric. This spice is used in the traditional diet and as an herbal medicine in India.[133] The frequency of Alzheimer's disease in India is roughly one-quarter of that in the US (e.g., 0.7 vs. 3.1% between 70 and 79 year).[134] Maybe not by chance, CUR is a free radical scavenger,[135] which protects the brain from lipid peroxidation,[99] and scavenges nitric oxide-based

radicals. Oral administration of CUR has been shown to be protective of the central nervous system. In 2001, Lim *et al.*[88] suggested that CUR was able to block Alzheimer's disease pathogenesis at multiple sites of the inflammation cascade, but the direct effects of CUR on the formation and destabilization of fAβ remain unclear. Looking at these information, in 2005 Yang *et al.*[89] worked on CUR as Aβ inhibitor both *in vitro* and *in vivo*. They showed that under aggregating conditions *in vitro*, CUR inhibited aggregation (IC_{50} = 0.8 μM) and disaggregated fibrillar $Aβ_{1-40}$ (EC_{50} = 1 μM). Later, other authors[86,87,94] reported lower IC_{50}. The effects of CUR did not depend on Aβ sequence, but on fibril-related conformation. Brain sections of Tg2576 mice with Alzheimer's disease were incubated with CUR and revealed preferential labeling of amyloid plaques. *In vivo* studies showed that CUR, injected peripherally into aged Tg mice, crossed the blood-brain barrier and bound Aβ plaques. When fed to aged Tg2576 mice, with advanced amyloid accumulation, CUR labeled plaques and reduced amyloid levels and plaque burden. Hence, CUR directly binds small β-amyloid species, thus blocking aggregation and fibril formation both *in vitro* and *in vivo*. These data suggested that low dose CUR is effectively able to disaggregate Aβ, as well as to prevent fibril and oligomer formation, supporting the rationale for CUR use in clinical trials preventing or treating AD. In 2007, Reinke *et al.*[136] studied the structure-activity relationships of amyloid β-aggregation inhibitors based on CUR. They studied the effect of three prominent features on the inhibition of amyloid aggregation: the presence of two aromatic end groups, the substitution pattern of these aromatics, and the length and flexibility of the linker region. They found that the modification of any one of the modules has profound effects on their activity. They assembled a collection of CUR related compounds, to establish the contribution of each structural module to activity. CUR is composed of two relatively polar aromatic groups, connected by a rigid linker. Reinke *et al.*, in their first experiments, investigated whether both aromatic groups were required for activity using the ThT assay.

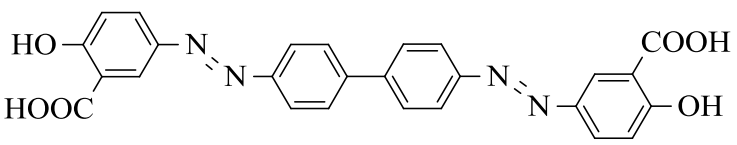

Figure 16: Structure of Chrysamine G.

They found that simple compounds with a single aromatic group, like vanillin, salicylic acid or ferulic acid, did not decrease aggregation of 25 μM $A\beta_{1-42}$, even at high concentrations (500 μM). They also studied the relation between the substituent on the two phenyl group and the activity, observing that the aromatic end groups require one or more polar, hydrogen bonding substitutions for optimal inhibition of Aβ aggregation.
In CUR, CR, and Chrysamine G (CG) (Figure 16) the distances between the terminal aromatic regions are all strikingly similar; it was hypothesized that the length of the linker would be important for the activity.

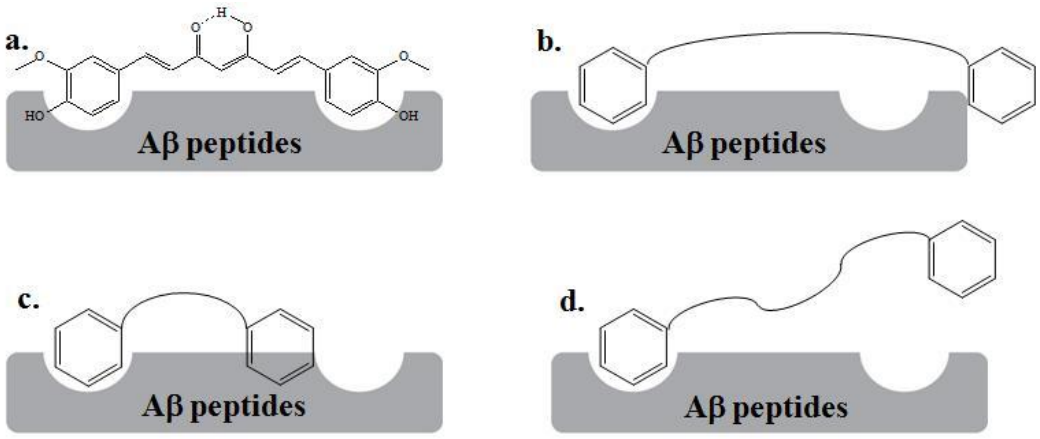

Figure 17: Representative model showing how linker characteristic contribute to potency. Linker too long (b), too short (c) or too flexible (d) can decrease the ability of the compound to interact with Aβ.

Reinke *et al.*[136] noticed that the length and the flexibility of the linker region are not independent variables and established that the optimal are rigid (less than two freely rotating carbons) and restricted between 8 and 16 Å. It is interesting to notice that many of the best amyloid ligands fall within the observed optimal range. For example, all CR, CG, NDGA, CUR (Figure 17) and rosmarinic acid meet these requirements. In addition, the linker requirement seems to be one of the most significant features, as the compounds that fulfill the other substructural requirements - such as the aromatic substitution - still fail to inhibit if they have a short linker. A remarkable exception to this observation is resveratrol. Despite its short linker length, this compound is active, suggesting a possible alternative mechanism for the inhibition or a possible different binding site on the amyloid peptide, such as the site occupied by ThT.

Overall, the anti-amyloidogenic molecules can be classified into four groups based on their activity. Dopamine and tannic acid were classified into the strongest anti-amyloidogenic group. Compounds like NDGA, CUR, rosmarinic acid or myricetin belonged to the second group. L-DOPA or β-carotene were classified into the third group and RIF or TC into the fourth group. Other molecules that are not presented above - such as Poly(vinylsulfonic acid, sodium salt), 1,3-propanedisulfonic acid, disodium salt, β-sheet breaker peptide and nicotine - exhibited anti-amyloidogenic activity in a μM range.

1.2. Crossing the blood brain barrier (BBB)

An endothelial cell monolayer associated with pericytes and astrocytes - known as the blood brain barrier **(**BBB) - separates the blood from the cerebral parenchyma; it is characterized by tight intracellular junctions and by the absence of fenestrations.[137-139] The BBB is the homeostatic defence mechanism against pathogens and toxins. Complex and highly regulated, the BBB screens the biochemical, physicochemical and structural features of solutes at its periphery, thus affording barrier selectivity in the passage of desired molecules into the brain parenchyma. The BBB provides the brain with nutrients, prevents the introduction of harmful blood-borne substances, and restricts the movement of ions and fluid to ensure an optimal environment for brain functions. It protects the brain from substances, which are neurotoxic in physiological concentrations. As a consequence of its barrier properties, the BBB also prevents the movement of drugs from the blood into the brain, and therefore acts as an obstacle for the systemic delivery of neurotherapeutics. The BBB determines whether a given drug - unless lipid-soluble, small (< 600 Da), electrically neutral and weakly basic molecules - could reach the central nervous system (CNS), either by passive diffusion or through carrier or receptor systems, limiting the brain penetration. Furthermore, the efflux transport systems may target the drugs that meet these criteria and export them from the brain. As a result, the BBB excludes many small-molecule pharmaceuticals and nearly all biopharmaceuticals - such as genes and proteins - fail to penetrate into the brain tissue to an appreciable extent. Although the surface area of the human brain microvasculature available for drug transport (~ 20 m^2) is more than adequate for treating the entire brain volume, the barrier properties of the BBB continue to restrict brain drug delivery via the bloodstream.[140]

There is growing evidence for BBB damage in AD.[141,142] Most Aβ plaques are located in the proximity, or are directly in contact with cerebral capillaries. Alterations of the expression and the distribution of the Aβ transporters and tight junction proteins have been observed at the level of endothelial basement membrane of cerebral microvasculature, where the efflux of Aβ from brain is regulated. These observation open the possibility of some potential therapeutic alternatives of AD, based on the sealing of a compromised BBB and the reversing AA deposition.

1.3. Cerebral clearance of Aβ across the BBB

The amyloid hypothesis states that a variety of neurotoxic Aβ species contribute to the pathogenesis of Alzheimer's disease. A key determinant of disease onset and progression is the appropriate balance between Aβ production and catabolism. It has been suggested that insufficient clearance of Aβ may account for elevated Aβ levels in the brain and the accumulation of pathogenic amyloid deposits in sporadic AD.[140] Ito *et al*. demonstrated that the efflux clearance of [^{125}I]Aβ in rats is 11.0 μL/(min g brain).[143] Experimental evidence suggests that brain and blood Aβ are in equilibrium through the BBB, and that peripheral sequestration of Aβ may shift this equilibrium towards the blood, eventually drawing out its excess from the brain ("sink" effect),[144] reducing Aβ-related pathology and dysfunction.[145] The clearance seems to be accomplished via two major pathways: proteolytic degradation and receptor-mediated transport from the brain.

Proteolytic degradation

A number of proteases are implicated in the proteolytic clearance of Aβ from the CNS; the two major endopeptidases involved in Aβ degradation are zinc metalloendopeptidases - called insulin degrading enzyme (IDE) or insulysin - neprilysin (NEP), endothelin converting enzyme, and plasmin.[146]

Receptor-mediated transport

The clearance is achieved by the brain-to-blood efflux transport system across the BBB. Increasing evidence suggests that the low-density lipoprotein receptor-related protein (LRP) and the receptor for advanced glycation end products (RAGE) are involved in receptor-mediated flux of Aβ across the BBB.[147] While LRP appears to mediate the efflux of Aβ from the brain to the periphery, RAGE has been strongly implicated in Aβ influx

back into the CNS. Therefore therapeutic strategies can be aimed at upregulation of LRP-1 or downregulation of RAGE.

ApoE, acting to traffic lipids throughout the brain, plays critical roles in regulating brain Aβ peptide levels, as well as their deposition and clearance.[148] Recently, Jiang Q. *et al* demonstrated that lipidated forms of ApoE act to enhance the clearance of Aβ peptides from the brain, facilitating the proteolytic degradation of Aβ. They demonstrated that an elevation of lipidated forms of ApoE results in reduced Aβ peptide and plaques levels in an animal model of AD.[149]

The molecular pathways responsible for the efflux and the influx of Aβ across the BBB suggest an array of potential therapeutic strategies that could reduce the accumulation of cerebral Aβ. The Aβ clearance should preferably be performed before the proteins cluster into the toxic oligomers and can be achieved in many ways, such as: 1) immunotherapy; 2) enzymatic degradation by metallo-endoproteases; 3) stimulating clearance by increasing transport over BBB by stimulating the LRP receptor or inhibiting RAGE (or P-gp).

More recently, immunological approaches have been implemented to reduce Aβ load in the CNS. Recent studies demonstrated that beta amyloid burden in transgenic animal models can be either peripheral or cerebral infusion of exogenous anti-Aβ antibodies (passive immunization) or by immunization with synthetic Aβ peptide. Two basic mechanisms have been proposed to account for the findings of reduced amyloid load in transgenic animals with high anti-Aβ antibody titers. First, anti-Aβ antibodies may cross the BBB and bind to Aβ in the brain, prompting digestion by activated microglia. In alternative, antibodies or agents that have high affinity for Aβ (ganglioside GM1 or gelsolin) may bind and sequester Aβ in the periphery; they may either promote the efflux from or inhibit the influx back into the brain.[144,150]

Another possibility to enhance the Aβ clearance from the brain is the upregulation of Aβ degradating enzymes; for example NEP activity can be upregulated by the administration of somatostatin.[150]

1.4. Current and novel therapeutic approaches for the treatment of AD

The objectives of pharmacologic therapy for AD are the stabilization and the modulation of the expected decline of cognitive, functional and behavioral symptoms.[151] The available

treatments are not intended to alter the progressive pathophysiology of the disease, but they are rather considered to be symptomatic therapies. Nowadays, cholinesterase inhibitors (ChEIs) are the first-line medications in the treatment of AD and they are effective in delaying cognitive impairment. The management of the non-cognitive psychiatric symptoms require some additional adjunctive medications, such as antipsychotics, antidepressants, and anxiolytics.[152] Alternate treatments, using nonsteroidal anti-inflammatory drugs (NSAIDs), Gingko biloba, and hormone replacement therapy, have been used with varying success in the treatment of AD. New anti-amyloid medications in various stages of clinical trials show promise in modifying the process of the disease. The glutamate-mediated toxicity in the cerebral cortex has been hypothesized to contribute to the neurodegeneration of AD. In 2003, the FDA approved memantine, a moderate-affinity non-competitive N-methyl-D-aspartate receptor antagonist, for the treatment of moderate to severe AD.[153] In patients with moderate to severe AD, receiving a stable dose of memantine, it results in significant improvement in cognitive, functional, and global outcomes, compared with placebo. Gingko extract has been used for thousands of years in traditional Chinese medicines for a variety of conditions. Recently, it has become more widely used in the United States to treat age-related physical and cognitive disorders.[152] The efficacy of gingko in the treatment of AD has been attributed to the flavonoid component, for its antioxidative and antiperoxidative properties and to the terpenoid component for its anti-inflammatory effects. [154] Estrogens are neuroprotective against oxidative stress, excitatory neurotoxicity, and brain ischemia. Several small short-term randomized clinical trials and some epidemiologic studies have suggested the efficacy of the hormone therapy in the treatment of mild to moderate AD.[155]

There are currently four categories of anti-amyloid drugs in clinical trials with promise to modify the AD process: 1) immunotherapies; 2) secretase inhibitors; 3) selective Aβ-lowering agents; and 4) anti-Aβ aggregation agents. Several anti-aggregation agents, which are in clinical testing, are thought to prevent fibril formation and facilitate Aβ clearance. Tramiprosate (Figure 18), a small glycosaminoglycan (GAG) mimetic, binds to soluble Aβ inhibiting fibril formation, and allows a decrease of soluble Aβ levels in CSF and reduces amyloid plaque formation. In a 3-month phase II study in subjects with mild to moderate AD, tramiprosate decreased CSF Aβ concentrations from baseline without effect on cognitive function compared with placebo.[156] Colostrinin, a proline-rich peptide, inhibits

Aβ aggregation and has demonstrated moderate improvements in the cognitive function for mild more than moderate AD. Unfortunately, these effects were not sustained over long term use.[157]

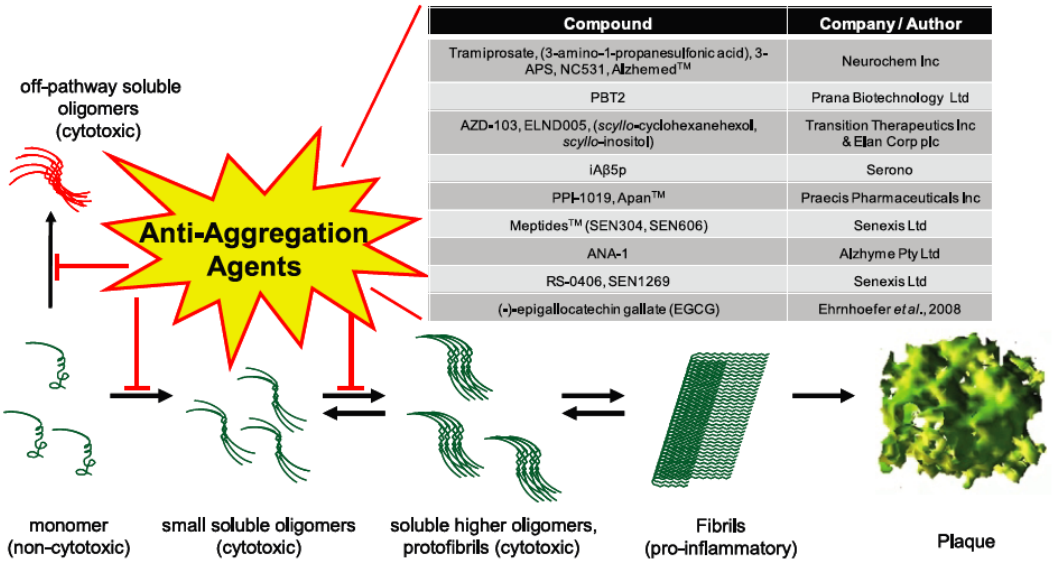

Compound	Company / Author
Tramiprosate, (3-amino-1-propanesulfonic acid), 3-APS, NC531, Alzhemed™	Neurochem Inc
PBT2	Prana Biotechnology Ltd
AZD-103, ELND005, (*scyllo*-cyclohexanehexol, *scyllo*-inositol)	Transition Therapeutics Inc & Elan Corp plc
iAβ5p	Serono
PPI-1019, Apan™	Praecis Pharmaceuticals Inc
Meptides™ (SEN304, SEN606)	Senexis Ltd
ANA-1	Alzhyme Pty Ltd
RS-0406, SEN1269	Senexis Ltd
(-)-epigallocatechin gallate (EGCG)	Ehrnhoefer *et al.*, 2008

Figure 18: Aβ aggregation pathways and points of therapeutic intervention.

1.5. Novel therapeutical promises exploiting nanoparticles

The currently available diagnostic tools do not allow to screen AD at an early stage, and the therapy is often compromised by the difficulty to cross the BBB.

The idea to exploit a sort of "cargo", that allows drugs and diagnostic to cross the BBB, is very actractive. To accomplish this task, one must take advantage of one of the molecular transport systems, that permits the uptake of nutrients into the brain. One of these transport systems - known as receptor mediated transcytosis (RMT) - employs the vesicular trafficking machinery of the endothelium to transport substrates into the brain. Once a chemical entity, able to cross the BBB exploiting RMT, is found, the drug can be covalently linked to it or encapsulated in it, generating a sort of cargo to cross BBB.

Recently, the emerging field of nanotechnology has generated new devices to solve this problem. Nanoparticles (NPs) - ranging in size from 10-1000 nm - have several advantages. They present a good physical stability in biological fluids; they can be designed, using a wide range of materials, to control release of encapsulated drugs; NPs

formulations can be suitable for either hydrophilic or lipophilic drugs. Moreover, NPs possess high drug-loaded capacities; they may offer protection from degrading enzymes to sensitive molecules (e.g. peptides) during transportation, and increase their half-life in the blood stream.[158,159] The NPs surface can be modified with specific molecules to avoid recognition by the macrophages of the reticuloendothelial system (RES) and for prolonging the NPs blood circulation residence time.[160] Finally, the NPs surface can be modified with specific ligands, in order to achieve a site-specific drug delivery and a successful penetration of the BBB.[161] Many Aβ ligands described in this review can't cross the BBB. The conjugation or the incorporation into NPs might overcome this problem.

Multiple presentation of a single ligand at the surface of NPs will exploit the cluster effect[162] that strongly enhances the adhesion properties. Furthermore, NPs can be functionalized with molecules performing different roles, such as 1) interaction with BBB, 2) stimulation to cross BBB, 3) PET and MRI contrast agents. Such NPs combine the different properties required for diagnosis and therapy.

1.5.1. Nanoparticles for drug delivery through blood-brain barrier

The blood-brain barrier (BBB) represents an effective obstacle for the delivery of neuroactive agents to the central nervous system (CNS). The presence of the BBB makes treatment of many CNS diseases difficult to achieve, because the required therapeutic agents can't be delivered across the barrier in sufficient amounts. It is estimated that more than 98% of small molecular weight drugs and practically 100% of large molecular weight drugs (mainly peptides and proteins) developed for CNS phatalogies do not readily cross the BBB.[163]

A variety of novel strategies have been proposed to improve the permeability of drugs into the CNS, including blood-brain barrier disruption, alternative routes to CNS drug delivery, chemical drug delivery, biological drug delivery. One of the possibilities to delivery drugs to the brain is the employment of NPs.[164] NPs can operate as carries for several classes of drugs, such as anticancer agents, antihypertensive, immunomodulators, and hormones; and macromolecules such as nucleic acids, proteins, peptides, and antibodies.

NPs are usually made of natural or artificial units, ranging in size between about 10 and 10000 nm (10 μm). Drugs or other entities may be dissolved into the NPs, entrapped, encapsulated and/or adsorbed or attached. The aim of using NPs is to increase the specificity towards cells or tissues, to improve the bioavailability of drugs by increasing their diffusion through biological membranes and/or to protect them against enzyme inactivation.[164]

The field of nanoparticles drug technology is not well developed in AD research, but NPs are promising candidates in the investigation of AD. In fact, NPs are capable of opening tight junctions, crossing the BBB, high drug loading capacities; they can also target towards mutagenic proteins of Alzheimer's disease.[158]

The generation of nanoparticles properly loaded with antiamyloidogenic ligands, which could be concentrated at the brain surface and/or able to cross the blood brain barrier (BBB), represents therefore a novel promising therapeutic approach.

Objectives

The grand aim of all science is to cover the greatest number of empirical facts by logical deduction from the smallest number of hypotheses or axioms.

A. Einstein

The goal of this study, developed in the field of nanotechnologies, is to create nanoparticles NPs able to cross the BBB and thus to reach the brain, which is the principal site of Alzheimer's disease. Molecules that can recognize (diagnosis) and destroy (therapy) the amyloid deposits, characteristic of the illness, will be attached to nanoparticles (NPs) and tested in vitro with different technologies. The results can have an enormous impact on the early diagnosis and therapy of a disease of high incidence, which has a heavy social cost.

The aim of this project is the use of NPs specifically functionalized with Aβ ligands, that can interact with the peptides both in the early stages of the aggregation and also with the Aβ plaque (Figure 19).

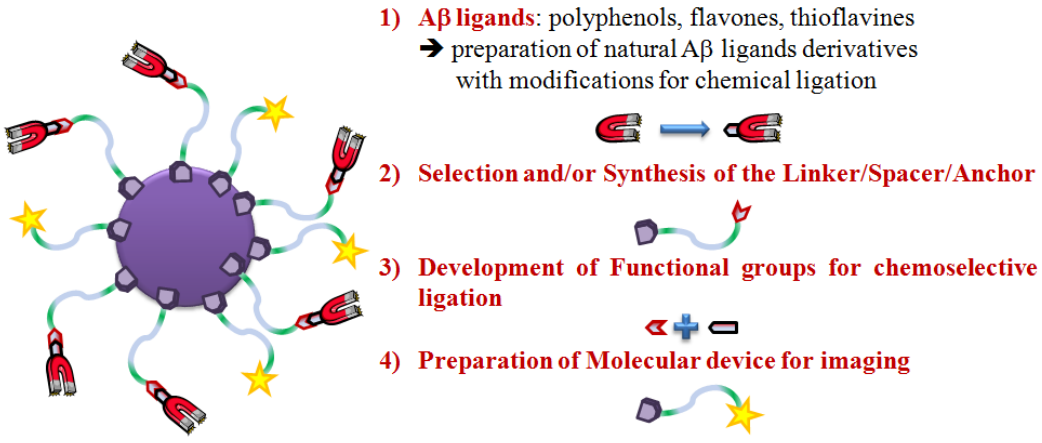

Figure 19: Strategy for functionalization of nanoparticles.

As already mentioned above, there are different classes of compounds with reported ability to interact with Aβ, among them there are: specific lipids, omo- and hetero-aromatic

polycyclic compounds such as flavones and thioflavins, polyphenols, peptidomimetics, tetracyclines and antibodies.

Many possible "lead compounds" have been identified, but we don't know any process of lead optimization ever been done. Moreover, since Aβ peptides are concentrated inside the brain or within the brain surface, the identified compounds must be concentrated near the BBB, for the interaction with circulating Aβ; they must also have the ability to cross this barrier, for the interaction with Aβ peptides or plaques inside the brain.

The work presented in this thesis aimed to synthesize novel chemical entities, such as small molecules and NPs, and was organized in different steps:

2.1. Preparation of Aβ ligands for NPs functionalization

Basing on the conformation/oligomerization hypothesis, molecules able to stabilize the soluble Aβ conformation and to prevent the required conformational transition could be effective inhibitors of the amyloid plaque formation and very potent drug candidates for AD treatment. These include naturally occurring or commercially available bioactive compounds, drugs, surfactants[79], Cu/Zn chelators[80], phenothiazines[81] and sulfonated dyes such as or Congo red and its derivatives[82]. According to Porat *et al.*,[86] who reviewed the possible mode of interaction with Aβ, small molecules with aromatic moieties can intercalate within grooves, created by β-sheets in both the soluble oligomeric forms and in the large fibrils (fAβ). It is not surprising to notice that many reported small molecule inhibitors are planar and with more than one aromatic moiety. Beginning from this information, we decided to use Curcumin (CUR) as starting natural material for our synthesis. CUR (diferuloylmethane) - a low molecular weight molecule - is an active principle of the perennial herb *Curcuma longa* (commonly known as turmeric), which is used in the traditional diet and as an herbal medicine in India.[133] The yellow-pigmented fraction of turmeric contains CUR as a major component and curcuminoids, which are chemically related to its principal ingredient.

In water environment CUR exists in enolic and β diketonic forms, because of its cheto-enol tautomerism. The fact that CUR in solution exists primarily in its enolic form[165]

has an important influence on the radical-scavenging ability of CUR and on its Aβ-binding activities.[166]

In 2001, Lim *et al.*[88] suggested that CUR was able to block Alzheimer's disease pathogenesis at multiple sites of the inflammation cascade, but the direct effects of CUR on the formation and destabilization of fAβ remained unclear. As presented above, Reinke *et al.*[136] noticed that, for the interaction with Aβ, the two aromatic rings need to be coplanar and the linker between them must be rigid and restricted between 8 and 16 Å. Modifications that don't influence these parameters, could improve the ability of CUR against Aβ. In 2008, Narlawar *et al.*[167] replaced the 1,3-dicarbonyl moiety with isosteric heterocycles to minimize the metal chelation properties of CUR and to lock its conformation into an enol-type arrangement. This modification provides potent ligands of Aβ aggregates, inhibitors of tau protein aggregation and they *de*-polymerized tau protein aggregates at low micromolar concentrations.

Considering this information, we synthesized a new series of compounds replacing the 1,3-dicarbonyl moiety with a pyrazole ring, not only for the reasons reported above, but also for improving water solubility and stability at physiological pH, preserving the best features for the interaction with Aβ-peptides.

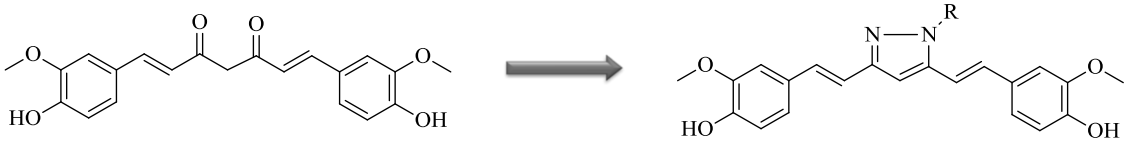

Figure 20: Chemical abstract of CUR-functionalization

2.2. Synthesis of different anchors and/or spacers for NPs Functionalization

Working on various types of NPs, we had to carry out different strategies for the functionalization/conjugation of NPs with Aβ ligands looking on the physical/chemical properties of these two building blocks.

In order to allow the generation of NPs functionalized at the same time with Aβ linkers, contrast agents and, eventually, molecules able to facilitate the transport through the BBB, building blocks of different NPs were synthesized, having the following characteristics (Figure 21): 1) an anchor for the insertion inside the NPs, 2) a chemical moiety, useful to

link an hydrophilic linker as polyethilenglycol (PEG), 3) a PEG chain of different length (30-40 bounds), 4) a functional group at the end of the PEG chain to link, alternatively, an Aβ ligand, a contrast agents, a BBB transporter or an antibody.

For the selective ligation we used the Huisgen 1,3-dipolar cycloaddition of azides and terminal alkynes, also called "Click reaction".

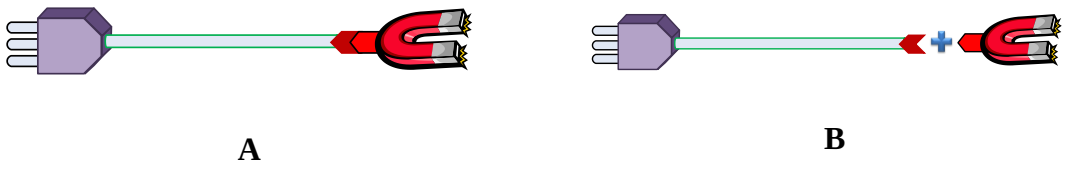

Figure 21: Chemical abstract of linker/spacer/anchor synthesis. A) preformed monomer bearing the Aβ ligand; B) preformed monomer with functional group for chemoselective ligation.

2.3. Functionalization of different NPs

Different strategies for the functionalization/conjugation of NPs with Aβ ligands have been developed: i) the linker/spacer has been first linked/conjugated to the surface of NPs and Aβ ligands were conjugated afterwards, using chemoselective ligation methods (Figure 22 A); ii) the linker/spacer/anchor have been conjugated to Aβ ligands for the subsequent functionalization/addition to NP (Figure 22 B).

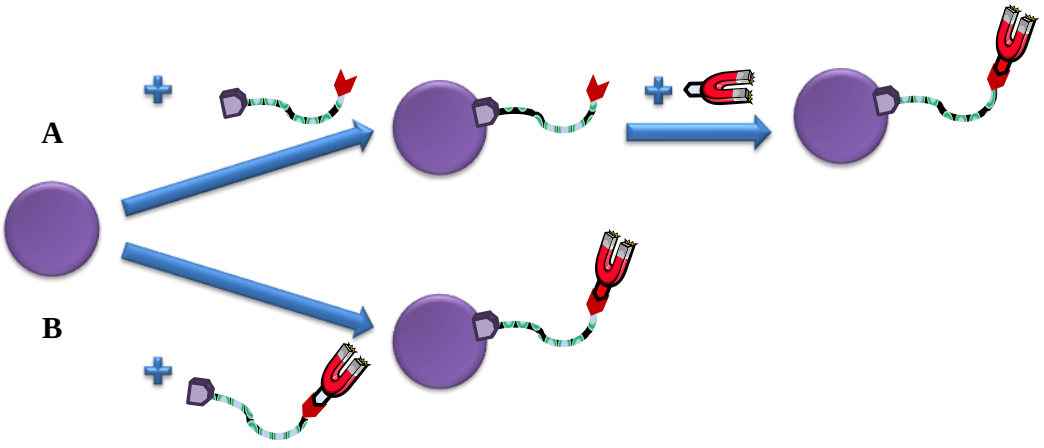

Figure 22: Chemical abstract of functionalization of NPs.

Results and Discussion

3.1. Preparation of Aβ ligands for NPs functionalization

As previously reported, curcumin (CUR) is a major component of the yellow spice turmeric.[168] This spice, used as an herbal medicine in India, is currently undergoing scientific evaluation for their efficacy as anti-inflammatory agents. In fact, it is believed to prevent and treat cancer[133,169] and it is being also studied for the treatment of human immunodeficiency virus (HIV) infection,[170] and for the treatment of cystic fibrosis.[171] It has been demonstrated that curcumin has anti-oxidant, anti-inflammatory and cholesterol lowering properties. These three properties are believed to play a crucial role in the processes involved in the pathogenesis of AD (Figure 23).

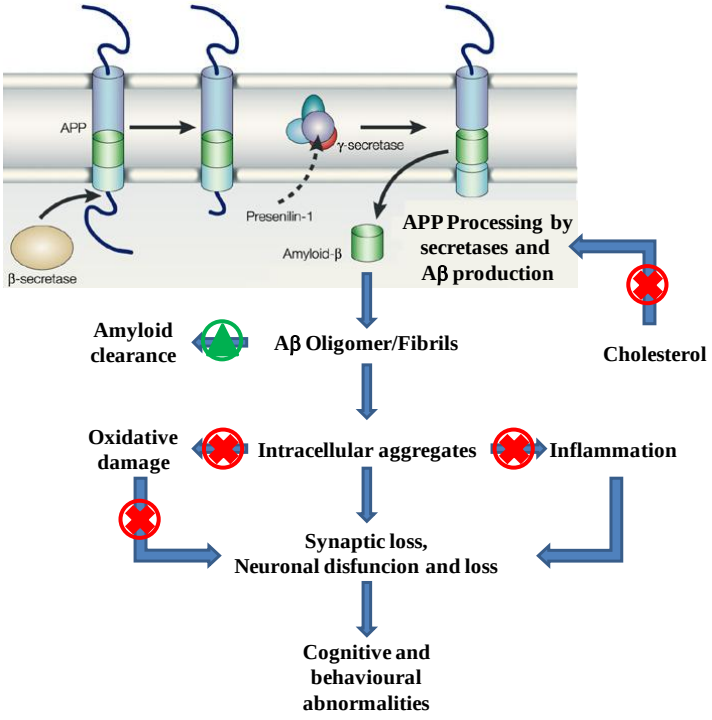

Figure 23: Curcumin's target in AD.

Oxidative damage plays a significant role in the pathogenesis of AD. Increased levels of the oxidated forms of various organic molecules - such as lipids, proteins, DNA and carbohydrates - have been found in the brain, in the cerebrospinal fluid (CSF), in the blood and/or in the urine of AD patients.[172,173] Epidemiological studies indicated an association between dietary antioxidant consumption and a reduced risk for the development of AD.[174] CUR displays a potent antioxidant activity: it reduces oxidative damage, synaptic loss and neuronal dysfunction. It shows anti-inflammatory effects and therefore it may have a role in slowing or halting AD. It also curtails the damage by inhibiting NF-kB induced iNOS, lipoxygenase and COX-2 and inflammatory cytokinin production by reactive glia.[175-178] Moreover, epidemiological studies have indicated that high levels of cholesterol may contribute to the pathogenesis of AD. In fact, it is unusually accumulated in the dense cores of Aβ plaques in the brain of AD patients. It is believed that cholesterol interacts with the amyloid cascade in the pathogenesis of AD. CUR can lower plasma and tissue cholesterol, potentially lowering Aβ production and inhibiting $A\beta_{1-42}$ fibril formation and disaggregating preformed fibrils.[179,180]

Altogether, these properties make CUR a potential druglike candidate for AD. The widespread use of CUR as a food additive and some relatively small short-term studies on humans demonstrate its safety and tolerability. However, some important information regarding CUR's stability, solubility, bioavailability, safety and tolerability - especially in an elderly population - is still lacking. In fact, the mixture of natural curcuminoids products is insoluble in water and ether, but soluble in ethanol, dimethylsulfoxide, and acetone. It is stable at acidic and high (> 11.7) pH but unstable at neutral and quite basic pH; it is degraded to (5*E*)-6-(4'-hydroxy-3'-mothoxyphenyl)-2,4-dioxo-5-hexenal as major product and vanillin, ferulic acid and feruloylmethane.[181-184] In fact, most CUR (> 90%) is rapidly degraded within 30 min of placement in phosphate buffer systems of pH = 7.2. In comparison, CUR is more stable in cell culture medium, containing 10 % fetal calf serum, and in human blood, < 20% of CUR being degraded within 1 h and approximately 50% by 8 h.

In water environment CUR exists in enolic and β diketonic forms, because of its cheto-enol tautomerism. The fact that CUR in solution exists primarily in its enolic form[165] has an important effect on the radical-scavenging ability of CUR and on its Aβ-binding activities.[166]

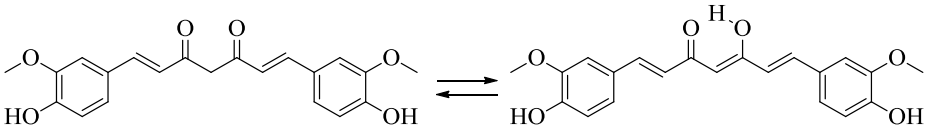

Figure 24: Cheto-enol tautomerism of Curcumin.

In 2001, Lim *et al.* [88] suggested that CUR was able to block AD pathogenesis at multiple sites of the inflammation cascade, but the direct effects of CUR on the formation and destabilization of fAβ remain unclear. In 2007, Reinke *et al.* [136] studied the structure-activity relation of Aβ aggregation inhibitors based on CUR. As presented before, they studied the effect of three prominent features on the inhibition of the amyloid aggregation: the presence of two aromatic end groups, the substitution pattern of these aromatics, and the length and flexibility of the linker region. They found that the modification of any one of the modules has profound effects on their activity. They noticed that the two aromatic rings need to be coplanar and the linker between them must be rigid and restricted between 8 and 16 Å. The modifications that don't influence these parameters could improve the ability of CUR against Aβ. In 2008, Narlawar *et al.*[167] replaced the 1,3-dicarbonyl moiety with isosteric heterocycles, to minimize the metal chelation properties of CUR and to lock its conformation into an enol-type arrangement. This modification provides some potent ligands of Aβ aggregates and inhibitors of tau protein aggregation and *de*-polymerized tau protein aggregates at low micromolar concentrations.

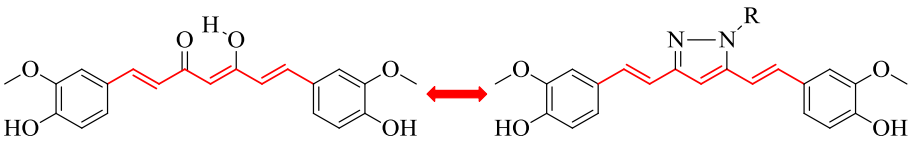

Figure 25: Locked enol conformation of Curcumin.

Starting from this information, we synthesized a new series of compounds replacing the 1,3-dicarbonyl moiety with a pyrazole ring. It was made not only for the reasons reported above but mainly for improving water solubility and stability at physiological pH, preserving the best features in interaction with Aβ-peptides.

3.1.1. Chemical synthesis

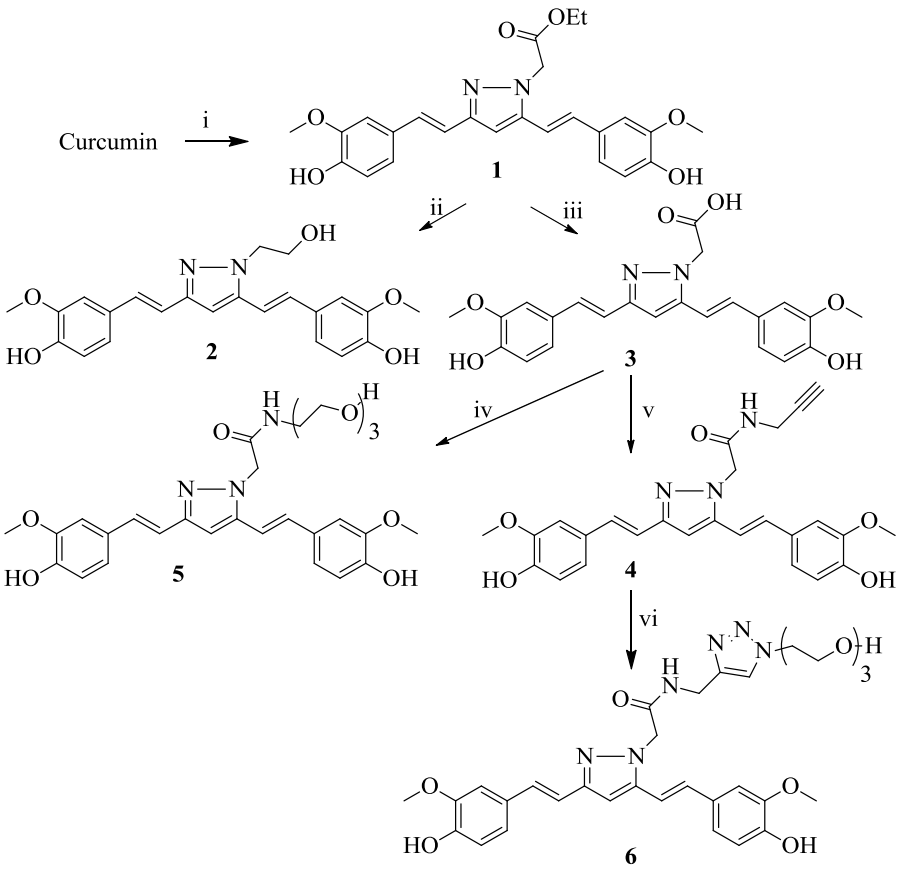

Scheme 1: Reagents and Conditions: (i) ethyl 2-hydrazinylacetate hydrochloride, TEA, TFA, reflux, 2.5 h. 87%; (ii) THF, $LiAlH_4$, 0 °C → r.t. 70%; (iii) KOH, MeOH, r. t., 12 h, quant.; (iv) HOBt, TBTU, DMF, r.t., 15 min., then 2-(2-(2-aminoethoxy)ethoxy)ethanol, TEA, r. t., 12 h, 37%; (v) HOBt, TBTU, DMF, r.t., 15 min., then propargylamine, TEA, r. t., 12 h, 68%; (vi) $CuSO_4 \cdot 5H_2O$, Sodium ascorbate, water/THF, 2-(2-(2-azidoethoxy)ethoxy)ethanol, 90 min., r.t. 72%.

In order to generate the small library of CUR derivatives in a straightforward manner, we first synthesised pyrazole derivative **1**, which was converted to all other derivatives (Scheme 1). The treatment of CUR with ethyl 2-hydrazinylacetate hydrochloride in refluxing toluene afforded the pyrazole derivative **1** in good yield (87%). The reduction of **1** with $LiAlH_4$ afforded product **2** in a 70% yield. The carboxylic acid **3** was obtained from **1** by basic hydrolysis of the ethyl ester in a quantitative yield. The derivatives **4** and **5** were obtained from **3**, through the coupling respectively with propargyl amine and 2-(2-(2-aminoethoxy)ethoxy)ethanol in the presence of the coupling agents hydroxybenzotriazole (HOBt) and O-(benzotriazol-1-yl)-N,N,N',N'-tetramethyluronium tetrafluoroborate

(TBTU) in 68 and 37% yield. Finally, Cu(I) chemoselective reaction of alkyne **4** with 2-(2-(2-azidoethoxy)ethoxy)ethanol, afforded the final compound **6** in 72% yield.

3.1.2. In vitro binding studies

3.1.2.1. *Solution Nuclear Magnetic Resonance studies*

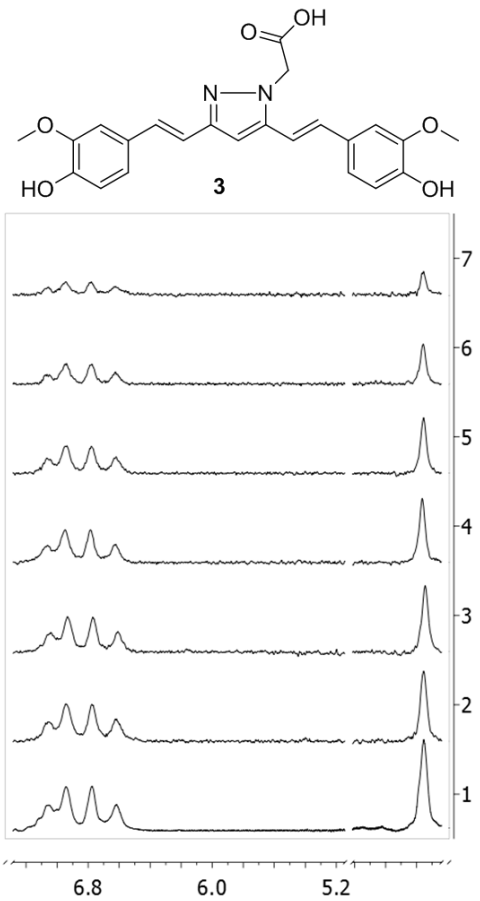

Figure 26: 1) $A\beta_{1-42}$-compound 3, at a 1:7 molar ratio, NS=64. 2-7), STD spectra of the mixture recorded at different peptide saturation times (2, 3 s; 3, 2 s; 4, 1.5 s; 5, 1 s; 6, 0.6 s; 7, 0.3 s). NS=128, on-resonance frequency=-1.0 ppm, off-resonance frequency=40 ppm. All spectra were recorded on the same sample; all samples were dissolved in PBS, pH = 7.4, at 37 °C.

The compounds **2**, **3**, **4**, **5** and **6** were tested for their ability to bind $A\beta_{1-42}$ peptide by exploiting Saturation Transfer Difference-Nuclear Magnetic Resonance (STD-NMR) spectroscopy. This technique has been used extensively as a comprehensive and efficient method to investigate enzyme–ligand interactions.[185-190] More recently, Airoldi *et al.* employed STD-NMR experiments to characterize tetracycline and ThT interaction with

$A\beta_{1-40}$ and $A\beta_{1-42}$ peptides.[191] The same methodology has been applied here, in order to check the effect of CUR chemical fictionalizations on $A\beta_{1-42}$ oligomer recognition and binding processes. As a matter of facts, some aggregated Aβ species, in particular the oligomeric assembly intermediates, are believed to trigger a cascade of events, which lead to the formation of neurofibrillary tangles and the disruption of the neuronal cytoskeleton, widespread synaptic loss and neurodegeneration.[192]

The binding studies were performed on the mixtures containing a batch of $A\beta_{1-42}$ enriched in oligomers and compounds **2**, **3**, **4**, **5** or **6** at the final concentration of respectively 80 μM and 0.5 mM.

Our data demonstrate that all the molecules retain CUR ability to bind peptide oligomers. In all cases, after selective irradiation of the peptide resonances at -1.0 ppm, some compound signals appeared in the STD spectra. This indicates the existence of magnetization transfer from the oligomers to the drug. STD spectra, recorded on a $A\beta_{1-42}$-compound **3** mixture at six different saturation times of the peptide envelope, are reported in Figure 26 as an example.

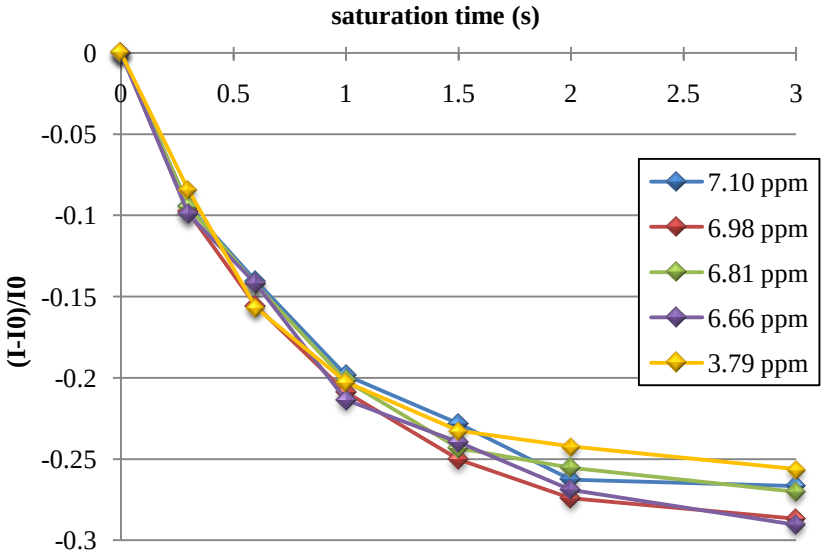

Figure 27: Fractional STD effects for compound 3 protons, calculated by $(I-I_0/I_0)$, where $I-I_0/I_0$ is the peak intensity in the STD spectrum and I_0 is the peak intensity of an unsaturated reference spectrum.

Fractional STD effects for the compound **3** protons revealed that all the hydrogen atoms, strictly related to the natural CUR moiety, interact in the same manner with the $A\beta_{1-42}$

soluble oligomers, as presented in Figure 27. A detailed ligand-epitope mapping disclosed that the two aromatics rings and the conjugates double-bounds are always implicated in the binding. On the other hand, the different chains present on the pyrazole ring do not contribute to the interaction, being the corresponding signals absent in STD spectra.

3.1.2.2.*Structural characterization by different microscopy techniques.*

Transmission Electron Microscopy (TEM) analysis, performed on fibers exposed to curcumin-derivatives, allowed a direct examination of self-assembling capacity of the peptide. EM microphotographs (Figure 28 - $A\beta_{1-42}$ alone) show structured amyloid fibrils, obtained with $A\beta_{1-42}$ after an incubation period of 5 days.

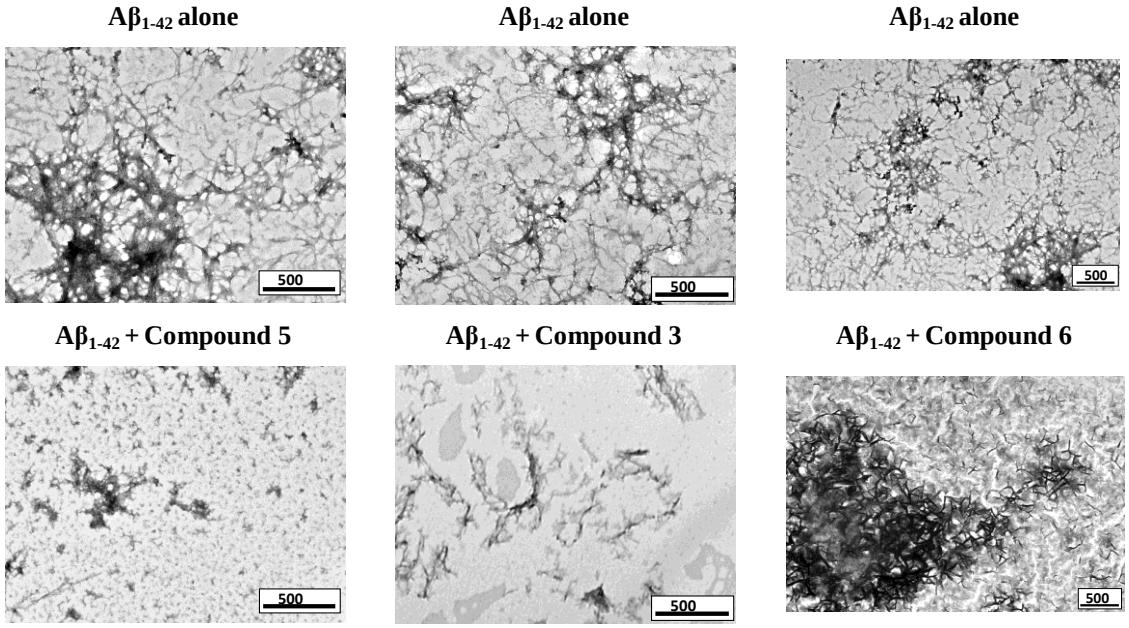

Figure 28: Electron micrographs of $A\beta_{1-42}$ alone and with compounds 3, 5, 6, after an incubation of 5 days.

The presence of test compounds during the incubation induced some morphological changes, altered the aggregation process and produced structural modifications. $A\beta_{1-42}$ appeared folded, enriched in oligomers, proto-fibrils and fibrils (Figure 28 - $A\beta_{1-42}$ alone). Compound **5** decreased the presence of aggregates (Figure 28 - $A\beta_{1-42}$ + Compound **5**), increasing the percentage of amorphous material. This compound co-precipitated with $A\beta_{1-42}$, forming tight agglomerates. The incubation with compound **3** also caused a

reduction of fibers, enhancing the development of amorphous structures (Figure 28 - $A\beta_{1-42}$ + Compound **3**). As reported in Figure 28 (Figure 28 - $A\beta_{1-42}$ + Compound **6)**, the presence of compound **6** during the aggregation process radically altered the structure of fibers: the samples showed an elevated amount of peptide in amorphous conformation and the presence of highly electron-dense material.

The interaction of test compounds with $A\beta_{1-42}$ was analyzed by Atomic Force Microscopy (AFM) as well. Aβ peptides were incubated for 5 days at 37 °C in the presence of the test compounds (peptide:compound, 1:2). After a centrifugation at 13.000 rpm for 15 min, the pellets were washed with 300 µL of buffer, centrifuged again and dissolved in 25 µL of formic acid. Finally, they were diluted to a concentration of 10 µM and spotted onto a mica disk. As reported in Figure 29 (Figure 29 - $A\beta_{1-42}$ alone), the samples of $A\beta_{1-42}$ after an incubation of 5 days were rich in oligomers, proto-fibrils and fibers aggregates. The test compounds apparently modify the aggregation process, as it was seen with the other techniques (Figure 29).

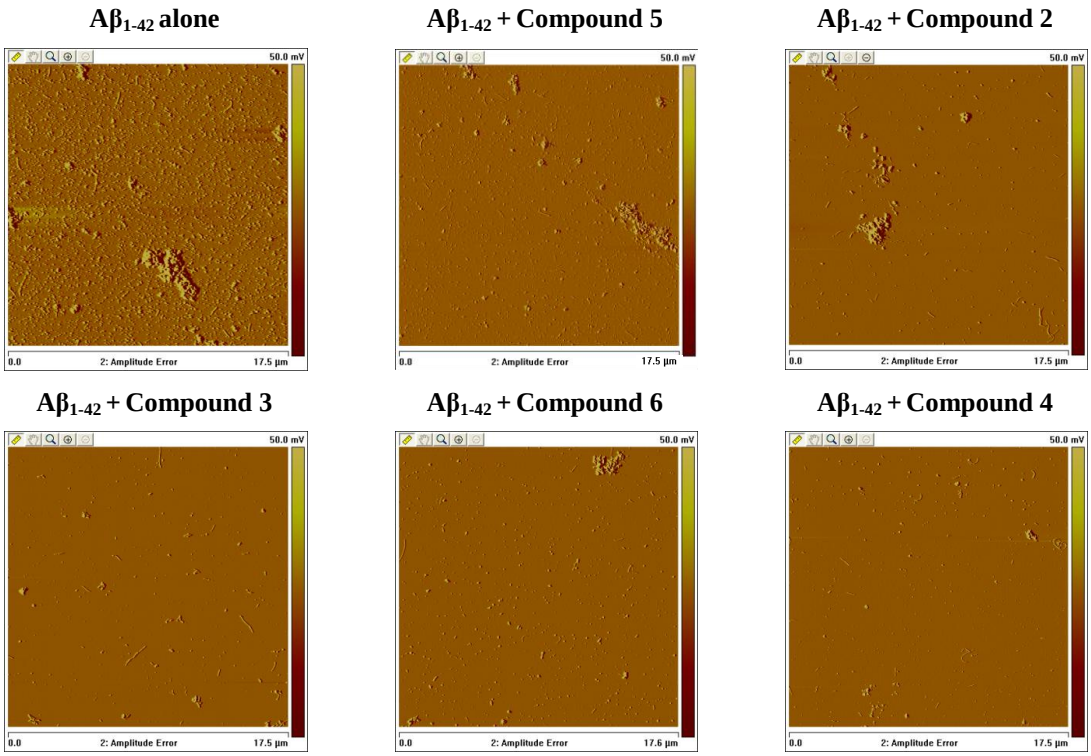

Figure 29: Tapping mode AFM images of $A\beta_{1-42}$: Morphology of aggregates of $A\beta_{1-42}$ alone and of $A\beta_{1-42}$ co-incubate with curcumin-derived compounds (1:2 molar ratio).

3.1.2.3.*Staining of amyloid deposits in Tg CRND8 mice.*

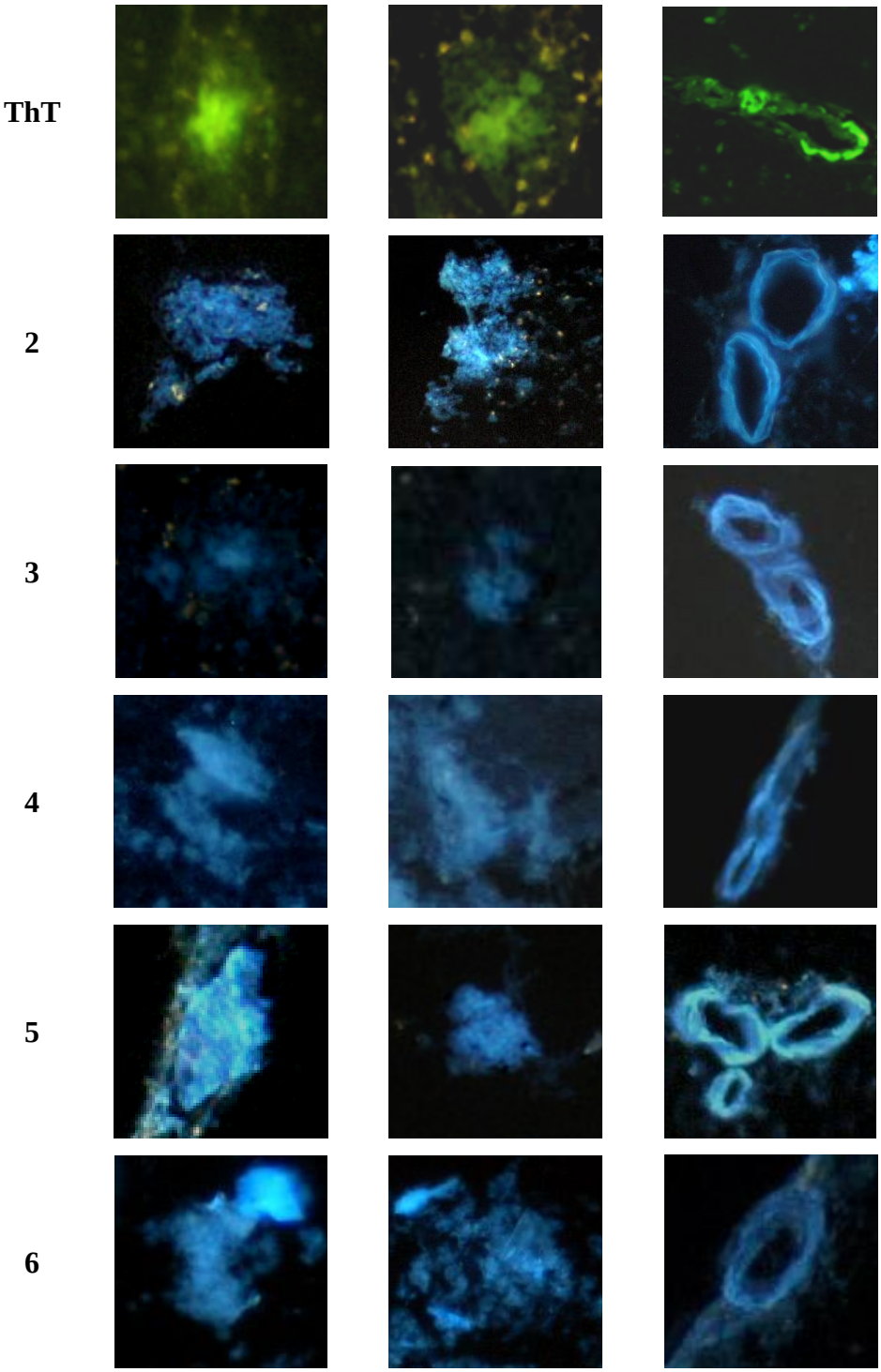

Figure 30: Staining of amyloid deposits in brain sections of Tg CRND8 mice: plaques and vascular walls stained with ThT, 2, 3, 5, 6 and 4. Fluorescent sections were viewed using fluorescence microscopy FITC for ThT and UV for curcumin-derived compounds.

A preliminary analysis was made on $A\beta_{1-42}$ samples that had been incubated for five days to form fibrils. After the aggregation, the samples were centrifuged and the formed fibers (pellet) were incubated with test compounds. These analysis enabled to determine the maximum absorption - around 335 nm - and important increases of the spectra of fluorescence was observed with a significant increase of the peak at 385 nm. Considering these results, the ability of test compounds to bind amyloid deposits was tested in brain sections from Tg CRND8 mice. These animals carry a human APP with double mutations and accumulate Aβ deposits in brain parenchyma and at cerebrovascular level. Cryostatic sections of 20 μm were obtained from fresh tissue, mounted on gelatin coated microscope slides and used for a staining assay. A solution of EtOH:water 50:50 (v/v) of test compounds was layered on tissue sections (the concentrations used were different, depending on the compound's ability to label amyloidogenic deposits). Fluorescent sections were viewed, using fluoromicroscope equipped with UV and FITC filters.
Thioflavin T (ThT) at 3 μM was used as a reference. All the test compounds were able to label amyloid plaques and vascular walls at concentration of 6 μM, but compound **6** and **5** were used at a final concentration of 12 and 18 μM, to obtain signal comparable to Thioflavin T staining. These results suggested that the test compounds recognize the β-pleated sheet structure of amyloid fibrils similarly to ThT and without being involved in aspecific binding to tissue preparations (Figure 30).

3.1.3. Discussion

CUR derivatives were synthesized in order to avoid the disadvantages of CUR itself, in particular regarding the solubility and also the stability in aqueous media. In fact, all the compounds present an improved solubility (in particular the compound **3** that has a solubility greater than 1 mM in PBS, pH = 7.4). This result is very important in relation to the bioavailability of the drug and also to its assimilation in the organism. Another enhanced property of our synthetic derivatives is their very high stability in all the types of organic and water mediums, as demonstrated by NMR studies; NMR experiments were carried out some months after the dissolution of the compounds in NaOD 10 mM and we noticed that the spectra presented the same shape and no new peaks of degradation. We also obtained another important goal, connected to their ability to interact with Aβ. In fact,

all the data presented above demonstrate that our derivatives retain CUR's ability to interfere with Aβ in all the different forms. From the NMR data we demonstrated that the blocked CUR's enol-tautomer is implicated in the interaction with the $A\beta_{1-40}$ and $A\beta_{1-42}$ oligomers and no substitution on the pyrazole ring modify this property. As a matter of facts, different microscopy experiments revealed that our compounds are able to modify the Aβ aptitude to form fibrils and fibers, obtaining some aggregates that are not related to these detrimental structures in AD patient's brains. The last property we found is the ability of staining the Aβ plaque in *ex vivo* models, without being involved in aspecific binding to tissue preparations.
All these characteristics are important for future applications, both in the therapy and in the diagnosis of Aβ related disease.

3.2. Synthesis of different anchors and/or spacers for NPs functionalization

3.2.1. Easy silica gel-supported desymmetrization of PEG

Polyethylene glycol (PEG) is a linear polymer that - because of its ideal properties, i.e., very low toxicity, excellent water solubility, extremely low immunogenicity and antigenicity - is used in a wide range of applications. Though not biodegradable, PEG is readily excreted after the administration into living organisms. In addition, it has excellent pharmacokinetic and biodistribution characteristics. All these properties[193-196] make PEG particularly useful for biomedical applications, as an ideal linker to graft biomolecules.
The main disadvantages of using PEG as a spacer are its symmetry and the difficulty in differentiating between the two terminal hydroxyl groups. Many authors have proposed different approaches for solving these problems. Some of them are based on the polymerization of differentially protected monomers and require multiple protection and deprotection steps. Others are based on the monoprotection of dihydroxy-PEG, which often leads to a mixture of mono-, bi- and non-protected compounds, very difficult to separate.
In order to exploit PEG as spacer in our project, we focused on the problem and proposed a new, simple, general method for the desymmetrization of PEG. This method is based on the connection of the polymer to a solid support through one of two terminal hydroxyl

groups. Then, the unbound hydroxyl group can be protected or converted into different functionalities (Br, N_3, SSH, OBn). The cleavage from the solid support, and the possible functionalization of the second hydroxyl group, generates the bi-functional polymer **X**-CH_2CH_2-$(O\text{-}CH_2CH_2)_n$-**Y**.

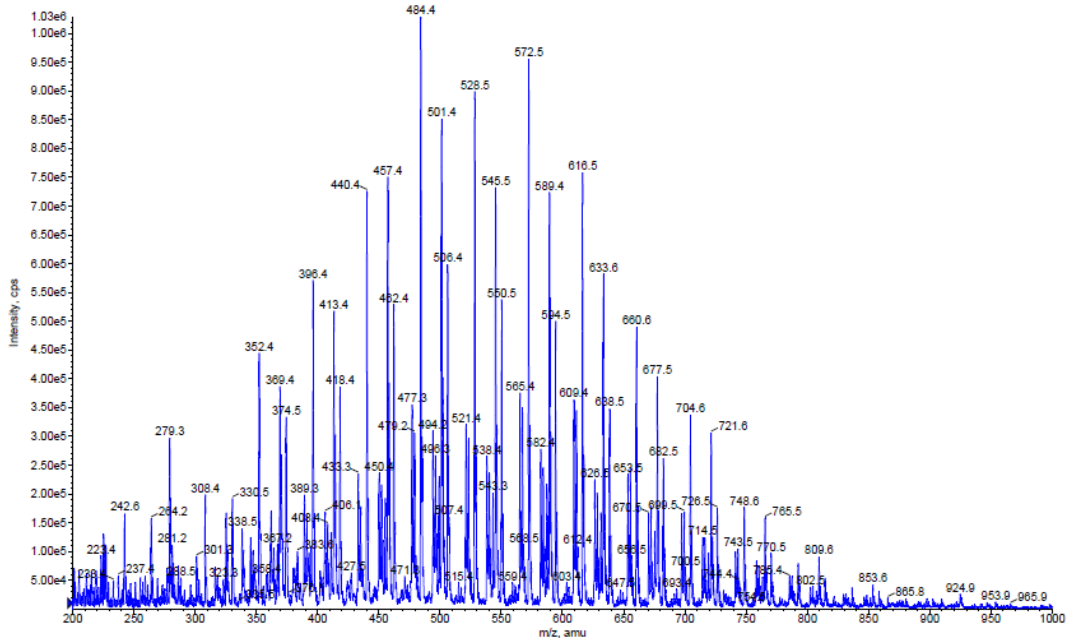

Figure 31: Typical mass spectrum of PEG 600.

We used Silica Gel 60 (mesh 230-400), as a solid support; in fact, it is a readily available material, generally used for the chromatography. The silanization[197,198] of a silica gel toluene suspension was obtained using (3-aminopropyl)triethoxysilane (Scheme 2) under reflux in a Dean-Stark apparatus. This technique led to a solid support with amino functionalities (**7**) (loading 0.53 mmol/g). The treatment of **7** with succinic anhydride introduced a carboxylic function, suitable for loading PEG, and permitted an easy cleavage from the support after proper modifications.

The treatment of a suspension of the solid support **7** in anhydrous tetrahydrofuran (THF) (r.t. for 12 h) with succinic anhydride, led to a carboxylic functionalized solid support **8** obtained in a quantitative yield, measured using TNBS test.[199] Next, the polyethylene glycol was loaded onto the generated solid support, through a simple coupling process: commercial PEG 600 (average MW 546) and **8** (1 g), suspended in anhydrous THF (10 mL), was reacted with *N*,*N*'-diisopropylcarbodiimide (DIC) and

4-(dimethylamino)pyridine (DMAP). This coupling provided **9**, with a loading of 0.1 mmol of PEG per gram of solid support. This, in turn, led to a loading lower than it was needed for solid support **7** (0.53 mmol/g). This can be explained considering the steric hindrance of the attached PEG chains. Even if the latter outcome is not very high it is satisfactory for our purposes.

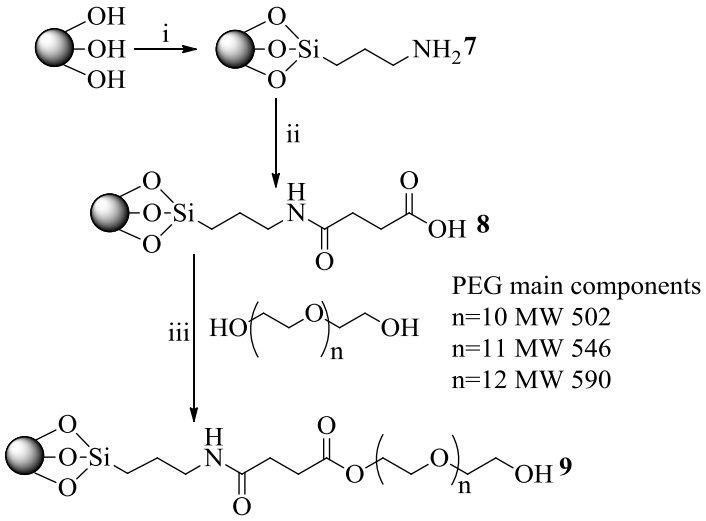

Scheme 2: ***Reagents and Conditions*****: (i) (3–aminopropyl)triethoxysilane, toluene, reflux, Dean–Stark apparatus; (ii) succinic anhydride, THF dry; (iii) commercial PEG 600, DIC, DMAP, THF dry.**

The "free" hydroxyl group of the silica gel-loaded polymer **9** was next functionalized as shown in Scheme 3. We followed two different synthetic strategies: the protection of the free OH as a benzyl ether by direct reaction with activated benzyl alcohols and the conversion of the free OH into a bromide and the subsequent displacement by other nucleophilic functional groups. The protection was carried out by suspending **9** (1 g) in benzyl 2,2,2–trichloroacetimidate (20 equiv.) in anhydrous CH_2Cl_2 (10 mL) and adding trifluoromethanesulfonic acid (10 equiv.). At the end of this process, we obtained derivative **10**. Bromide **11** was generated through the reaction of the suspension of **9** (1 g) in anhydrous CH_2Cl_2 (10 mL) containing phosphorus tribromide (10 equiv., 12 h). Bromide displacement with an azide or thiol nucleophile led to the formation of derivatives **12** and **13,** respectively. Functionalized silica gel **11** was washed with CH_2Cl_2, toluene and CH_3CN to remove excess reagent prior to being suspended in *N*,*N*-dimethylformamide (DMF) (1g/10 mL) and reacted with NaN_3 (10 equiv.) or caesium thioacetate (10 equiv.).

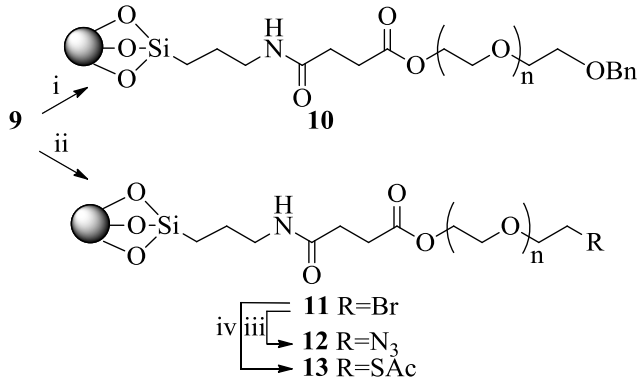

Scheme 3: ***Reagents and Conditions*****: (i) benzyl 2,2,2–trichloroacetimidate, triflic acid, CH_2Cl_2 dry, r.t.; (ii) PBr_3, CH_2Cl_2 dry, r.t.; (iii) NaN_3, tetrabuthylammonium iodide, DMF dry, 80 - 100°C; (iv) caesium thioacetate, DMF dry, r.t.**

All PEG derivatives (compounds **10**, **11**, **12**, **13**) were suspended in a solution of ammonia in methanol (7 M, 10 mL per gram of pegylated silica gel) and stirred for 12 h; this allowed the cleavage of the functionalized molecules from the solid silica support. Then, all the different suspensions of silica gel were filtered and washed with MeOH (Scheme 4). The filtrates were concentrated under reduced pressure, affording the mono derivatized poly(ethylene glycol) compounds **14**, **15**, **16**, **17** with good yields (Table 2), without further purification procedures. As previously reported,[200] the treatment of a thioacyl compound with basic conditions can lead to the dithiosulfide derivative as the only product. We investigated the structure of compound **17** and found that it was the dithiosulfide derivative. This can be used without further modifications and can be easily converted into the corresponding thiol (compound **18**) derivative by the treatment with $NaBH_4$ in MeOH. The obtained compounds were characterized by ^{1}H-NMR, IR and mass spectroscopy (Table 2). After a meticulous analysis of the mass peaks shown in Table 2, we determined that harsh reaction conditions (PBr_3, 7M NH_3 in MeOH) did not influence the poly-dispersion of the starting commercial PEG.

In order to verify the possibility of using the functionalized solid support in successive cycles, silica gel **9** was cleaved and we used an aqueous basic solution, to avoid amide formation (compound **20**). Next, 1 g of **9** was experimentally treated with 10 mL of a sodium hydroxide solution (NaOH 1.25M) and washed with MeOH.

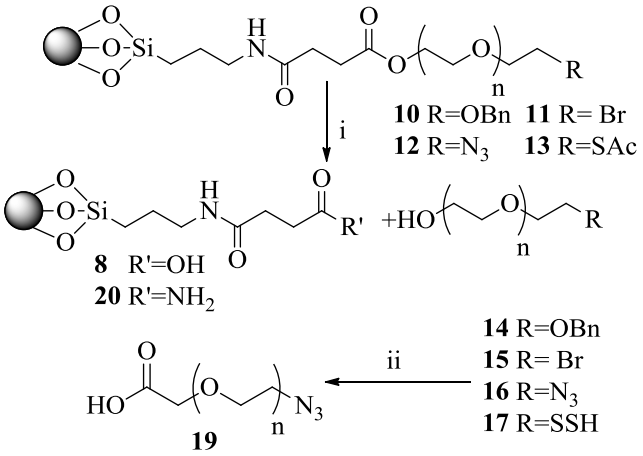

Scheme 4: ***Reagents and Conditions*****: (i) NH_3 7 M in methanol, r.t. (NaOH 1,25M, R.T. to generate 2); (ii) $KMnO_4$, NaOH 4 M.**

Table 2: Summary of the yields of desymmetrized PEG 14-17 and 19, and significant characterization signals; [a]calculated from 3, [b]oxidation yield from 16 [c]400 MHz, $CDCl_3$, 25 °C; [d]typical signals of commercial polymers; [e] the most intense peaks.

Compound	**Yield[a,b] (%)**	**Characterization**
14	54[a]	^{1}H NMR[c] δ 7.25–7.40 (m, 5H, Ar), 4.57 (s, 2H, OCH_2Ph), 3.55–3.75 (m)[d]; MS–ESI[e]: (n=10) M+H^+ (593.5), M+NH_4^+ (610.6), M+Na^+ (615.3); (n=11) M+H^+ (637.5), M+NH_4^+ (654.6), M+Na^+ (659.5); (n=12) M+H^+ (681.5), M+NH_4^+ (698.6), M+Na^+ (703.5).
15	78[a]	^{1}H NMR[c] δ 3.80 (t, J=6.3 Hz, 2 H, OCH_2CH$_2$Br), 3.55–3.75 (m)[d], 3.47 (t, J=6.3 Hz, 2H, OCH$_2$CH_2Br); MS–ESI[e]: (n=10) M+H^+ (565.5-567.5), M+NH_4^+ (582.6-584.6), M+Na^+ (587.5-589.5); (n=11) M+H^+ (609.6-611.6), M+NH_4^+ (626.1-628.3), M+Na^+ (631.5-633.7); (n=12) M+H^+ (653.6-655.6), M+NH_4^+ (670.6-672.6), M+Na^+ (675.6-677.6).
16	75[a]	^{1}H NMR[c] δ 3.55–3.75 (m)[d], 3.38 (bt, J=4.9 Hz, 2H, -CH_2N$_3$); IR band 2104.6 cm^{-1} st asymmetric; MS–ESI[e]: (n=10) M+H^+ (528.5), M+NH_4^+ (545.5), M+Na^+ (550.5); (n=11) M+H^+ (572.5), M+NH_4^+ (589.4), M+Na^+ (594.5); (n=12) M+H^+ (616.5), M+NH_4^+ (633.6), M+Na^+ (638.5).
17	71[a]	^{1}H NMR[c] δ 3.55–3.75 (m)[d], 2.84 (bt, J=6.99 Hz, 2H, OCH$_2$CH_2SSH). MS–ESI[e]: (n=10) M+H^+ (551.4), M+Na^+ (573.4); (n=11) M+H^+ (595.4), M+Na^+ (617.4); (n=12) M+H^+ (639.9), M+Na^+ (661,9).
19	73[b]	^{1}H NMR[c] δ 3.86 (s, 2 H, HOOCCH_2O), 3.55–3.75 (m)[d], 3.38 (bt, J=4.9 Hz, 2H, –CH_2N$_3$); MS–ESI[e]: (n=10) M+H^+ (542.5), M+Na^+ (564.5); (n=11) M+H^+ (586.5), M+Na^+ (608.5); (n=12) M+H^+ (630.5), M+Na^+ (652.5).

The silica was then acidified with HCl 0.1 M, until the filtrate pH was moderately acidic. After these steps, the silica was suspended in toluene and dried using a Dean-Stark apparatus. The commercial PEG was then loaded on the recycled solid support, as

presented in Scheme 2. This coupling afforded **9** with a loading of 0.091 mmol of PEG per gram of solid support; it is a result similar to the one achieved for the first coupling on silica **8**.

The remaining hydroxyl group of the obtained compounds can be further modified to generate other desired hetero-bifunctional polymers. For example, compound **16** was efficiently oxidized to the corresponding carboxylic acid **19**, by the treatment in aqueous media at pH > 12 with potassium permanganate (2 equiv.) (Scheme 4).

In conclusion, we reported a successful, efficient, easy and direct procedure for the monofunctionalization of commercial polyethylene glycol, exploiting inexpensive silica gel as a solid support. The monofuctionalized desymmetrized products can be used after their cleavage from the silica support without purification, and eventually, can be directly exploited for additional solid-supported synthesis.

3.2.2. Synthesis of monomer for lipid-base NPs.

The synthesis of functionalized derivatives of phospholipids analogs as effective agents for the preparation of targeted and/or stealth lipid-based NPs was carried out.

The analog was synthesized to allow the generation of NPs, that can be functionalized at the same time with Aβ ligands and contrast agents, and eventually even molecules able to facilitate the transport through the BBB.

Looking to the natural lipids and commercially available compounds, we decided to synthesize monomers which have the following characteristics (Figure 32): 1) two fatty acid chain, 2) a group to link the hydrophilic chain (Y), 3) a PEG chain of different length (30-40 bounds), 4) a functional group at the end of the PEG chain (Z) to link alternatively an Aβ ligand or a contrast agents or a BBB transporter or an antibody. We also planned to avoid the presence of charges, avoiding both ammonium and phosphate groups usually present in natural phospholipids.

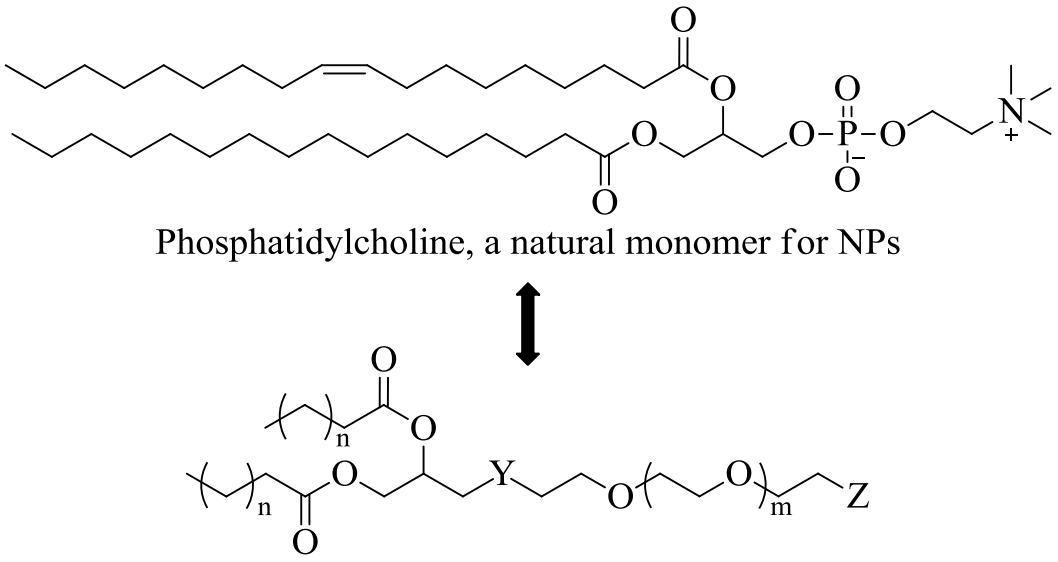

Figure 32: Structure of natural lipid analogs: Y = linking group between anchor and linker; Z = functional group for selective ligation.

Different chemical ligation methods and functional groups (Z) were taken into account, concerning the physical-chemical properties of both NPs and Aβ ligand. In fact, we had to choose a method which avoids the use of organic solvent that can destroy the NPs structure and doesn't interfere with the presence of double bonds of the CUR. We identified the Huisgen 1,3-dipolar cycloaddition of azides and terminal alkynes, the "click chemistry", as the best reaction for the conjugation of the Aβ ligand on the surface of all lipid-based NPs. After this, we moved our attention to the linker (Y) between the hydrophobic fatty acid chains and the hydrophilic PEG chain. The most important property of this moiety is that this group must be as polar as possible, to ensure the correct insertion of the lipid into the NPs. It is well known that the polarity ranking of functional groups is Amide > Acid > Alcohol > Ketone ~ Aldehyde > Amine > Ester > Ether > Alkane; so, the formation of an amide bond may be the best solution for the linkage and also for an improved *in vivo* stability. In order to obtain an even better hydrophilicity, we added a triazole ring in this "polar head". In fact, in substituted triazoles, the substituted carbon atom and the C–H bond can act respectively as an electrophilic site and hydrogen-bond-donor, while the pyridine-type lone pair of electrons on the nitrogen atom serves as a hydrogen-bond-acceptor element. As a result, the overall dipolar moment of the triazole system is larger than the one of amide bond and its hydrogen-bond donor and acceptor properties are

therefore more marked than those of an amide bond, increasing the polarity of this important part of the monomer.

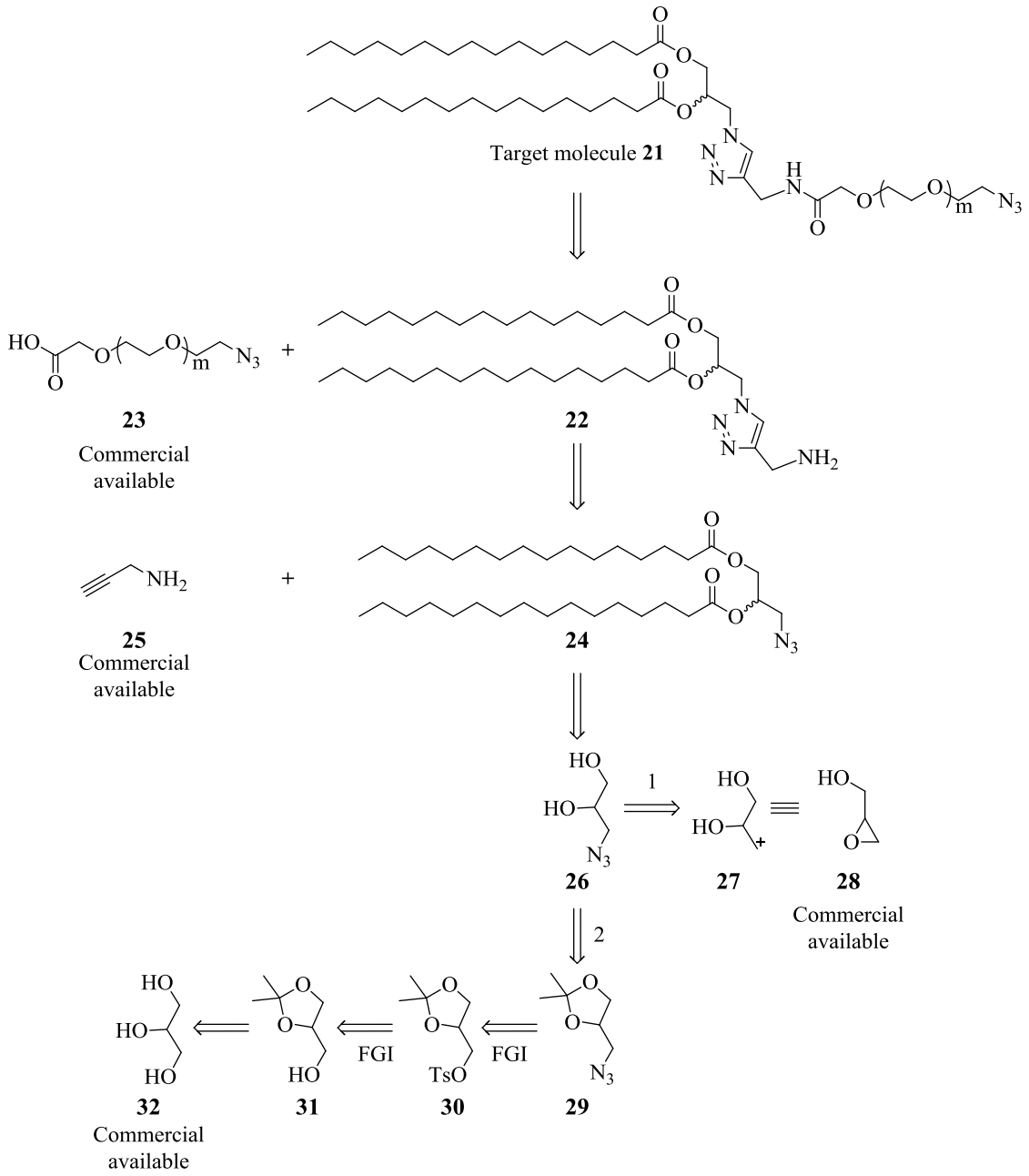

Scheme 5

Our strategy for the synthesis of the monomer **21** for lipid based NPs is presented in the retrosynthetic analysis shown in Scheme 5. We envisioned one key product in our disconnection approach: this is compound **26** which is a glycerol analog with an azide moiety. To obtain it, we tried both reaction routes; the best results were obtained using the

compound **28** as starting material - the synthetic route is presented below (Scheme 6). These reactions allowed to obtain pure product in very high overall yield (60 %).

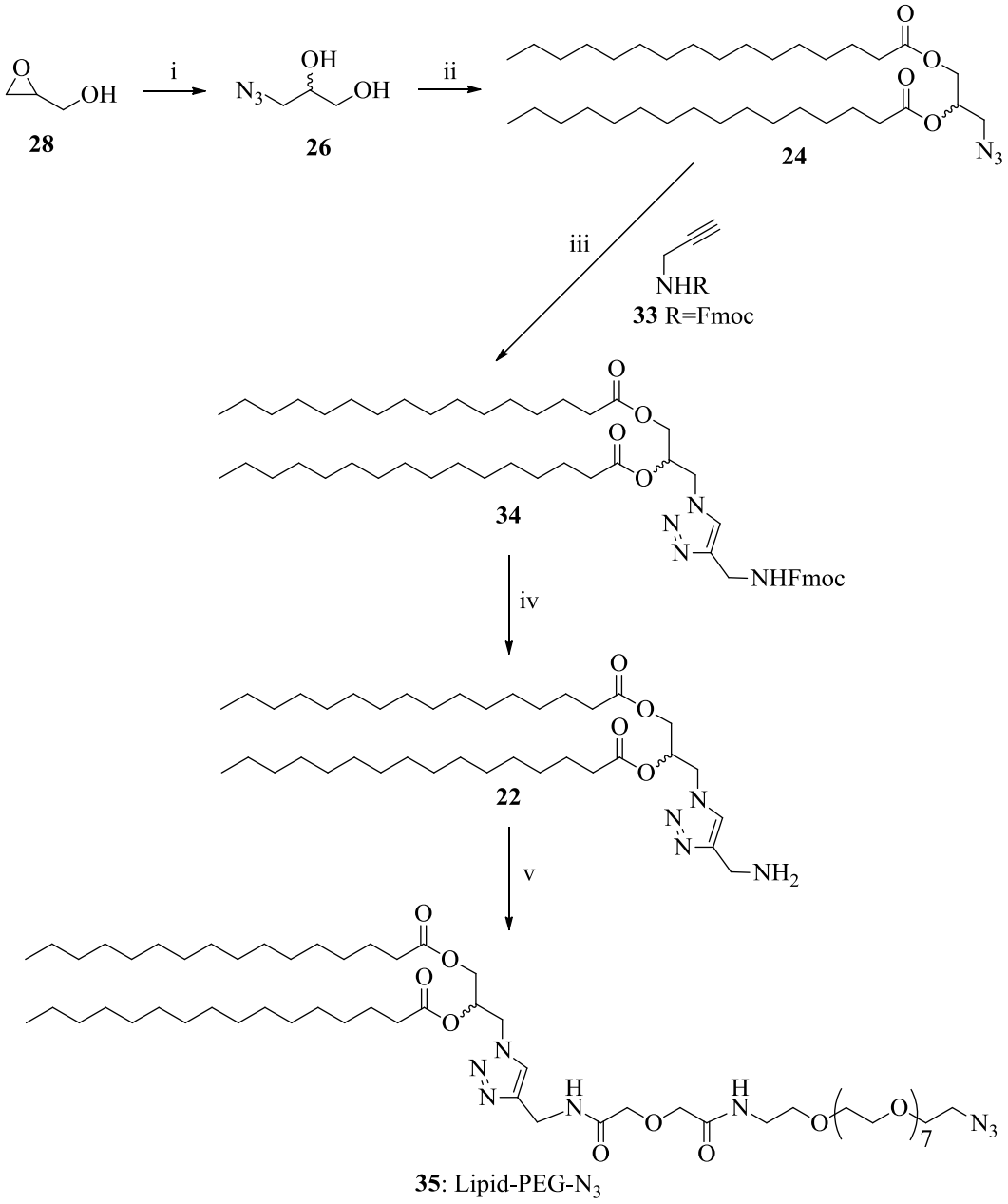

Scheme 6: Reagents and Conditions: (i) $LiBF_4$, NaN_3, t-BuOH/H_2O, reflux, 1 h; (ii) PalmitoylCl, Py, CH_2Cl_2 dry, r.t., O.N., 75 % over two steps; (iii) Cu(I), THF/H_2O, r.t., O.N., 87 %; (iv) Piperidine, DMF, r.t., 2 h; (v) TBTU, O-(2-azidoethyl)-O'-(N-diglycolyl-2-aminoethyl) heptaethyleneglycol, DIPEA, CH_2Cl_2 dry, r.t., 3 days, 92 % over two steps.

3.3. Curcumin-decorated Nanoliposomes with very high affinity for $A\beta_{1-42}$ peptide

Another possibility for the application of the beneficial effects of CUR could be the attachment of it, in a stable way and active structural conformation, on the surface of biocompatible/biodegradable and stealth nanoparticles. Such attachment (on the surface of nanoparticles), might help to increase the drug bioavailability and perhaps it will further increase the binding affinity of CUR for Aβ peptides, because of multivalency.[201-203] Among the known nanoparticles types, liposomes have many advantages for drug delivery applications, for their non-toxic and non-immunogenic, fully biodegradable and structurally versatile nature.[204]

Liposomes were first produced in the United Kingdom in 1961 by Alec D. Bangham, who was studying phospholipids and blood clotting. A liposome is a spherical vesicle, with a membrane composed of a lipidic bilayers, usually used to deliver drug or genetic material into a cell. In fact, the bilayer can fuse with other bilayers (i.e. cell membranes) delivering the liposome contents inside the target cells. Depending on the structure, there are two type of liposomes (Figure 33): A.) small unilamellar vescicles (SUV - unilamellar liposomes have a single phospholipid bilayer sphere enclosing aqueous solution) and B.) multilamellar vescicles (MLV) with an onion structure (usually unilamellar vesicles - up to 14 - will form one inside the other in diminishing size, creating a multilamellar structure of concentric phospholipid spheres, separated by layers of water).

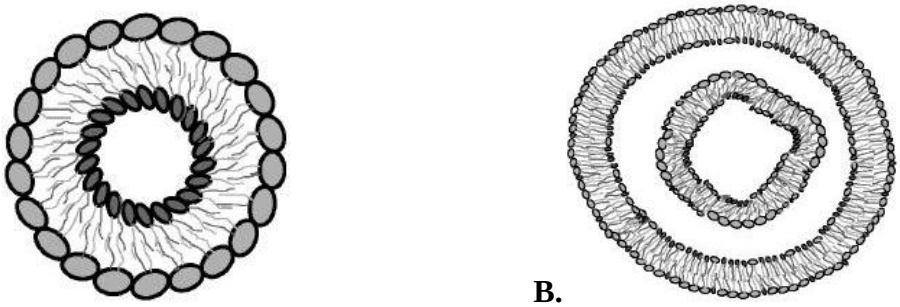

A. **B.**

Figure 33: Different types of liposome: A. Small unilamellar vescicles; B. Multilamellar vescicles.

Both the two types of liposomes are usually composed of natural phospholipids and cholesterol as stabilizing agent. So, these devices can be introduced in the body without triggering any immune rejection reaction. As a matter of facts, phospholipid bilayers are the core structure of the liposomes and the cell membrane formations. Different

approaches exist for the production of finely dispersed vescicles. In particular, they can be prepared using methods like the extrusion, the handshaking method, the sonication method, the reverse phase evaporation method and the freeze dried rehydration one.

Among them, the sonication methods are the best for the preparation of SUV. They can be divided into two techniques: probe sonication and bath ones. In particular, in the first one the sonicator tip is directly submerged into the MLV dispersion until the liposome dispersion is completely clear. This procedure is the most widely used to obtain nanosized liposomes, even if it has some disadvantages like the local overheating - that can de-esterify the lipid - or the contamination with titanium sloughing off from the tip.

Using these methods SUV are usually surrounded by a single lipid bilayer and are 25 to 150 nm in diameter. These small dimensions are very important, because in this way the liposomes could avoid to be uptaken by the cells of the reticulo endothelial system (RES) and mononuclear phagocyte system (MPS). Besides the technique used for their formation and the dimensions, the lipid composition of liposomes is also - in most cases - very important. For some bioactive compounds, the presence of net charged lipids not only prevents the spontaneous aggregation of liposomes, but also determines the effectiveness of the entrapment of the solute into the liposomal vesicles. Natural lipids - particularly those, with aliphatic chains attached to the backbone by means of ester or amide bonds (phospholipids, sphingolipids and glycolipids) - are often subject to the action of various hydrolytic (lipolytic) enzymes, when injected into the animal or human body. These enzymes cleave off acyl chains and the resulting lysolipids have destabilizing properties for the lipid layer and cause the release of the entrapped bioactive component(s) and recognition by RES. As a result, new types of vesicles - that should merely bear the name of liposomes as their components are lipids only by similarity of their properties to natural (phospho)lipids - have been elaborated. In particular further advances in liposome research had been able to allow liposomes to avoid the detection by the body's immune system . These liposomes are known as "stealth liposomes", and are constructed with PEG-lipids with the hydrophilic polymer studding the outside of the membrane. Surface modification of liposomes with PEG can be achieved in several ways: by physically adsorbing the polymer onto the surface of the vesicles, by incorporating the PEG-lipid conjugate during liposome preparation, or by covalently attaching reactive groups onto the surface of preformed liposomes. Grafting PEG onto liposomes has shown several biological and

technological advantages. First of all, the PEG chains on the liposome surface avoid the vesicle aggregation,[205] increasing the stability of formulations. Moreover, it is certain that the molecular mass of the polymer, as well as the graft density, determine the degree of surface coverage and the distance between graft sites. These properties influence the behavior of PEGylated liposomes.[206] As a matter of facts, the most evident characteristic of PEG-grafted liposomes (PEGylated-liposomes) is their circulation longevity, regardless of their surface charge or of the inclusion of a stabilizing agent such as cholesterol. This property is caused by the decrease in RES and MPS uptake and thus improves the distribution in perfused tissues. This increased blood circulation time also results in a reduced interaction with plasma proteins and cell-surface proteins.[207,208] Although other studies have found no direct evidences of this reduced interaction with plasma components.[209] There are sufficient conflicting data to warrant a reassessment of the mechanism(s) by which surface grafted PEGs improve liposome properties.[210] However, the common opinion is that PEG increases the circulation longevity of drug carriers, by reducing or preventing protein binding and/or by inhibiting cell binding/uptake.

In addition to a PEG coating, most stealth liposomes have also some sort of biological species attached as a ligand to the liposome, in order to enable binding via a specific expression on the targeted drug delivery site. These targeting ligands could be monoclonal antibodies (making an immunoliposome), vitamins, or specific antigens. Targeted liposomes can target nearly any cell type in the body and deliver drugs that would naturally be systemically delivered. Naturally toxic drugs can be much less toxic if delivered only to diseased tissues.

In the study presented below, we designed and formulated two types of nanosized liposomes, functionalized with CUR derivatives (on their surface) and evaluated their ability to bind to Aβ fibrils by Surface Plasmon Resonance (SPR). The two types of decorated liposomes were obtained either by a conventional synthetic method or by "click chemistry" technique.[211-214] When the conventional synthetic method is used (it is the conjugation of curcumin with functionalized phospholipid and the use of this lipid-conjugate for liposome formation), the planarity of the curcumin molecule is disrupted because of the introduction of a tetra-substituted carbon atom in the linker region. On the contrary, the "click chemistry" technique allowed conjugation of an appropriate curcumin

derivative, designed to preserve the planarity of the compound and opportunely functionalized for the conjugation.

3.3.1. Synthesis of lipid and curcumin derivatives for click chemistry

The details about the synthesis of all intermediate are reported in the paragraphs 3.1 and 3.2.

The compound **36**, formed by click reaction between lipid-peg-azide **35** and CUR-alkyne derivative **4** in organic solvents was synthesized according to Scheme 7. This new compound was used (as standard) for the determination of the yield of the click reaction on liposomes (liposomes bearing Lipid-PEG-N_3 **35** in their lipid bilayers reacted with curcumin-alkyne **4** under click conditions, as described below).

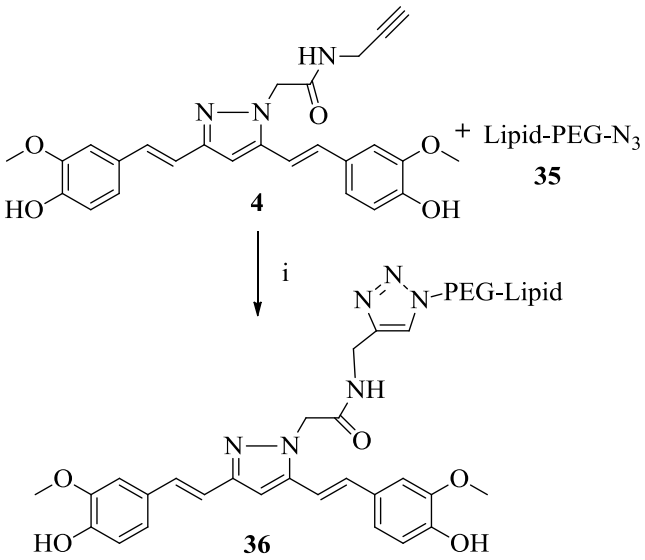

Scheme 7: ***Reagents and Conditions*****: (i) Procedure A: $CuSO_4 \cdot 5\ H_2O$, Sodium ascorbate, THF-H_2O, r.t., 87%; Procedure B: CuBr, PMDTA, Sodium ascorbate, AcCN-H_2O, r.t., 10 min, 92%.**

3.3.2. Synthesis of curcumin-phospholipid conjugates via Michael addition.

For the second preparation of curcumin-decorated nanoliposomes, a phospholipid conjugate of curcumin - 1,2-dipalmitoyl-3-(2-(1,7-bis(4-hydroxy-3-methoxyphenyl)-3,5-dioxohept-6-enylthio)ethyl phospho)-*sn*-glycerol (DPS-curcumin) **37** - was synthesized via Michael addition of 1,2-Dipalmitoyl-*sn*-Glycero-3-Phosphothioethanol (Sodium Salt)

[DPSH] to CUR,[215] as presented in synthetic Scheme 8. Some details about the synthesis and characterization of this compound are included in the Supporting Information.

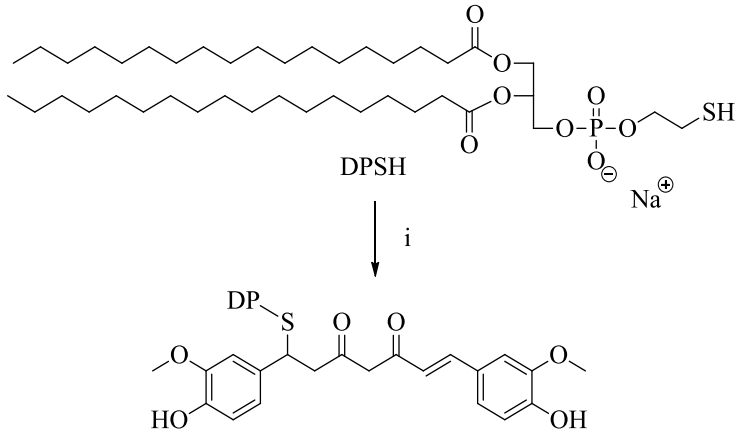

Scheme 8: ***Reagents and Conditions*****: (i) Curcumin, CH_2Cl_2, DIPEA, r.t., O.N., 75 %.**

3.3.3. Nanoliposomes preparation

3.3.3.1. *Curcumin-decorated liposomes by click chemistry*

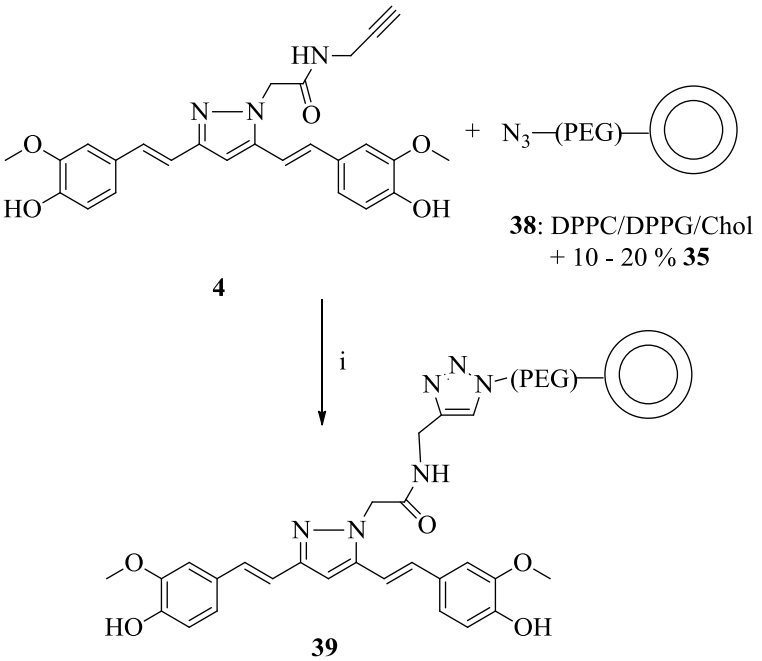

Scheme 9: ***Reagents and Conditions*****: (i) $CuSO_4 \cdot 5\ H_2O$, Sodium ascorbate, Bathophenanthrolinedisulfonate, buffer PBS 6,5 (No NaN_3), N_2, r.t., 6-8 hours.**

Liposomes, functionalized with the curcumin derivative **4** by the click chemistry method, were prepared as described in synthetic Scheme 9; this follows the method recently reported,[211,214] and, more specifically, the Huisgen 1,3-dipolar cycloaddition of azides and terminal alkynes.[212]

Here is a most detailed explanation: a dispersion of liposomes (DPPC/DPPG/Chol + 10-20 mol% Lipid-PEG-N_3 in PBS pH = 6.50) was added in an aqueous solution of bathophenanthrolinedisulfonate catalyst (28 mM), mixed with a preformed aqueous solutions of $CuSO_4$ (8 mM) and sodium ascorbate (145 mM). Then, compound **4** (0,44 mg solubilized in a small volume of DMSO) was added, and the reaction was gently stirred for 8-10 hours at 25-27^{o}C under continuous flow of N_2. Any aggregates, that may have formed during the reaction were disaggregated by gentle bath sonication (~ 2-5 min) and the resulting mixture was placed in a 10.000 MW cutoff dialysis tubing (Servapore, Serva) and dialyzed against PBS buffer overnight. The vesicle dispersion was further purified by a column chromatography (Sephadex 4B). A quantification of **36** in final liposomal dispersion **39** after liposomal click reaction was achieved by a HPLC analysis of a specific quantity of freeze-dried liposomal dispersion and an integration of the corresponding peak (see Supporting information).

3.3.3.2. *Curcumin decorated liposomes by curcumin-phospholipid conjugate incorporation*

For the preparation of SUV DPPC/Chol (2:1) liposomes incorporating 10-20% DPS-curcumin conjugate **37**, the appropriate amounts of lipids and Chol were dissolved in a chloroform/methanol (2:1 v/v) mixture. They were subsequently evaporated under vacuum, until they formed a thin lipid layer. The lipid film was treated with gas N_2 and it was subsequently connected to a vacuum pump for 12 h, in order to remove any traces of organic solvent. The lipid film was hydrated with PBS buffer (pH = 7.4) at 45°C [or a 100 mM solution of calcein, prepared in the same buffer, in case of integrity experiments]. After the complete lipid hydration and the formation of liposomes, the vesicle dispersion was placed under the microtip of a probe sonicator for 10 min, or until the liposome dispersion was completely clear. The liposome dispersions **40** rested for

annealing structural defects, at a temperature above the lipid transition temperature, for 1-2 hours.

3.3.4. Characterization of Nanoparticles

3.3.4.1. *Size, polydispersity and ζ-potential*

The size, polydispersity and ζ-potential of the liposome were determined using a NanoZeta series particle sizer and ζ-potential analyzer (Malvern). The size and polydispersity measurements were performed at 25 °C. Liposomes, prepared in 10 mM PBS, 150 mM NaCl, 1 mM EDTA, pH = 7.4, were diluted at 0.25 mM total lipid concentration. The particle size was assessed by dynamic laser light scattering with a 652 nm laser beam. The particle size and the polydispersity index were obtained from the intensity autocorrelation function of the light scattered at a fixed angle of 173° (conditions which avoid errors due to back-scattering). The ζ-potential was measured at 25 °C. Each measurement was performed on freshly prepared liposomes samples. For some of the liposome types prepared, the vesicle stability was measured when the liposomes were dispersed in the buffer (at various lipid concentrations) and stored at 4 °C, by following their size, polydispersity index and ζ-potential (which were measured by dynamic laser light scattering, as described above) for periods of 3 – 30 days.

3.3.4.2. *Liposome integrity studies*

The integrity of the vesicles, with lipid membrane compositions similar to the ones used for surface decoration by the click chemistry methodology, was evaluated in order to establish the optimum conditions for the reaction. The integrity of DPPC/DPPG/Chol liposomes was evaluated under the conditions and in presence of the solutions required for the click reaction to take place. So, the latency (%) of calcein in the vesicles was measured at various time points, during the incubation of liposomes at 25 °C or 37 °C, in presence of reaction media. Lipid/reaction compound ratios of 1:1 mole/mole and 1:2 mole/mole were used. The lipid concentration in the incubated dispersions was always constant at 1 mM, and calcein was initially encapsulated in the vesicles at a quenched concentration

(100 mM). For % calcein latency calculation,[216] some samples from the liposomes (20 μL) were diluted with 4mL buffer, pH = 7.40, and the fluorescence intensity (*F*) was measured (EM 470 nm, EX 520 nm), before and after the addition of Triton X-100 at a final concentration of 1 % v/v (that ensures the liposome disruption and the release of all encapsulated dye). The percent latency (% latency) was calculated from the equation 1:

$$\% \text{ Latency} = \frac{1.1 \cdot (F_{AT} - F_{BT})}{1.1 \cdot F_{AT}} \cdot 100 \quad \textbf{Equation 1}$$

where: F_{BT} and F_{AT} are calcein fluorescence intensities, respectively before and after the addition of Triton X-100.

After establishing the conditions at which the liposomes remain stable, and carrying out the click chemistry reaction for the decoration of the vesicle surface as described above, the vesicles produced were studied for their integrity, during an incubation in absence and in presence of serum proteins. So, the liposomes that encapsulated calcein were prepared as described above and subjected to the click reaction to allow the CUR's attachment to their surface. They were subsequently incubated in absence or presence of serum proteins (80 % v/v, FCS) and their integrity was evaluated during their incubation at 37 °C for 24 or 48 h.

3.3.5. Binding of liposomes to $A\beta_{1-42}$, investigated by Surface Plasmon Resonance

3.3.5.1. *Preparation of $A\beta_{1-42}$ in different aggregation forms*

A depsi-$A\beta_{1-42}$ peptide was synthesized at first, as previously described.[217,218] This depsi-peptide is much more soluble than the native peptide. It also has a much lower propensity to aggregate, so it prevents the spontaneous formation of 'seeds' in solution. The native $A\beta_{1-42}$ peptide was then obtained from the depsi-peptide, by a "switching" procedure, involving a change in the pH.[217-219] The $A\beta_{1-42}$ peptide solution obtained immediately after the switching is seed-free, as shown in carefully conducted previous works. [218,219] The $A\beta_{1-42}$ peptide obtained with this procedure is therefore in its very initial state and, to simplificate, it will be referred to here as "monomers".

To prepare $A\beta_{1-42}$ fibrils, the switched peptide solution was diluted with water to 100 μM, acidified to pH = 2.0 with 1 M HCl. Then it was left to incubate for 24 hours at 37 °C.[220] Kinetic studies with circular dicroism and thioflavin-T clearly indicated that these conditions enable to reach the maximal level of β-sheet structures, whereas the presence of amyloid fibrils was directly confirmed by the atomic force microscopy (AFM).[219]

3.3.5.2.*Surface Plasmon Resonance analysis*

For these binding studies with Surface Plasmon Resonance (SPR) technique, we used the ProteOn XPR36 (Biorad) apparatus, which has six parallel flow channels that can be used to immobilize uniformly some strips of six "ligands" on the sensor surface. $A\beta_{1-42}$ "monomers" or fibrils were immobilized in two of these parallel-flow channels of a GLC sensor chip (Biorad), using amine-coupling chemistry. Briefly, after the surface activation, the peptide solutions (10 μM in acetate buffer pH = 4.0) were injected for 5 min at a flow rate of 30 mL/min, and the remaining activated groups were blocked with ethanolamine, pH = 8.0. The bovine serum albumin (BSA) was also immobilized in another parallel flow channel, as a reference protein. The final immobilization levels were similar, about 2500 Resonance Units (1 RU = 1 pg protein/mm^2). A fourth surface was prepared, using the same immobilization procedure, but without addition of the peptide ("empty" reference surface).

The fluidic system of Proteon XPR36 can automatically rotate 90°, so that up to six different "analytes" (e.g. different liposomes preparations, or different concentrations of the same preparation) could be injected simultaneously, over all the different immobilized molecules.[221] Some preliminary injections were done, in order to check for the binding features of the immobilized $A\beta_{1-42}$ species. Then we injected the anti-Aβ antibody 4G8 (Covance) which, as expected, bound both to Aβ fibrils and to "monomers" (not shown), whereas Congo-Red - a dye specifically recognizing β-sheet-containing species - only bound to Aβ fibrils but not to "monomers" (not shown).

The ProteOn analysis software (BioRad) was used for the fitting of sensograms, to obtain the association and the dissociation rate constants of the binding (k_{on} and k_{off}) and the corresponding K_D value. The simplest 1:1 interaction model (Langmuir model) is used at first.

3.3.6. Results

3.3.6.1. *Preparation of curcumin decorated nanoliposomes by click chemistry*

Integrity of liposomes during the click reaction

Before using preformed liposomes for the click chemistry reaction, their integrity during the incubation in presence of the required chemicals was investigated. As seen in Figure 34, when the incubation was done at 37 °C (Figure 34 A), the liposomes were not stable, since the liposome encapsulated dye (calcein) leaked out of the vesicles at significant amounts, even during the first 2-3 hours of incubation, while approximately 50 % of the vesicle-encapsulated dye was released after 6 h of incubation. This result suggests that the click reaction should not be carried out on liposomes (with this lipid composition) at 37 °C.

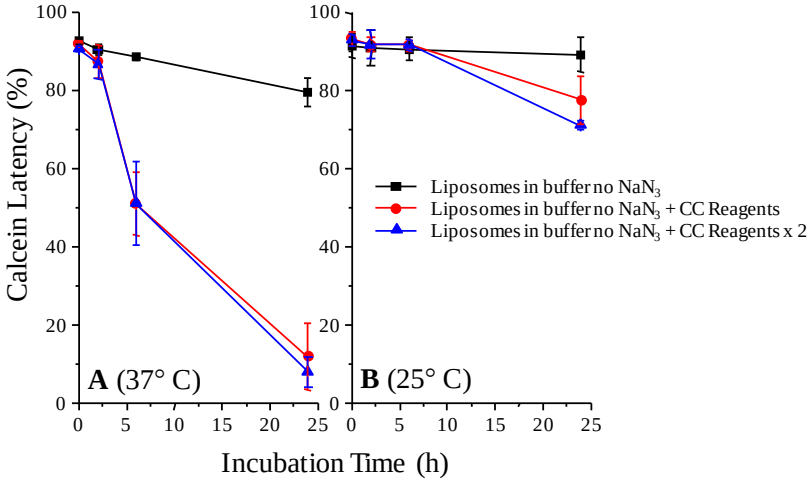

Figure 34: Integrity of liposomes (DPPC/DPPC/Chol 8:2:5), expressed as latency of vesicle encapsulated calcein, during incubation in PBS buffer (control) or in presence of the reagents required for the click chemistry (CC) reaction to take place. Vesicle integrity was studied in presence of the normal quantities of reagents required, as mentioned analytically in the Methods section or in presence of double amounts, at 37 °C (A) or 25°C (B). Each data point is the mean of at least 3 different experiments and the bar is the SD of the mean.

On the contrary, at 25 °C the liposomes are stable for the first 6 hours of incubation, in presence of the reactants required for the click reaction to take place (Figure 34 B) and also in presence of double amounts of reactants. Even after 24 h incubation at room temperature the vesicle are more or less stable, since the percent of dye released is very low. This

proves that it is important to carry out the reaction at room temperature and not at 37 °C, especially when valuable drug molecules are entrapped in the vesicles, before the click reaction takes place.

*Confirmation of compound identity -Yield of Click chemistry reaction- liposomes **39***

A final confirmation that the click reaction is indeed taking place and liposomes **39** are forming was provided by the identification of the presence of compound **36** in the liposome dispersion after the liposomal breakage and the HPLC analysis of the resulting mixture (for more details about HPLC and ESI-MS graphs, see Supporting information). The yield of the click reaction was determined by quantifying the amount of product **36** in weighted quantities of freeze dried liposomal dispersions, and proved to range between 75 and 95 percent.

Table 3: Physicochemical characteristics of the various liposome types prepared, depending on the percent (theoretical) of curcumin moiety present on the vesicle surface. Vesicle mean diameter (in nm), polydispersity index and ζ-potential (mV) are measured, as described in the methods section and values reported are the mean values from at least 5 measurements of 3 different preparations.

Liposome	**Curcumin moiety (mol%)**	**Mean diameter (nm)**	**Polydispersity Index (PI)**	**ζ-Potential (mV)**
39 - CTRL	0	52.8 ± 5.5	0.097	-7.6 ± 1.7
39	5	130.9 ± 1.1	0.108	-24.30 ± 0.42
39	10	168.9 ± 1.3	0.164	-20.3 ± 1.4
40 -CTRL	0	63.1 ± 6.2	0.195	-6.44 ± 0.49
40	1	135.30 ± 0.70	0.209	-
40	5	180 ± 13	0.193	-14.5 ± 2.4
40	10	207.2 ± 8.0	0.255	-10.5 ± 1.2

3.3.6.2.*Physicochemical properties of liposomes*

The mean diameters and ζ-potential values measured for the various types of nanoliposomes prepared are presented in Table 3. As seen, the vesicle size increases as a function of the percent of curcumin decoration on the vesicle surface, for both liposomes

39 and liposomes **40**. In all the cases, the polydispersity indices measured were low (ranging from 0.097 – 0.255), indicating that the nanoliposomes prepared have very narrow size distributions. The surface charge of CUR decorated vesicles is negative in all the cases, indicating that the curcumin on the surface influences the ζ-potential of the vesicles. This influence is normal, if considering that CUR has two phenol groups which are partly ionized at pH = 7.40.

3.3.6.3.*Vesicle size stability and Integrity studies*

The stability (mean diameter and ζ-potential values) of two different preparations of liposomes **39**, during storage at 4 ^{o}C, for a period of 15 days is presented in Figure 35.

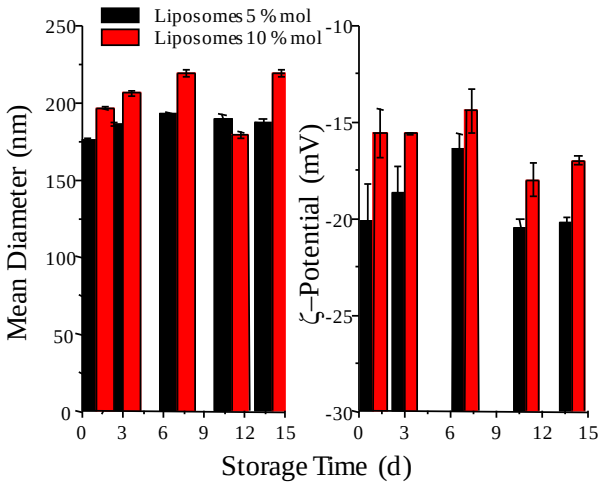

Figure 35: Size (d-hydrodynamic diameter, nm) and ζ-Potential values of two different vesicle batches of liposomes 39 (decorated with 5 mol% or 10mol% curcumin derivative), dispersed in PBS buffer at a lipid concentration of 10 – 15 mg/mL, during storage at 4 °C. Each value is the mean of at least 5 different measurements and bars are the SD values of each mean.

As seen, both liposome preparations are very stable for the storage period, in terms of size distribution and surface charge value. No signs of liposome aggregation was evident when the liposomes were stored as dispersed at the specific lipid concentrations used herein (up to 5 mg/mL). Liposomes **40** were also found to be stable under identical conditions, for more than 20 days of storage (results not shown).

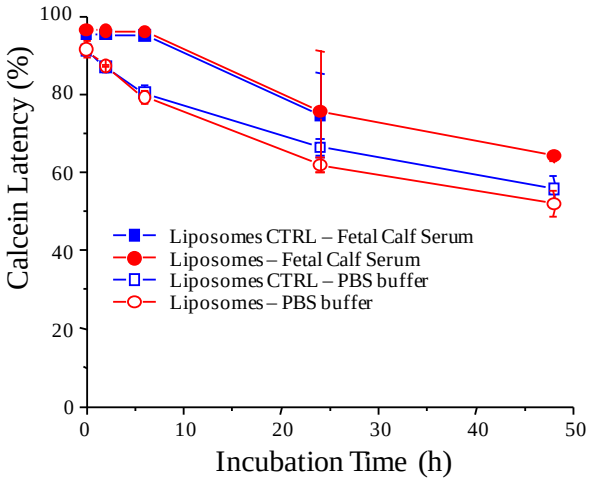

Figure 36: Integrity of liposomes 39 (A) and their corresponding control liposomes - CTRL - (with no "clicked curcumin" on their surface), during the incubation in buffer or FCS (80% v/v) at 37 °C. Each data point is the mean of at least 3 different experiments and the bar is the SD of the mean.

The integrity of the selected type of liposomes **39**, during the incubation in presence of serum proteins and PBS, is presented in Figure 36. In both cases, the integrity of **control** liposomes (**CTRL** - with the same lipid composition) are studied in parallel, while both types of liposomal dispersions (**CTRL** and curcumin-decorated) are also incubated in presence of plain buffer for comparison. As seen, the liposomes are equally stable when compared with the relevant control liposomes, during the incubation in buffer, and in the presence of FCS, for a period of at least 24 h. This indicated that these liposomes possess the required stability for *in vivo* applications.

In the case of liposomes **39**, the control liposomes were actually the same liposomes before the click reaction step was carried out. This result proves that under specific conditions, liposomes, which are pre-formed to encapsulate active drugs or other types of bioactive molecules, can be subjected to click reaction and, after appropriate purification, they can be used for in vivo applications.

3.3.6.4.*Binding of functionalized liposomes to Aβ$_{1-42}$*

Before using compound **4** for the preparation of curcumin-decorated liposomes **39**, its affinity for Aβ$_{1-42}$ fibrils was confirmed by SPR studies. The results of this initial confirmatory experiment are presented in Figure 37.

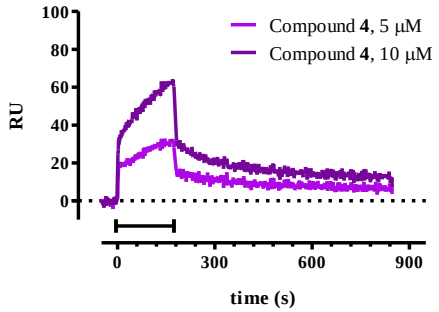

Figure 37: SPR studies of Compound 4 for $A\beta_{1-42}$ fibrils, immobilized on the sensor chip. The figure shows representative sensograms (resonance units, RU, *versus* time) obtained by simultaneous injection of two concentrations of the compound, for 3 min (as indicated) over sensor chip surfaces. The reported sensograms are indicative of a specific binding to $A\beta_{1-42}$, since they were obtained after subtraction of the signal detected in the reference surface, thus correcting for binding-independent responses, such as bulk effects due to buffer exchanges or drift effects.

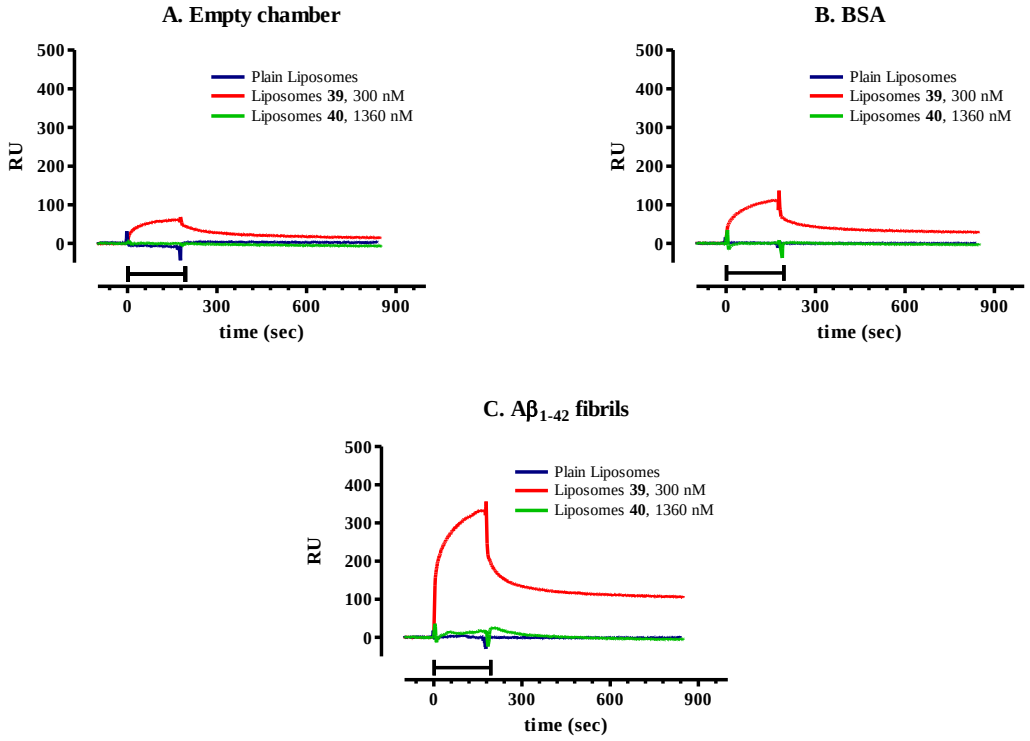

Figure 38: SPR studies comparing the binding properties of liposomes 39, liposomes 40 and plain liposomes when injected onto sensor surfaces immobilizing bovine serum albumin (BSA) (B.) or $A\beta_{1-42}$ fibrils (C.), at similar densities; panel A. refers to the signal measured in the reference, empty, surface. The figure shows representative sensograms (resonance units, RU, versus time) obtained by simultaneous injection of the different liposomes, for 3 min (as indicated) over all the sensor chip surfaces . Liposomes 39 (red) were injected at a concentration corresponding to 300 nM of exposed curcumin-derivative; liposomes 40 (green), as well as plain liposomes were injected at a concentration corresponding to 1360 nM of exposed curcumin.

Liposomes **39**, **40** and plain (not functionalized) liposomes were flowed over parallel flow channels of the same sensor chip, immobilizing $A\beta_{1-42}$ fibrils, BSA (to check the specificity of the interaction). They were also employed over an empty surface.

No binding was detected, when using plain liposomes and liposomes **40** on the different sensor surfaces, even at highest CUR concentrations (green lines, Figure. 38). On the contrary, liposomes **39** interacted with immobilized $A\beta_{1-42}$ species, in particular with $A\beta_{1-42}$ fibrils (Figure 38 C). A lower binding was observed on BSA (Figure 38 B) and an even lower binding was detected on empty surface (Figure 38 A).

Figure 39 shows the concentration-dependence of the specific binding of liposomes **39** to the immobilized $A\beta_{1-42}$ fibrils (i.e. after correction of the signal measured in the reference surface). In particular, for these experiments, we used liposomes with a different density of functionalization (5 or 10 %); we injected three concentrations, so we obtained 100, 300 and 600 nM of exposed CUR-derivative.

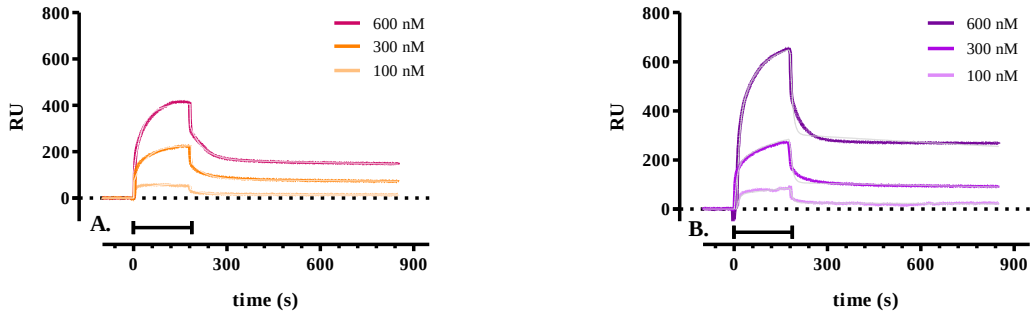

Figure 39: Concentration-dependent binding of liposomes 39 to $A\beta_{1-42}$ fibrils immobilized on the SPR sensor chip. For this session, liposomes with two different densities of functionalization with the compound 4 (A. = 5% and B. = 10%) were used. Liposomes were injected at concentrations corresponding to 100, 300 and 600 nM of exposed curcumin-derivative. The figure shows representative sensograms (resonance units, RU, versus time) obtained by simultaneous injection of the liposomes, for 3 min over sensor chip surfaces (as indicated). The reported sensograms are indicative of a specific binding to $A\beta_{1-42}$, since they were obtained after subtraction of the signal detected in the reference surface, thus correcting for binding-independent responses, such as bulk effects due to buffer exchanges or drift effects. The fitting of these sensograms, with a "two-sites" model, are shown in white.

The resulting sensograms, shown in Figure 39, could not be fitted by a simple 1:1 interaction model (Langmuir equation), but require more complex interaction models. This is clearly evident by the dissociation phase, which cannot be fitted by a mono-exponential curve (as expected for simple interactions). It indicates that there are at least two binding components with two different rate constants, one faster and one slower. The fitting of

these sensograms with a "two-site" model is represented as white lanes in Figure 39. It allowed to estimate the binding constants of the two putative components, highlighting, in particular, the presence of a component representing about 40 % of the binding characterized by a very low dissociation rate constants ($< 3x10^{-4}$ s^{-1}, pseudo-irreversible binding). The corresponding K_D values of the exposed CUR-derivative was calculated to be in the low nM range (2-10 nM). It is important to underline that the sensograms obtained with the different concentrations could not be globally fitted; it suggests that even the binding of this high affinity component is complex and likely involve avidity effects.[222]

3.3.7. Discussion

CUR-decorated liposomes were prepared and studied for their integrity, stability and binding affinity to $A\beta_{1-42}$ fibrils. For the preparation of curcumin decorated vesicles **39**, a click chemistry method was performed using appropriate CUR alkyne derivative **4** and azido containing lipid. Some initial vesicle integrity experiments revealed that the click chemistry reaction should be carried out at room temperature (Figure 34 B), since at 37 °C the liposome integrity is highly affected (Fig 34 A) by the reaction media required for the click to occur.[212] Of course, this is the case of the specific liposomes (with lipid composition of DPPC/DPPG/Chol 8:2:5 mol/mol/mol) evaluated herein. Perhaps, other lipid compositions may be more or less stable; in this case, it would be required the use of milder conditions for click attachment[223] (in order to preserve the vesicle integrity during the reaction performed to decorate their surface). For the construction of liposomes as negative controls, a second method was used for the attachment of CUR on the surface of vesicles (liposomes **40**). In this case the planar structure of CUR, required for its activity,[136] is disrupted.

Both this techniques we used for the formation of CUR-decorated NPs were successful. They allowed to prepare nanosized liposomes (Table 3) with the appropriate stability for *in vivo* applications (Figures 34, 36) and high stability during storage (Figure 35). As the amount of CUR molecules attached to the vesicle surface increases, the produced vesicles (by both techniques evaluated) demonstrated an increase in mean diameter (as anticipated for the CUR coating). However, the vesicle population was still homogeneous, as judged by the low polydispersity indices of the dispersions (Table 3).

SPR binding results (Figure 38) show that the liposomes (**40**), on which CUR was attached without preservation of its structural planarity, do not show any binding affinity to the immobilized $A\beta_{1-42}$ fibrils. On the other hand, the vesicles exposing a CUR derivative maintaining the planarity showed a very high binding. This result proves that this specific structural characteristic is indeed required for CUR binding to the fibrils. Furthermore, the current results enhance the opinion that CUR predominantly exists in the enol form during the binding to Aβ aggregates and that the enolization of CUR is crucial for binding to the Aβ aggregates.[224]

In more details, the CUR derivative **4** showed a clear binding to immobilized $A\beta_{1-42}$ fibrils, with an estimated K_D value of 7 μM. In particular, a significant amount of binding to fibrils dissociates very slowly, indicating a persistent interaction.

It is interesting that the affinity of the CUR derivative - exposed on liposomes **39** – for $A\beta_{1-42}$ fibrils (2-10 nM) was much higher than the affinity of a corresponding compound not attached to liposomes. We suggest the involvement of multivalent interactions (i.e. different molecules of CUR derivative on the same liposome) contribute to the binding to the immobilized $A\beta_{1-42}$ fibrils. In fact, it has been previously shown that a multivalent ligand (dendrimer[202], nanoparticles[203]) has a binding affinity for its target, which can greatly exceed, even by 2-3 orders of magnitude, the binding affinity of the same ligand, if monovalent. This increase of affinity was caused, in particular, by a decrease of the dissociation rate constants; it approached those of a pseudo-irreversible binding, and the same finding was actually found with our liposomes decorated with the CUR derivatives. The binding of the decorated liposomes for BSA was much lower and this is consistent with the lack of binding of the CUR derivative for this plasmatic protein.

These data indicate that the decoration of liposomes with this CUR derivative provide these NPs with a specific and high affinity binding for $A\beta_{1-42}$ fibrils. This is potentially very useful in the attempt of targeting these AD pathogenic markers for diagnostic and/or therapeutic purposes.

3.4. Preliminary studies on functionalization of SLNs with curcumin derivative

For a decade, trials are being made to utilize solid lipid nanoparticles (SLN) as a drug delivery system alternative to the colloidal one - such as lipid emulsions, liposomes and

polymeric nanoparticles. SLNs consist of spherical solid lipid particles in the nanometer range, which are dispersed in water or in aqueous surfactant solution. They are generally made up of solid hydrophobic (i.e. lipids solid at room temperature and also at body temperature) and stabilized by a surfactant coating. By definition, the lipids can be highly purified triglycerides, complex glyceride mixtures or even waxes.[225] Recently, SLN based on para-acyl-calix[4]arenes have been prepared and studied.[226,227] The carrier system SLN has been characterized and reviewed intensively, thanks to the work of various research groups.[228-230] The main features of SLNs, with regard to *in vivo* application, are the excellent physical stability, the protection of incorporated labile drugs from degradation, the controlled drug release (fast or sustained) - depending on the incorporation model, the good tolerability and the site-specific targeting. Potential disadvantages, such as insufficient loading capacity, drug expulsion after polymorphic transition during storage and relatively high water content of the dispersions (70-99.9%), have been observed. The drug loading capacity of conventional SLN is limited (generally up to approximately 25% with regard to the lipid matrix, up to 50% for special actives such as Ubidecarenone) by the solubility of drug in the lipid melt, the structure of the lipid matrix and the polymorphic state of the lipid matrix.[229,231-237]

Therefore, the use of more complex lipids (mono-, di-, triglycerides, different chain lengths) is more sensible for higher drug loading.

SLNs combine the advantages of polymeric nanoparticles, fat emulsions and liposomes and simultaneously avoid their disadvantages.[238] The advantages of SLNs include the following:

- The nanoparticles and the SLNs, particularly those in the range of 120–200 nm, are not taken up readily by the cells of the RES (Reticulo Endothelial System) and so bypass liver and spleen filtration.[229]
- The controlled release of the incorporated drug can be achieved for up to several weeks. Further, by coating with or attaching ligands to SLNs, there is an increased scope of drug targeting.[239]
- SLN formulations, stable up to three years, have been developed. This is very important for the other colloidal carrier systems.[240]
- The high drug payload.

- The excellent reproducibility, with a cost effective high pressure homogenization method, as the preparation procedure.[238]
- The feasibility of incorporating both hydrophilic and hydrophobic drugs.[241]
- The carrier lipids are biodegradable and hence safe.[242,243]
- The avoidance of organic solvents.
- The feasible large scale production and sterilization.[229]

Table 4: Literature survey of methods of preparing SLNs of different drugs and the resulting particle size distribution and surfactant used for preparation of the SLNs.

Drug	**Lipid matrix**	**Preparation method**	**Mean diameter (nm)**	**Cosurfactant**
Apolipoprotein E	Dynasan 114	HH	186 245	Polysorbate Poloxamer
Ascorbil palmitate	Witepsol E 85	HPH	228	Tegocare
Clobetasol propionate	Monostearin	SD	143	PVA
Clozapine	Dynasan 114	HH	150	Poloxamer 188 Epikuron 200
Clozapine	Dynasan 116	HH	163.3	Poloxamer 188
Clozapine	Tristearin	HH	96.7	Poloxamer
Diazepam	Acidan N 12	μE	70	Epikuron 200
Diazepam	Glyceryl behanate	μE	86.0	Epikeron 200
Diminazine	Stearic acid	HH	78.5	Polysorbate 80
Doxorubicin	Stearic acid	μE	80	Epikuron 200
Mifepristone	Glyceryl monostearate	m-HSH	106	Tween 80, glycerol
***trans*-retinoic acid**	Tricaprin	MH	233-487	Tween 80
Vitamin A	Glyceryl Behanate	HPH	300-500	Hudroxypropyl distarch

Many different approaches exist for the production of finely dispersed SLN, with all the advantages presented above. They have also scaling up possibility, which is a prerequisite for the introduction of a product to the market. In particular, they can be prepared by methods like the microemulsification (μE), the solidification, the hot

homogenization (HH), the modified high shear homogenization (m-HSH), the ultrasound solvent diffusion (USD), the solvent injection, the solvent diffusion (SD), the melt homogenization (MH), and the high pressure homogenization (HPH) techniques.

Among them, one of the most used is the production of SLN via microemulsions technique. It was developed and optimized by Gasco's group in Turin.[244-248] First, a warm microemulsion is prepared by stirring - containing typically ~10% molten solid lipid, 15% surfactant and up to 10% cosurfactant. This warm microemulsion is then dispersed under stirring in excess of cold water (typical ratio ~1:50), using an especially developed thermostated syringe. The excess of water is removed either by ultra-filtration or by lyophilisation, in order to increase the particle concentration.

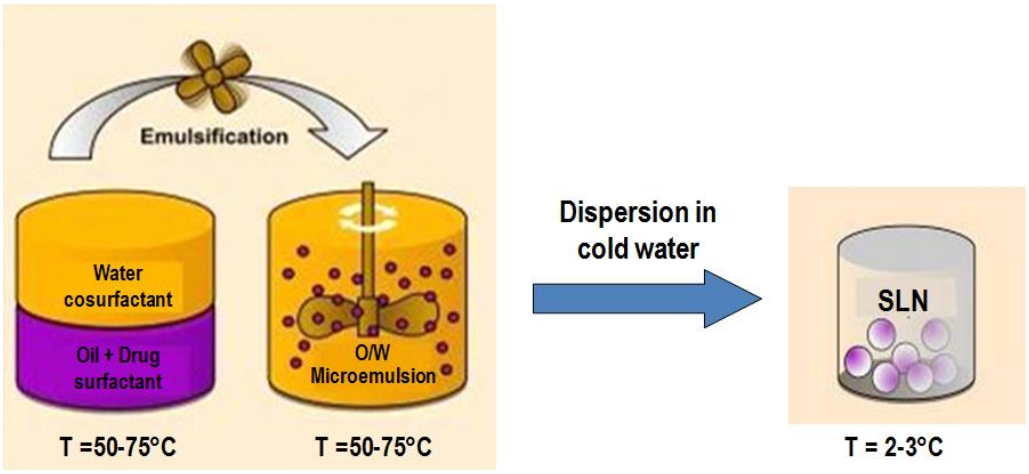

Figure 40: Preparation of Solid Lipid Nanoparticles (SLN) by Microemulsion procedure.

The effects of experimental factors - such as the microemulsion composition, the dispersing device, the temperature and the lyophilisation - on the size and the structure of the obtained SLNs have been studied intensively. It has to be critically remarked, that the removal of excess of water from the prepared SLNs dispersion is a difficult task, regarding their particle size. Also, high concentrations of surfactants and co-surfactants (e.g. butanol) are necessary for the formulating purposes, even if they are less desirable for the regulatory purposes and application.

Recently, a new method, based on the solvent emulsification-evaporation for the preparation of SLNs loaded with hydrophilic drugs, has been introduced to the scientific community.[246] Here, the hydrophilic drug is encapsulated-along with a stabilizer, to

prevent drug partitioning to the external water phase, during solvent evaporation in the internal water phase of a w/o/w double emulsion.

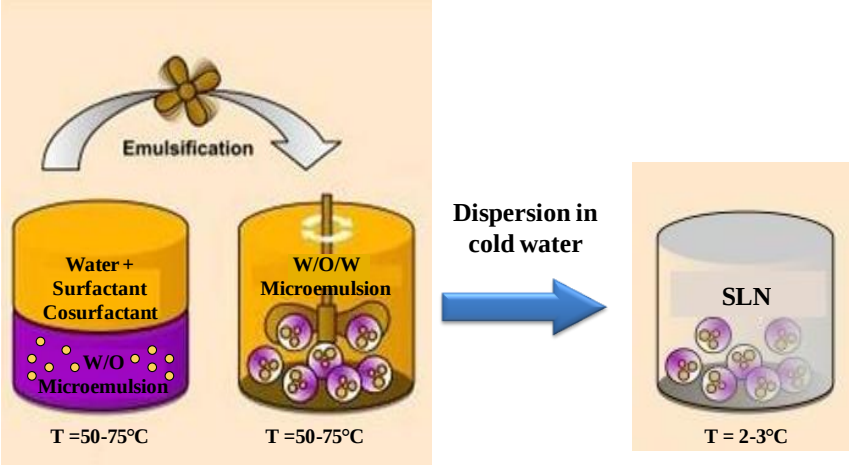

Figure 41: Preparation of Solid Lipid Nanoparticles (SLN) by w/o/w double microemulsion.

In the study presented below, we designed and formulated different SLNs dispersions, using o/w microemulsion, in order to obtain new clickable NPs. After these preparations, we set up a method to link our CUR derivative **4** on them, achieving Aβ ligand functionalized SLNs.

3.4.1. Development of HPLC-UV coupled method for SLN characterization.

A specific HPLC-UV method was studied and developed for the compound **35** (Lipid-PEG-N_3) and the compound **36** (the product of click reaction), in order to evaluate and quantify the amount of different lipids and compounds inerted or linked on SLN.

The compound **36** was dissolved in Chloroform/Methanol 60:40 v/v, the UV spectrum was acquired in the range 200-700 nm and two maxima were observed at about 210 e 330 nm.

At the beginning it was analyzed on an amino phase column (Zorbax NH_2, 4,6 x 250 mm, 5 μm) with Acetonitrile/Methanol(70:30 v/v)/$NH_4H_2PO_4$(10 mM pH = 4,8) 92:8 v/v mobile phase. The compound eluted at about 8 minutes, showing an area/concentration proportionality. On the basis of the very low absorbance observed, it was supposed the micelle formation and the necessity to work in completely organic conditions.

On a Zorbax Eclipse XDB-C8 analytical column (250 x 4,6 mm, 5 μm) with Acetonitrile/2-Propanol 60:40 v/v as mobile phase, a significant peak was eluted at a early retention time. Such an early retention time was improved, decreasing the propanol percentage but the peak shape was worse.

As matter of facts, in a quantitative HPLC analysis the shape of a peak is very important. To enhance it some runs were executed on other columns (Zorbax SB-C18, Tracer Extrasil CN), using Acetonitrile/2-Propanol or Acetonitrile/Methanol as mobile phases in different proportions, but it wasn't obtained any good result.

Some promising results were obtained on the Zorbax Eclipse XDB-C8 column, using Acetonitrile/Methanol as mobile phase. It revealed the presence of a second interfering peak, probably a structural isomer not revealed by NMR and mass spectra analysis. One peak was obtained only with 2-Propanol as organic modifier in the mobile phase. Trial runs were executed using Acetonitrile/Methanol/2-Propanol in different volume percentages, sorting in the 80:15:5 as the best eluent composition. In these conditions the peak shape was good with an acceptable asymmetry. The retention time was about 12.5 minutes. After the set-up of the analysis, a solution of the compound in the same eluent was scanned in the 200-700 nm range to be sure that this eluent doesn't interfere in the UV spectra; also in this solution the two maxima were observed at about 210 e 330 nm

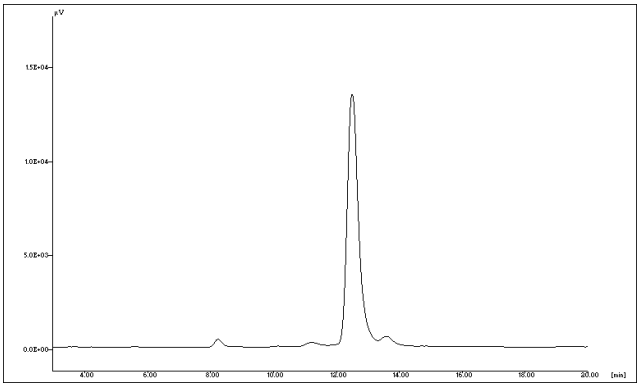

Figure 42: HPLC profile for compound 36 at 330 nm.

The same analysis was set up for compound **35**, but UV spectrum showed just a maximum at about 210 nm. Basing on this information, it was eluted in the same analytical conditions of compound **36** with a retention time of about 20 minutes. A calibration curve was prepared in the 6.05-60.5 μg/mL range.

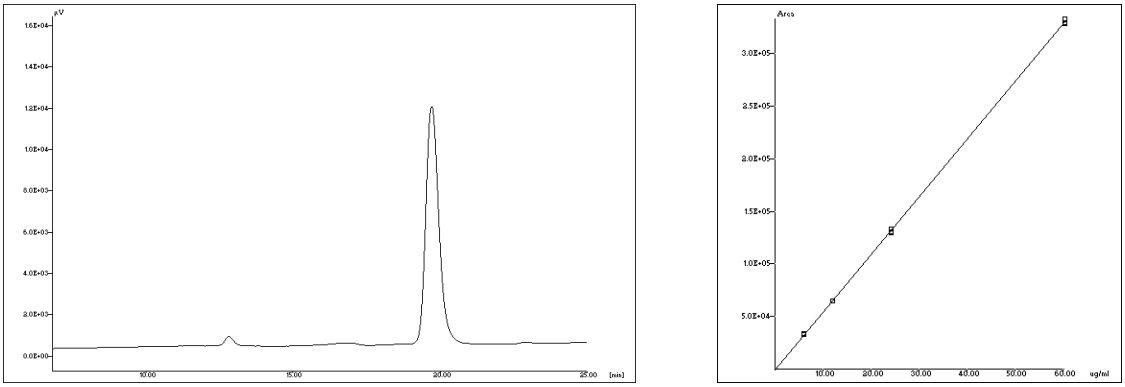

Figure 43: HPLC profile and calibration curve (r^2 = 0.99993) for lipid 35 at 210 nm.

3.4.2. Incorporation of lipid-PEG-N_3 35 into SLN

In order to incorporate Lipid-PEG-N_3 **35** into SLNs, different Stearic acid SLNs were prepared using the O/W warm microemulsion technique, substituting different molar percentage soybean phosphatidylcholine (PC) with compound **35**. We prepared the microemulsion starting from a mixture of solid stearic acid (SA), natural PC, surfactant and Lipid-PEG-N_3 in the exact ratios covered by different patents. After putting them together, we warmed the mixture at more than 70 °C and dispersed it in cold ultrapure water at different dispersion ratios. So, we obtained different formulations of Lipid-PEG-N_3 containing SLN **41** (Scheme 10 and Table 5).

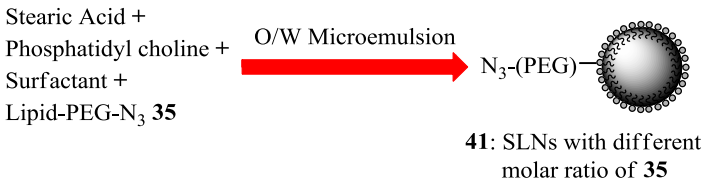

Scheme 10

Table 5: Different Lipid-PEG-N_3 containing SLN 41.

Formulation	**Lipid 35 (%mol PC)**	**Dispersion ratio in cold water**
AZD-A1-1	2.5	1:10
AZD-A1-2	5	1:10
AZD-A1-3	7.5	1:5

A HPLC-UV analysis was performed after the dispersion in cold ultrapure water. A complete recovery of Lipid-PEG-N_3 **35** was observed; it indicates a good stability (temperature) of the compound during the preparation process. We also carried out some structural studies on SLNs **41**. In particular, they were characterized in terms of average diameter, size distribution, lipid composition and incorporation efficiency (Table 6). After the preparation process, we achieved the purification of SLNs dispersion with tangential ultrafiltration; this process allowed us to remove compound **35** not inserted inside the SLNs and also to evaluate its incorporation into NPs. After tangential ultrafiltration, we can assume that all the free constituents of SLNs have been removed and that the dispersion is formed by the nanodevices. So we analyzed only the compounds which form the NPs using the HPLC-UV methods. We observed a reduction of the quantity of synthetic Lipid-PEG-N_3 in SLNs dispersion, as expected for its amphipatic nature (Table 6). In fact, this reduction is similar to the entity of the decrease usually find for PC; it happens because their behavior in aqueous environment is similar too. The same outcomes were obtained for all the formulations (not shown).

Table 6: SLN characterization after microemulsion dispersion in water and tangential ultrafiltration.

Sample	**Mean diameter (nm)**	**PI**	**Lipid 35 (mg/mL)**	**PC (mg/mL)**	**Cosurfactant (mg/mL)**	**Lipid matrix (mg/mL)**
AZD-A1-1 recovery	36.5	0.198	0.20 (100%)	4.44 (97%)	15.93 (95%)	8.29 (95%)
After purification	41.5	0.188	0.134 (67%)	3.37 (75%)	4.58	7.87 (95%)

To confirm these promising results, some NMR analysis were performed on different samples of SLN dispersions. These studies were carried out in different aqueous and organic environment, to test both the structural properties and the composition of SLNs. From the analytical point of view, we worked in $CDCl_3/CD_3OD$ 1:1 solution, avoiding the formation of new aggregates to be sure that all the NPs were destroyed and all the components in the sample solubilized. After some quantification NMR experiments we

confirmed the presence of Lipid-PEG-N_3 **35** into the SLN dispersions and also the results previously obtained by HPLC-UV methods (Figure 44).

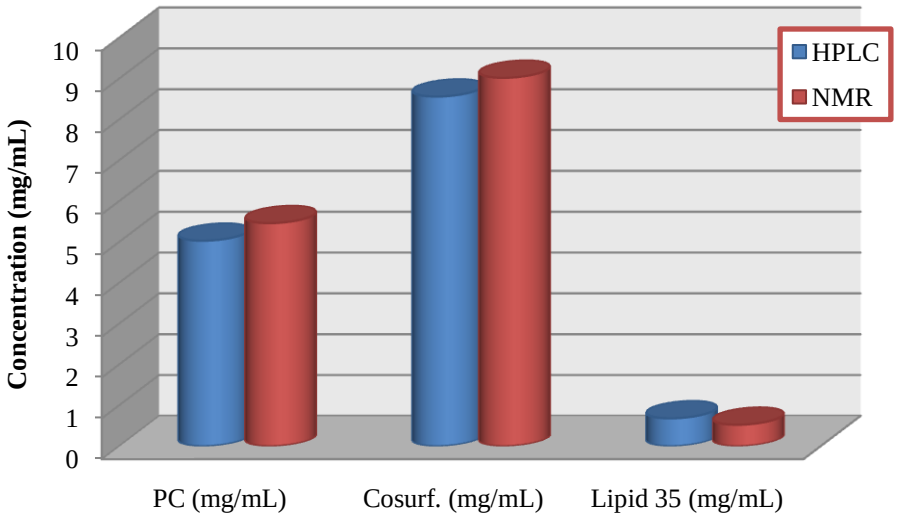

Figure 44: Comparison of analytical methods.

The two analytical methods are in good accordance for all the compounds that form the NPs. The little deviations may be caused by the behaviours that they have in the different experimental conditions, such as temperature, solvent and/or detector sensibility.

3.4.3. Functionalization of SLNs with curcumin derivative 4

After the preparation of SLNs **41**, we investigated the possibility of using "click chemistry" to functionalize their surface with Aβ ligands. In particular, SLNs decorated with the CUR derivative **4** by the click chemistry method were prepared as described in Scheme 11, and more specifically using the Huisgen 1,3-dipolar cycloaddition of azides and terminal alkynes.

First of all, we studied the stability of the stearic acid based SLNs in different reaction's aqueous solutions. This was important to judge the maximum amount of organic solvent (in particular DMSO) that could be used to dissolve the CUR derivative **4**. DMSO might be used because the solubility of CUR derivative **4** is not high enough, compared to the small volume of water in which the NPs are dispersed. We evaluated this reaction condition, verifying the modification in mean diameters of the SLNs.

Table 7: SLN stability in different water/DMSO solutions. Formulation AZD-A2-1 (1 mL) with addiction of different solvent mixture; M.D. (Mean Diameter).

Time (h)	STD		AZD-A1-1 + Water/DMSO 8:2 (1 mL)		AZD-A1-1 + Water (0.2 mL)		AZD-A1-1 + DMSO (0.2 mL)	
	M.D. (nm)	PI	M.D. (nm)	PI	M.D. (nm)	PI	M.D. (nm)	PI
0	53.9	0.184	54.8	0.172	53.4	0.176	65.2	0.274
2	86.9	0.158	105.6	0.166	88.8	0.168	148.6	0.241
4	---	---	---	---	123.0	0.158	193.6	0.308
6	153.2	0.141	153.7	0.208	145.7	0.138	237.2	0.400

Table 8: SLN stability in different water/DMSO solutions. Formulation AZD-A1-1 (0.4 mL) with addiction of different solvent mixture; M.D. (Mean Diameter).

Time (h)	STD		AZD-A2-1 + Water/DMSO 8:2 (0.4 mL)		AZD-A2-1 + Water (0.4 mL)	
	M.D. (nm)	PI	M.D. (nm)	PI	M.D. (nm)	PI
0	54.8	0.149	55.4	0.155	56.3	0.143
2	91.7	0.151	124.5	0.141	99.8	0.140
4	135.3	0.144	162.7	0.133	141.6	0.145
6	165.3	0.161	184.7	0.155	164.5	0.158

Looking at the results presented above (Table 7, 8), we had the possibility to use quite large amounts of DMSO (~ 10 %) without significant variation in the dimension of the nanodevices.

We used AZD-A2-1 and AZD-A3-1 SLN **41** preparations containing different concentrations of Lipid-PEG-N_3 **35**, in order to evaluate the comeback of the different formulations to reaction conditions. The click reactions were performed at room temperature, in presence of variable amounts of copper sulfate and sodium ascorbate - which produce fresh Cu(I) catalyst *in situ* - and modifying the number of equivalent of CUR derivative **4**.

The valuation of different reaction conditions was established on the variation of mean diameters, HPLC-UV profiles and peaks of Lipid-PEG-N_3 **35**. This allowed us to check both the concentrations of reagents and copper catalyst and the time of the click chemistry procedure.

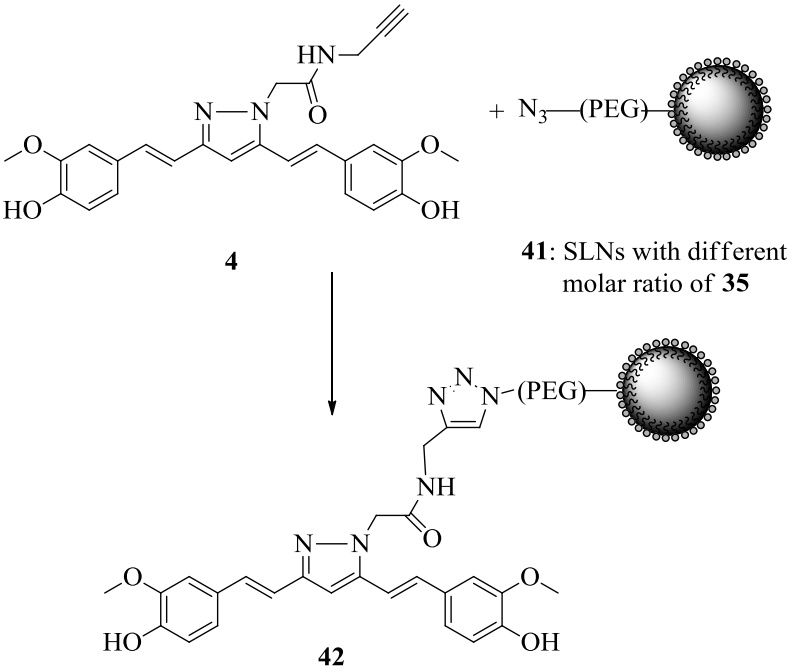

Scheme 11: ***Reagents and Conditions*****: (i) $CuSO_4 \cdot 5\ H_2O$, Sodium ascorbate, DMSO/water, r.t., 4-6 h.**

As presented in the scheme above, we decided not to use chelators in our reactions, to avoid the presence of interfering compounds during the purification of this type of NPs.
Preliminary trials (click I and II below) were performed with SLN formulation AZD-A2, that presented a Lipid-PEG-N_3 **35** concentration of 0.25 mM. We chose to modify only the concentration of copper sulfate and sodium ascorbate in the reaction conditions. In both these reactions we used a large excess of both CUR derivative **4** (e.g. 3.2 eq) and copper (I) catalyst. In particular for:

- **"Click I"**: we formulated 1.6 mL of aqueous solutions of freshly prepared Cu (I) catalyst mixing together $CuSO_4 \cdot 5\ H_2O$ and sodium ascorbate; the final concentrations of the two species were 1.02 mM and 1.36 mM respectively. This catalyst was added to 0.362 mL of a solution of CUR derivative **4** (4.36 mM) in DMSO. This orange suspension was then added to 2 mL of SLN aqueous dispersion AZD-A2-1, obtaining a DMSO/water ratio less than 10 %.

- **"Click II"**: we prepared the fresh catalyst in higher equivalent ratio, against the CUR derivative **4**. In particular, 1.6 mL of an aqueous solution of Cu(I), combining $CuSO_4 \cdot 5\ H_2O$ and sodium ascorbate, obtaining a final concentration of respectively 5.09 mM and 6.81 mM. The solution was added to 0.362 mL of a solution of CUR alkyne **4** (4.36 mM) in DMSO; in this test, the mixture was maintained under magnetic stirring for 30 min, protected from light, to verify if this activation of the triple bond can improve the result. After half an hour, it was added to 2 mL of SLN aqueous dispersion AZD-A2-1, affording a DMSO quantity - also in this case - less than 10 %.

Both the reaction mixtures were stirred at room temperature protected from light and were analyzed for the average diameter of SLNs, the size distribution and the concentration of Lipid-PEG-N_3 **35**.

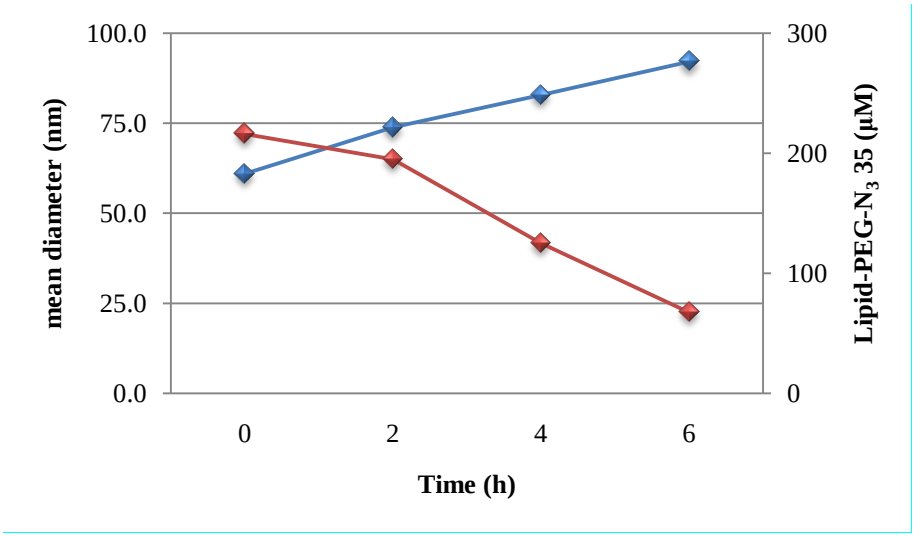

Figure 45: Mean diameters (blue) and Lipid-PEG-N_3 (red) ongoing in "click I".

As presented above, for **"click I"** we used a lower concentration of freshly prepared Cu (I), obtaining that in six hours more that 70 % of Lipid-PEG-N_3 **35** disappeared (Figure 45). Unfortunately, we observed a gradual increase of SLN diameters, even if they were lower than 100 nm also after the reaction ended. After six hours, we changed the HPLC-UV method and we noticed the presence of the peak of compound **36**; this result confirmed the reaction between the azide on lipid **35** and the triple bond on compound **4**.

As reported in Figure 46, good results were more quickly obtained for **"click II"**, in which we used an higher concentration of catalyst. In four hours we observed a faster increase of SLNs diameters and a complete disappearance of the reagent Lipid-PEG-N_3 **35**. Changing the HPLC-UV method, we confirmed the presence and the formation of compound **36**. Looking at the results presented below, the increase in the diameters was not so worrying, because they stayed under the 200 nm and so the particles were in the nano-range.

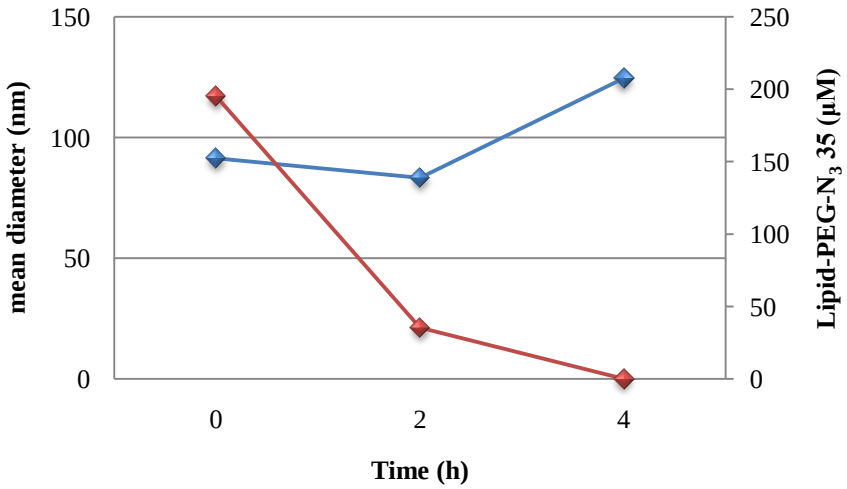

Figure 46: Mean diameters (blue) and Lipid-PEG-N_3 (red) ongoing in "click II".

Following trials were performed with SLN **41** formulation AZD-A3, containing an higher amount of Lipid-PEG-N_3 **35**; in particular its concentration was 0.57 mM. Also in the experiments reported in the next paragraphs, we worked in less excess of CUR alkyne **4** (i.e. 2 eq), varying the concentration of Cu (I) in the reaction's conditions.

In particular for:

- **"Click III"**: we decide to use a smaller amount of catalyst to check the comebacks and to simplify the further purification. In particular, we managed to prepare 1.23 mL of an aqueous solutions of Cu (I) catalyst freshly prepared mixing $CuSO_4 \cdot 5 H_2O$ and sodium ascorbate, in a final concentration of respectively 1.43 mM and 1.93 mM. The orange suspension was added to 0.27 mL of a solution of CUR derivative **4** (6.36 mM) in DMSO; the obtained mixture was stirred for 30 min, protected from light and then added to 1,5 mL of SLN aqueous dispersion AZD-A3-1.

- **"Click IV"**: we arranged 1.23 mL of catalyst combining, as usual, aqueous solutions of $CuSO_4 \cdot 5\ H_2O$ and sodium ascorbate in higher quantities than **"click III"**; we obtained a final concentration of respectively 7.15 mM and 9.64 mM. The mixture was added to 0.27 mL of a solution of CUR derivative **4** (6.36 mM) in DMSO. The obtained orange suspension was, also in this case, maintained under magnetic stirring for 30 min, protected from light, and then added to 1.5 mL of SLN aqueous dispersion AZD-A3-1.

Both the reaction mixtures were stirred at room temperature, protected from light, and were analyzed for the average diameter of SLNs, the size distribution and the concentration of Lipid-PEG-N_3 **35**.

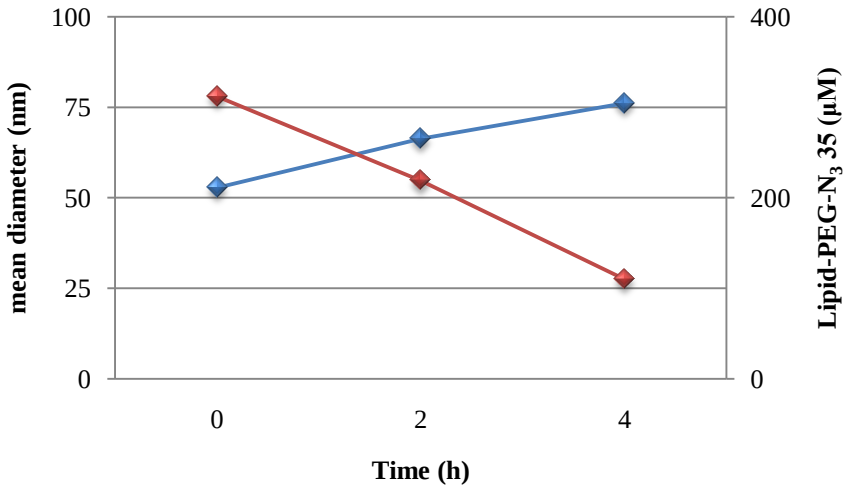

Figure 47: Mean diameters (blue) and Lipid-PEG-N_3 (red) ongoing in "click III".

As presented above for **"click III"** as for **"click I"**, we observed a gradual increase of SLNs diameters, a reduction of the azido-containing reagent **35** and, after changing the HPLC-UV method, the presence of compound **36** in the final dispersion. Looking at the data reported in Figure 47, the slight growth of diameter was not significant and the particles remained under 100 nm. The disappearance of lipid **35 "click III"** reaction proceeded quicklier than **"click I"**; it is probably caused by the activation of triple bond before the addiction to SLNs **41** dispersion.

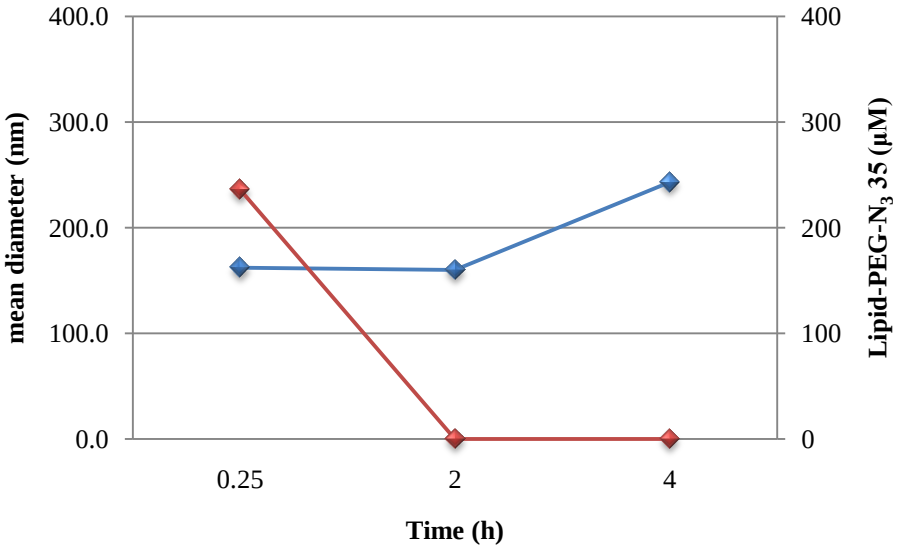

Figure 48: Mean diameters (blue) and Lipid-PEG-N_3 (red) ongoing in "click IV".

As reported in Figure 48, in **"click IV"** we observed an increase of SLNs diameters higher than other trials of click and a more rapid decrease of Lipid-PEG-N_3 **35**, confirming also in this case a faster course of the reaction. We evaluated that the increase in diameters was not a problem, because the complete disappearance of compound **35** was obtained when the diameters was under 200 nm; looking at all the parameters analyzed and at the speed of the reaction we considered it was a good result. The HPLC-UV method set up for compound **36** revealed also in this case the presence of clicked compound in the final dispersion.

During the experiments, we performed a control click reaction to be sure that no interfering compounds were present in the final dispersions. This was carried out with SLNs without Lipid-PEG-N_3 **35**, using the same reaction conditions (i.e. incubation time, concentration of catalyst and CUR derivative **4**) of **"click III"**. HPLC-UV analysis didn't reveal the formation of any compounds with the same retention time of compound **36**, revealing that it was synthesized during all our trials.

3.4.4. Purification of click reaction mixture

Many different purification procedures were studied and analyzed, in order to improve the purification from both the unbound CUR derivative **4** and the other chemicals in the

reaction mixture, such as different copper and ascorbate species. After some preliminary trials, the best possible procedure was pointed out. Operatively, after the incubation the reaction mixture was:

- filtered by syringe filter 0.45 μm to remove any particulate matter from SLNs dispersion
- centrifuged at 15000 g at 3 °C in order to remove a light blue precipitate; this might be caused by the oxidated form of copper (i.e. copper (II) sulfate) obtained after the complete removal of the ascorbate reductive agent
- centrifuged with the ultrafiltration device Vivaspin 500 with PES membrane 300 kDa, in order to separate all the low molecular weight reactants as unbound CUR derivative **4**, soluble copper species and/or degradated ascorbate species from SLNs **42** formulation.

During the different steps of the purification procedure, we characterized the SLNs dispersion for the average diameter, the size distribution and the concentration (HPLC-UV) of different components; we noticed that no significant variations of all these monitored parameters was observed.

The same properties were evaluated after 1 month storage at -20 °C, to check the stability of the SLN dispersions and also in this case there weren't any modifications in diameter and size distribution; this confirmed the effectiveness of the method proposed.

3.4.5. Discussion

In this part of the work, we set up the method for the first functionalization of SLNs with Aβ ligands. This works allowed us to check different reaction conditions, to obtain the best results in the shorter time. In particular, we saw that in all the different set up of the experiments, we obtained yield in compound **36** greater than 75 %, with peaks of quantitative transformations. Looking at all the trials, the analysis revealed that there was a slight increase in the diameters but they always were below the nanodevice limit. Only in **"click IV"**, after 4 hours, we noticed an higher growth but, mixing together with disappearance of Lipid-PEG-N_3 **35** (Figure 48), we could say that in 2 hours we achieved the quantitative removal of azido-compound, with no significant increase in diameters. We worked also on the purification technique and we arranged a method that allowed the

complete removal of the small interfering molecules and the recovery of stable storaged SLNs **42** dispersions. We didn't performed binding studies on this type of NPs yet, but we are managing to do them with our European project partners.

3.5. Curcumin-decorated PACA NPs: preparation, functionalization and interaction studies

Among suitable nanodevices for drug delivery, nanoparticles based on biodegradable poly(alkyl cyanoacrylate) (PACA) polymers have appeared as an established technology for colloidal nanomedicine. Introduced more than 25 years ago in the field of pharmacology,[249] NPs developed from poly(alkyl cyanoacrylate) (PACA) biodegradable polymers have opened new and exciting perspectives in the field of drug delivery. In fact, they have some almost ideal characteristics as drug carriers, in connection with biomedical applications.[250-254] Thanks to the direct implication of organic chemistry, polymer science and physicochemistry, multiple PACA nanoparticles with different features can be obtained: nanospheres (matrix type NPs)[249,255-257] and nanocapsules (vesicular-type NPs, either oil- or water-containing),[258-260] as well as nanoparticles with controlled-surface properties[255,258,261-264] - the later being considered as the second generation of drug delivery devices. The major breakthrough of this recent class of advanced PACA nanoparticles is undoubtedly the grafting of poly(ethylene glycol) (PEG), named "PEGylation". Also in this field, PEG gives rise to several potential beneficial effects, including the increased bioavailability and plasma half-lives, the biocompatibility/decreased immunogenicity, the reduced proteolysis and the enhanced solubility and stability; these are considered as a key material in this field.[265]

Alkyl cyanoacrylates monomers are also well-known for their very high reactivity and the excellent adhesive properties of the resulting polymers. On the one hand, the famous Superglue (manufactured by Henkel), which contains short alkyl chain cyanoacrylates, is commonly employed by the general public for the repairing and do-it-yourself activities. On the other hand, longer alkyl chain cyanoacrylates have been developed for biomedical purposes, such as surgical glue for the closure of skin wounds[266-268] and embolitic material for endovascular surgery.[266,267,269] However, this unique feature tends to make the synthesis of well-defined and/or functionalizable poly(alkyl cyanoacrylate) architectures extremely

difficult - or even impossible. A significant step could circumvent this important drawback, *via* the synthesis of random poly[(hexadecyl cyanoacrylate)-*co*-methoxypoly(ethylene glycol) cyanoacrylate] (P(HDCA-*co*-MePEGCA)) comblike *co*-polymers with amphiphilic properties.[270] This original approach derived from tandem Knoevenagel condensation-Michael addition reaction to build the polymeric backbone, where the corresponding cyanoacetates were reacted with formaldehyde, in the presence of dimethylamine as the catalyst (Scheme 12). To simplify, the term *co*-polymer will be employed in the text to refer to the oligomers mixture resulting from the polymerization reaction.

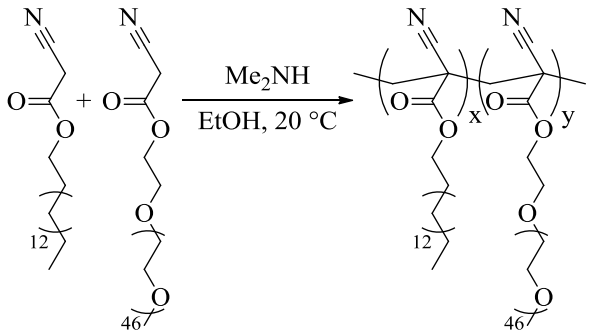

Scheme 12

However, even though these "PEGylated" nanoparticles have demonstrated a noticeable brain-targeting effect,[251] they suffer from a crucial lack of specificity toward cells and/or tissues and can't be efficiently addressed. Thus, for the forthcoming years, the most exciting challenge in drug delivery, whatever the nature of the drug carriers (i.e., liposome, nanoparticles, etc.), will be undoubtedly the synthesis of efficient ligand-functionalized colloidal devices, to achieve specific cells targeting based on a molecular recognition process. Looking at the last decade, there are some examples of functionalization of PACA NPs - the so-called third generation PACA NPs; one of them involves poly[(hexadecyl cyanoacrylate)-*co*-aminopoly(ethylene glycol) cyanoacrylate] (P(HDCA-*co*-H_2NPEGCA)) nanospheres displaying folic acid groups to target the folate receptor, which is overexpressed at the surface of many tumor cells.[271,272] However, this approach was restricted to amine-reactive compounds; to overcome this constraint Nicolas *et al.*[273] proposed a general method to prepare highly functionalizable PACA-PEG copolymers and associated NPs. This approach relied on the synthesis of a novel P(HDCA-*co*-N_3PEGCA) copolymer by Knoevenagel condensation-Michael addition reaction, able to react

efficiently with alkyne derivatives via Huisgen 1,3-dipolar cyclo-addition. As a proof of concept, in this work, model molecules have been quantitatively coupled either to the P(HDCA-*co*-N_3PEGCA) copolymers in homogeneous medium followed by nanoprecipitation, or directly at the surface of the P(HDCA-*co*-N_3PEGCA) NPs in aqueous dispersed medium - that acts here as a clickable colloidal scaffold (Figure 49).

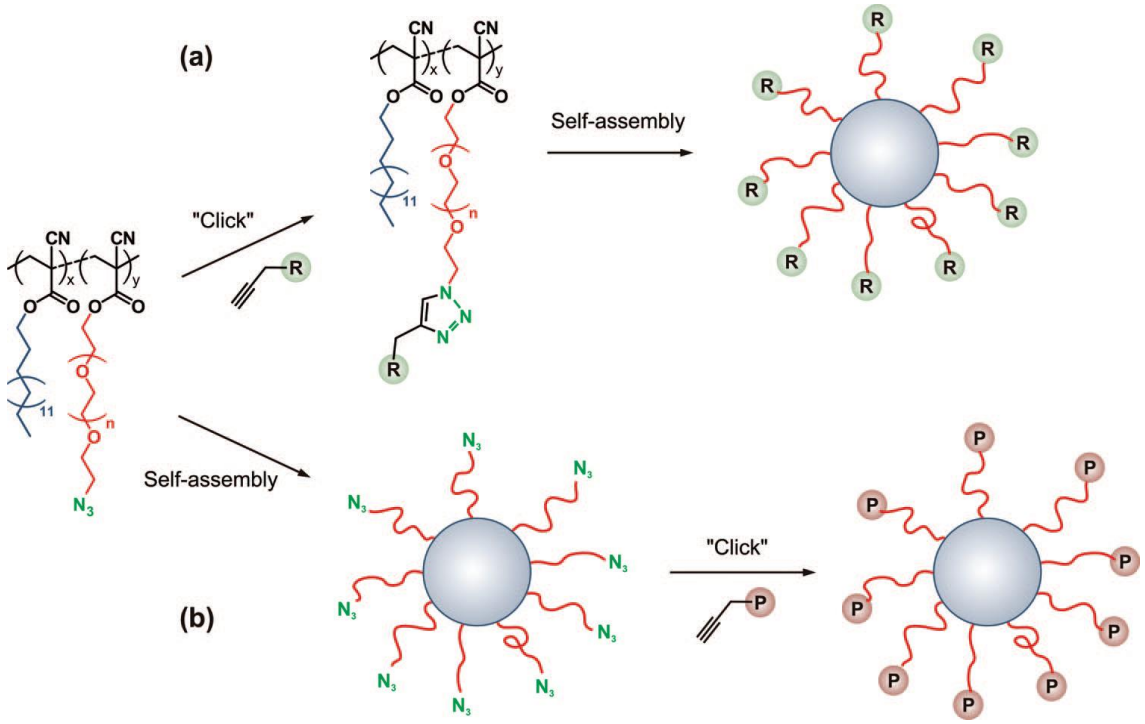

Figure 49: General approach to prepare functionalized poly(alkyl cyanoacrylate) nanoparticles.

Starting from this information, we decide to functionalize these type of NPs with our CUR derivative **4**; from the results presented above, we demonstrated that this compound is useful for the functionalization of lipid based NPs. As a consequence, it can give some promising results in the field of Aβ ligand decoration of PACA nanodevices. These linked nanotools could be a nice solution, because they may combine both the quality of the polymeric NPs (i.e. brain-targeting effect, biodegradability, stability) and the ability of derivative **4** to interact with Aβ peptides in their different forms.

3.5.1. Functionalization of PACA NPs

Basing on the literature data reported above, we decide to try the CUR decoration of polymeric NPs in two different ways. First of all, we evaluated the possibility to functionalize preformed NPs and/or *co*-polymers and then we considered the opportunity to synthesize the starting material for the polymerization.

3.5.1.1. *Functionalization of preformed P(HDCA-co-N_3PEGCA) co-polymer and NPs*

As shown above (Figure 49), we tried to decorate performed NPs or *co*-polymers using the technique presented by Nicolas *et al.*[273] in 2008. Stable nanoparticles from the starting P(HDCA-*co*-MeOPEGCA-*co*-N_3PEGCA) were prepared by the nanoprecipitation technique and analyzed by DLS. From these measurements, azide-functionalized NPs exhibited an average diameter very close to P(HDCA-*co*-MePEGCA) NPs (~ 100 nm). After the nanoprecipitation, we performed the click chemistry reaction in the homogeneous media; after the removal of the catalyst, we performed an extensive dialysis against a 1:2 acetone/buffered water (sodium chloride 1 M, sodium phosphate 50 mM) mixture, in order to have an efficient removal of the unreacted compounds. Unfortunately, we didn't obtain any results with this technique and so we moved to the functionalization of P(HDCA-*co*-MeOPEGCA-*co*-N_3PEGCA) itself. We tried the copper catalyzed 1,3 cycloaddition between azide and alkyne, also for this decoration; in this case, we chose to avoid the use water and to employ only organic solvent to prevent the formation of NPs during the reaction. After the removal of the copper catalyst, we purified the reaction mixture in different ways; also in this case no results were gained and some kinds of *de*-polymerization were obtained.

3.5.1.2. *Synthesis of monomer, co-polymerization and NPs preparation*

To overcome the problem of functionalization of preformed NPs and *co*-polymer, we set up the synthesis of the monomer starting from the CUR derivative **4** and the difunctionalized PEG-2000. We had to use this long chain polymer - instead of the

600 Da one - because the stability of the PACA NPs is strictly associated to the length of hydrophilic moiety and the best one is the 2000 Da PEG. Compound **43**, HDCA and MePEGCA were synthesized according to the procedure presented by Nicolas *et al.*[273] and Brambilla *et al.* [274] in very good yields. As presented in Scheme 13, after this first step we move to the linkage of the CUR derivative **4** to the hydrophilic linker of the cyanoacrylate monomer using the copper (I) catalyzed cycloaddition.

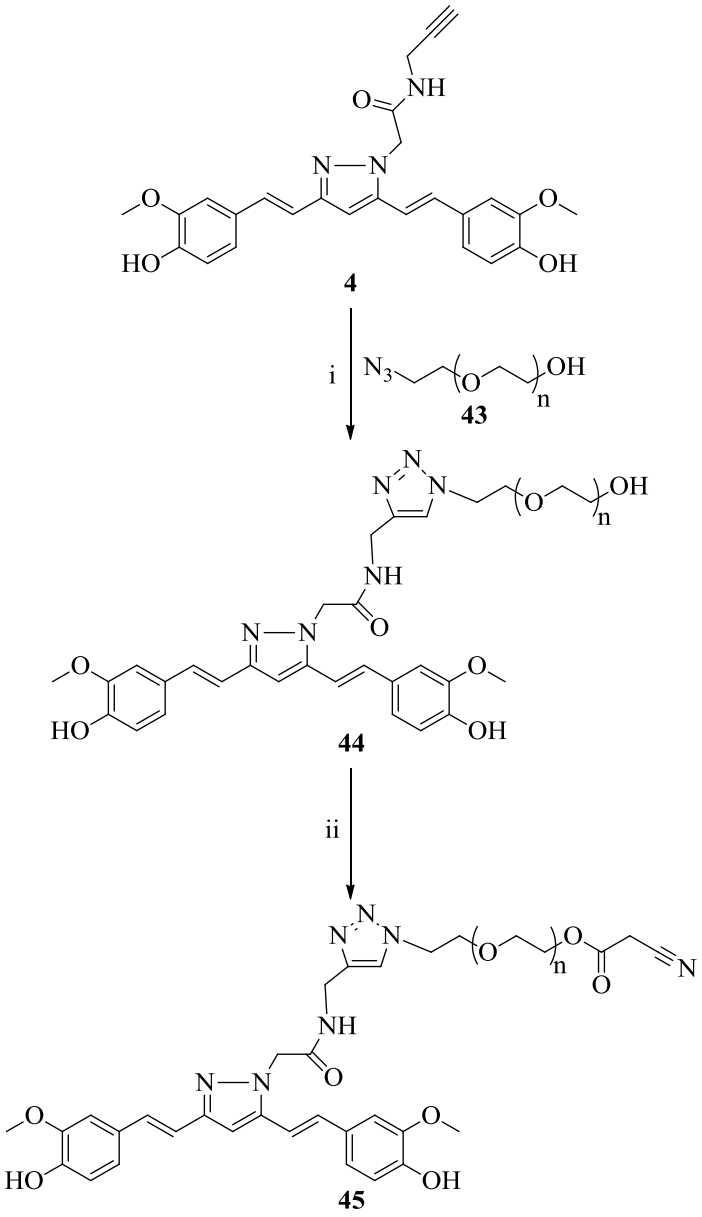

Scheme 13: i) $CuSO_4 \cdot 5\ H_2O$, Sodium ascorbate, THF/water, r.t., 4-6 h; ii) 2-cyano acetic acid, DCC, DMAP, CH_2Cl_2, r.t., 24 h.

After 12 h, we removed the catalyst and performed an extensive dialysis (2 kDa as membrane cut-off) against water, in order to remove efficiently all the undesired compounds. The NMR analysis confirmed the functionalization of starting PEG-2000 in quantitative yield.

After the recovery of desired compound **44**, we obtained the esterification of aliphatic -OH, using standard coupling method in controlled reaction conditions; after the precipitation of the cyanoacetate derivative, NMR experiments confirmed the presence of compound **45** (CurPEGCA) with no undesired products.

The synthesis of P(HDCA-*co*-CurPEGCA-*co*-MePEGCA) copolymers was then achieved from HDCA and PEG containing monomers, with 4:1 initial molar ratio via Knoevenagel condensation-Michael addition reaction. The total hydrophilic monomers were constituted by MEPEGCA and CurPEGCA in an initial molar ratio of 9:1. ^{1}H NMR spectra (data not shown) of the resulting materials were consistent with the expected structure of the copolymers **46** (Scheme 14); they are also in very good agreement with previous results concerning P(HDCA-*co*-MePEGCA) or P(HDCA-*co*-N_3PEGCA) copolymers.[273]

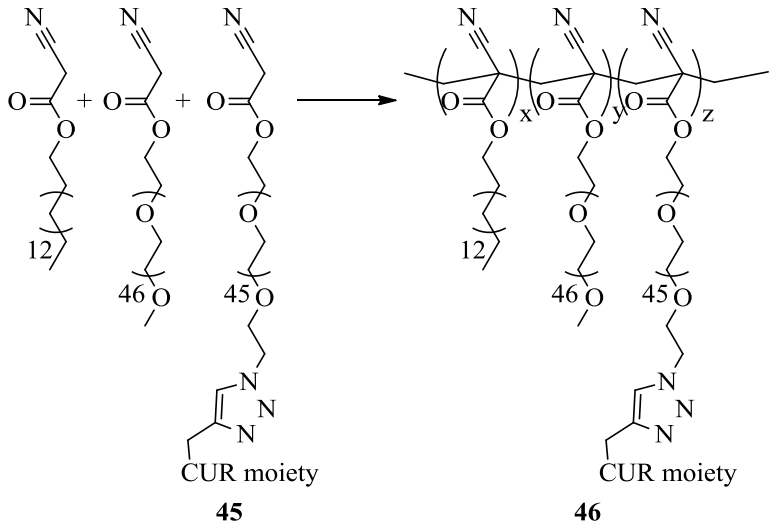

45 **46**

Scheme 14: formaldehyde, pyrrolidine, CH_2Cl_2, r.t., 24 h.

After this fundamental synthetic step, we went forward to the preparation of CUR decorated polymeric NPs adopting the nanoprecipitation technique. This method is based on the dissolution of the starting *co*-polymer in an acetone solution and on its dropping into a stirred cosurfactant water solution. For our purpose we used an aqueous solution of Pluronic F68 0.5 % m/v. Unfortunately, looking at the mean diameter, the

nanoprecipitation of our P(HDCA-*co*-CurPEGCA-*co*-MePEGCA) **46** allowed to get a dispersion of NPs with two different populations (data not shown); both of them were in the nanometer range but this was not sufficient for our goal.

To overcome this problem, we tried to make the population of the NPs dispersion homogeneous with other *co*-polymers; the best solution was achieved using the P(HDCA-*co*-RCA-*co*-MePEGCA) synthesized according to the procedure presented by Brambilla *et al.* This is a Rhodamine B-tagged poly(alkyl cyanoacrylate) amphiphilic copolymer, that has been successfully used to prepare fluorescent nanoparticles for human brain endothelial cell imaging, allowing their uptake and intracellular trafficking to be finely observed.[274]

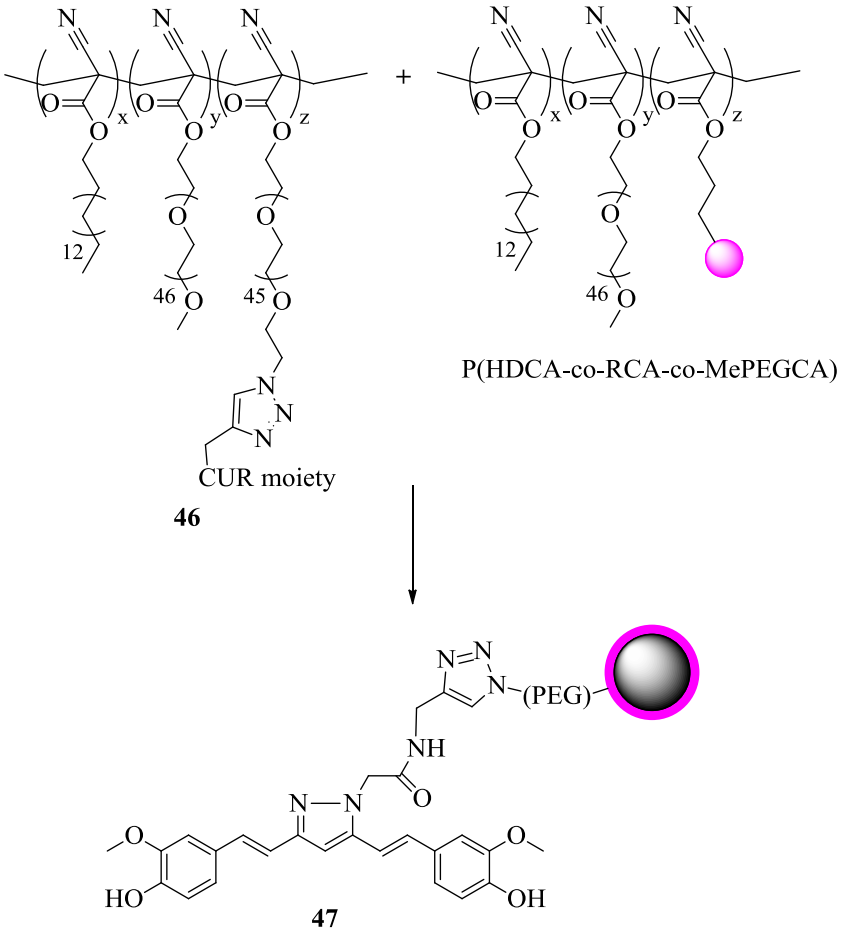

Scheme 15

As presented in Scheme 15, we prepared decorated and fluorescent NPs using nanoprecipitation technique; in particular, we dissolved in an acetone solution both the *co*-

polymer **46** and P(HDCA-*co*-RCA-*co*-MePEGCA) in initial 1:1 molar ratio. After the complete dissolution, we added dropwise the mixture to a stirring solution of Pluronic F68. Then we evaluated the mean diameters and the dispersion was in nanometer range, with only one population (Figure 50 A). After the nanoprecipitation phase, acetone was evaporated under reduced pressure and nanoparticles were purified by ultracentrifugation. The supernatant was discarded and the pellets containing NPs **47** were resuspended in the appropriated volume of water or PBS or other aqueous solution.

The stability (mean diameter) of the two different preparations - whereas they had been ultracentrifuged or not - of NPs **47**, stored at 4 °C or 37 °C, for a period of 3 days is presented in Figure 50.

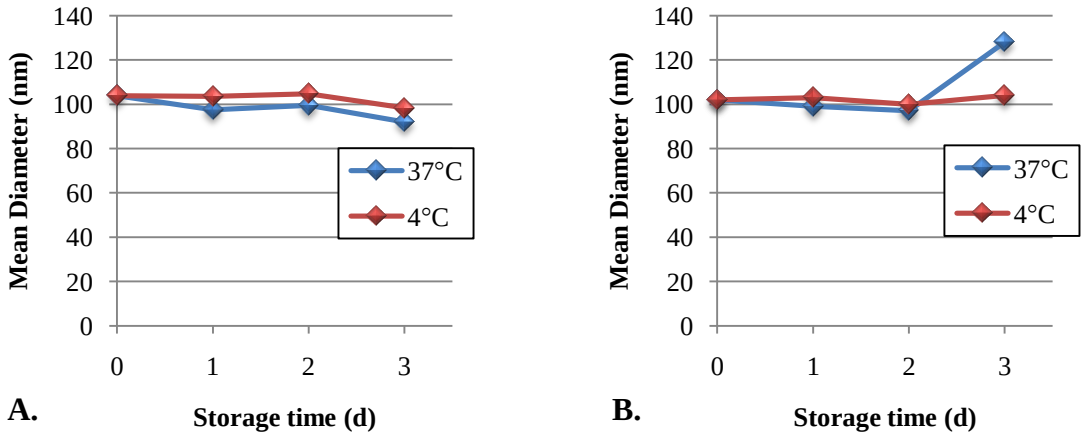

Figure 50: Stability studies of NPs 47: A. not ultracentrifuged NPs; B. ultracentrifuged NPs.

As seen, both polymeric NPs preparations are very stable for the storage period in terms of size distribution and no signs of aggregation were evident.

It is important to notice that during the NPs' formation by self-assembly in aqueous medium, PHDCA homopolymer is produced; even if these intrinsic features of alkyl cyanoacrylate chemistry might be considered as a drawback regarding polymer synthesis, the homopolymers are entrapped into the core of the NPs stabilized by P(HDCA-*co*-PEGCA) *co*-polymers and they eventually lead to well-defined colloidal objects. Besides, this is the only method available to yield biodegradable PACA nanoparticles covered by PEG chains in mild conditions (as opposed to direct emulsion polymerization of alkyl cyanoacrylates in strong aqueous acidic media).

3.5.2. Interaction studies

3.5.2.1. *Capillary electrophoresis*

Capillary electrophoresis (CE) with UV detection had previously been used for the *in vitro* identification of small molecules, as potential inhibitors of Aβ aggregation.[275,276] However, this work was limited, since the high concentrations of peptide required for the screening were about 5 orders of magnitude higher than those found in vivo. More recently, Kato *et al*.[277] reported a CE-LIF method, that allows the antiaggregation features of molecules toward fibrils to be monitored. However, those species are no longer considered to be the main toxic species for AD. As a consequence, an analytical method tailored to Aβ monomers and resulting soluble oligomers is enforced to understand the therapeutic or diagnostic perspective of NPs.

Starting from the work of De Lorenzi's research group, related to the screening of antifibrillogenic activity of small molecules[276] and from the work of Brambilla *et al*.,[278] related to the interaction between the Aβ peptide and NPs, we have applied capillary electrophoresis (CE) coupled to laser-induced fluorescence (LIF) detection to screen the ability of our NPs **47** to efficiently bind $A\beta_{1-42}$. This method is able to monitor in real time the binding of soluble $A\beta_{1-42}$ monomers or soluble oligomers to NPs.

The CE-LIF method used in this study was capable on investigating the interaction between NPs **47** and HiLyte Fluor labeled $A\beta_{1-42}$. The LIF detection allowed the use of a lower concentration of peptide to be used than in UV detection, so it better fits with physiological processes and conditions. As a matter of facts, Aβ peptide is found in biological fluids, such as the cerebro-spinal fluid (CSF), at nanomolar concentrations; therefore, a sensitive and discriminative analytical method is required.

The CE-LIF analysis of a solution of the fluorescent $A\beta_{1-42}$ showed a single peak migrating at ~ 8.5 min (with a highly reproducible migration time for each batch) and mainly constituted by the soluble form.

It is interesting that the electrophoretic profile of the peptide sample stayed constant over time up to 15 h (Figure 51 A), demonstrating an excellent stability of the fluorescent peptide in its soluble form, at this concentration in the buffer. Remarkably, when the same

concentration of $A\beta_{1-42}$ peptide solution was incubated with 20 µM of both free compound **4** and NPs **47** suspension, a gradual decrease of the monomeric peptide peak was observed (Figure 51 B and C).

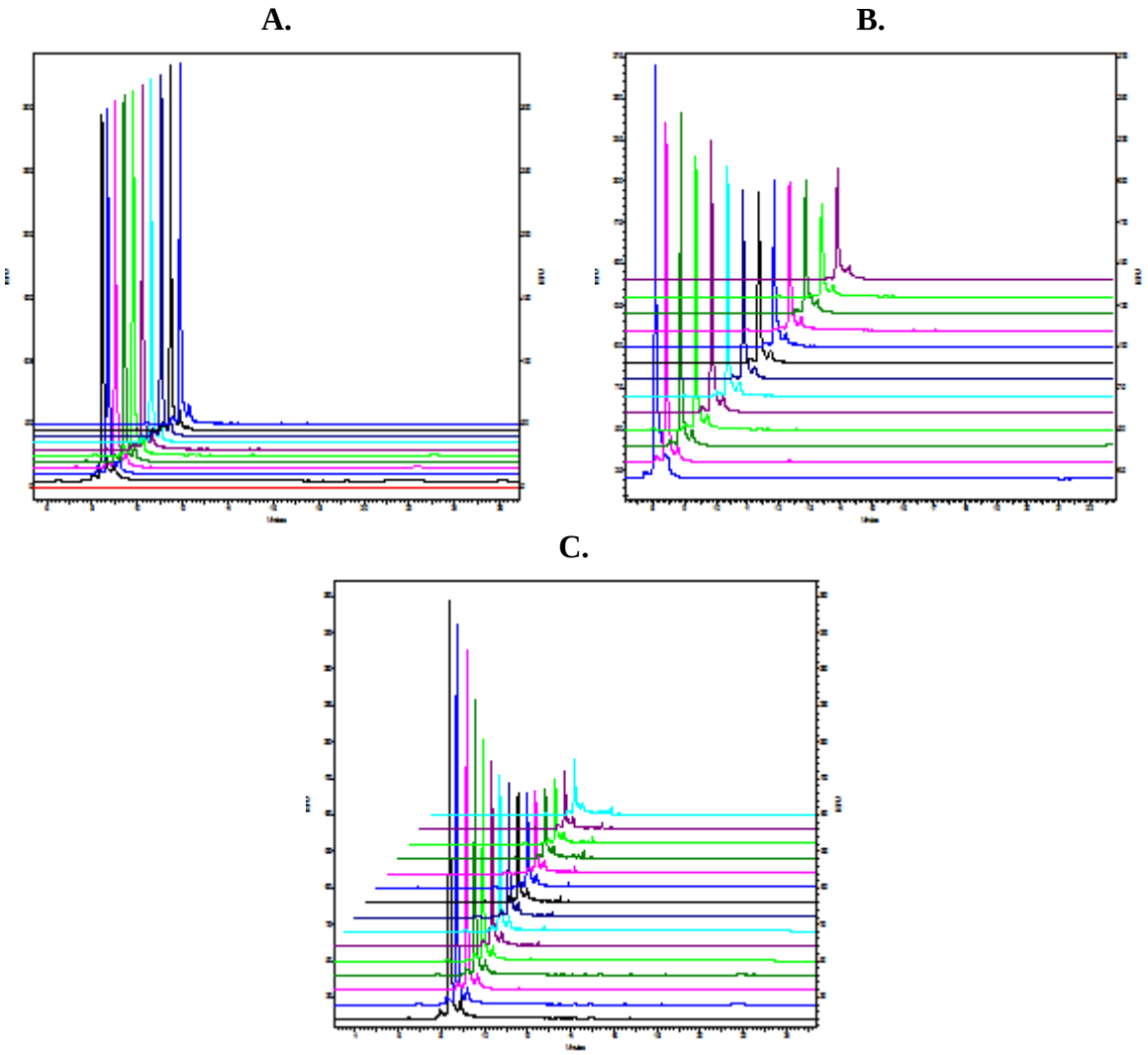

Figure 51: A. Evolution of the CE-LIF profile as a function of time at 37 °C of a 5 µM HiLyte Fluor $A\beta_{1-42}$ solution alone, B. in the presence of a 20 µM compound 4 solution and (c) in the presence of a 20 µM NPs 47 suspension; Elapsed time = 80 min.

These results indicate some kinds of interaction between the peptide and both compound **4** and NPs **47**. As presented above (see 3.1.2.), we obtained, also in this *in vitro* experiment, a formation of some not soluble aggregates in the solution or on the surface of NPs with both the analyte. These aggregates were visible after the recovery of sample vials, confirming this behavior of Aβ peptide in presence of CUR derivatives.

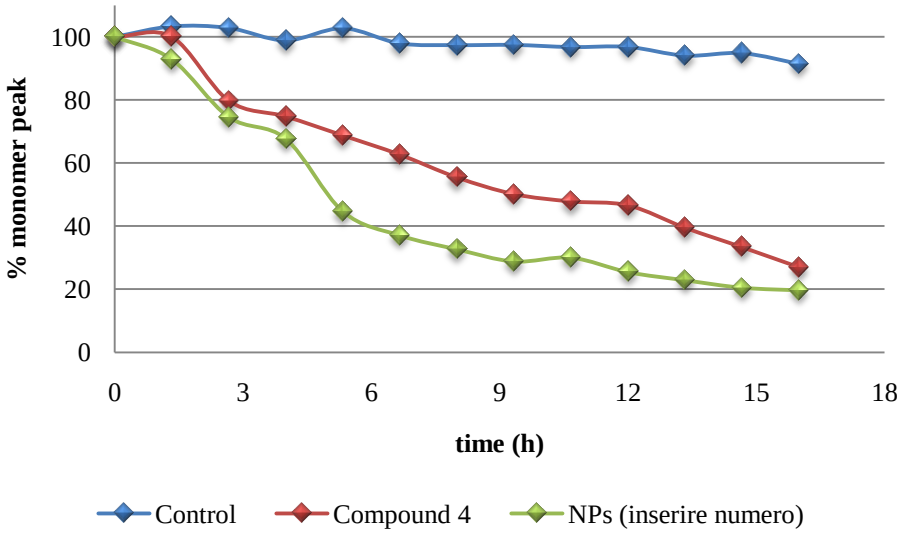

Figure 52: $A\beta_{1-42}$ monomer peak intensity as a function of time: control and upon incubation of $A\beta_{1-42}$ in the presence of compound 4 and NPs 47.

These experiments also allowed to monitor the evolution of monomer peak %, as a function of incubation time. Monomer peak % is calculated as the ratio between the absolute peak area of the monomer observed at t = 0 and the one observed at each incubation time. This tool was used to evaluate the kinetics of disappearance of the monomeric peptide, as a function of the concentration ratio between compound **4**, NPs **47** and $A\beta_{1-42}$. As shown in Figure 52, whatever the concentration ratio, there was a clear uptake of peptide by the Aβ interacting species with a capture varying from 26 % for the compound **4** to 90 % at t = 21 h (data not shown) for NPs **47**. It is important to underline that this process was strictly dependent on the peptide availability in solution. The higher the peptide presence in solution, the faster and the higher the capture ratio.

In an interesting analyzing of these data, we observed a non-linear disappearance of the monomeric peak over time, suggesting the formation of peptide aggregates in the sample solution or at the surface of the nanoparticles.

3.5.2.2.*Surface Plasmon Resonance*

We used the ProteOn XPR36 (Biorad) apparatus also for these binding studies with SPR technique. $A\beta_{1-42}$ fibrils were immobilized in one of the parallel-flow channels of the sensor chip (Biorad), using amine-coupling chemistry. As presented above, after surface

activation, the peptide solutions were injected for 5 min at a flow rate of 30 mL/min and the remaining activated groups were blocked with ethanolamine. BSA was also immobilized in another parallel flow channel, as a reference protein. The final immobilization levels were similar - about 2500 RU (1 RU = 1 pg protein/mm^2). A fourth surface was prepared, using the same immobilization procedure but without addition of the peptide ("empty" reference surface).

Preliminary injections were done, to be sure that Aβ fibrils were correctly immobilized. So we injected the anti-Aβ antibody 4G8 (Covance) and the Congo-red solution which, as expected, bound and recognized Aβ fibrils (data not shown).

After the sample analysis, ProteOn software (BioRad) was used for the fitting of sensograms with the Langmuir model (the simplest 1:1 interaction model). This allowed to obtain the association and dissociation rate constant of the binding (k_{on} and k_{off}) and the corresponding K_D value.

Looking at the formulation of NPs **47**, we decided to use NPs derived from P(MePEGCA-*co*-RCA-*co*-HDCA) *co*-polymer, instead of plain P(HDCA-*co*-N_3PEGCA) NPs as control (ctrl). This was done to be sure that we could distinguish all the components that were liable for the interaction with Aβ fibrils.

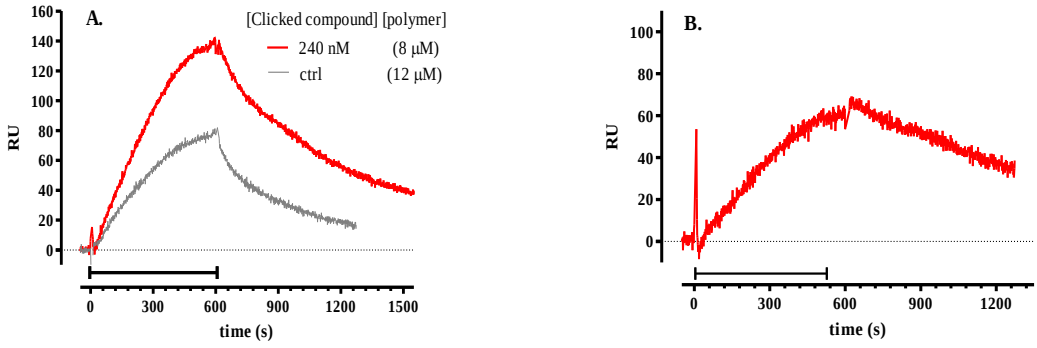

Figure 53: A. Typical sensograms obtained for NPs 47 and fluorescent ones (ctrl); B. sensograms of the interaction after the subtraction of the rhodaminated NPs signal.

PACA NPs **47**, as well as fluorescent NPs **47**, were flowed over parallel flow channels of the same sensor chip, immobilizing $Aβ_{1-42}$ fibrils, BSA and on the empty surface.

As presented in Figure 53 A, some interactions were detected when using both type of NPs, even if at different total concentrations of *co*-polymer. On the contrary, they didn't revealed interactions with immobilized BSA and on empty surface (data not shown). From

the sensograms obtained with the same total concentration of *co*-polymer, we were able to differentiate the contribution of the fluorescent fraction of NPs and the clicked compound **4** (Figure 53 B). Looking at these results, we could underline the improved binding ability obtained with CUR decorated NPs instead of fluorescent ones. These outcomes agree with results reported for liposomes and CUR derivative **4**.

Figure 54 shows the concentration-dependence of the specific binding of NPs **47** to immobilized $A\beta_{1\text{-}42}$ fibrils, before the correction of the signal measured with the fluorescent NPs, used as control. In particular, for these experiments we used polymeric NPs with different concentrations of exposed clicked CUR derivative **4**.

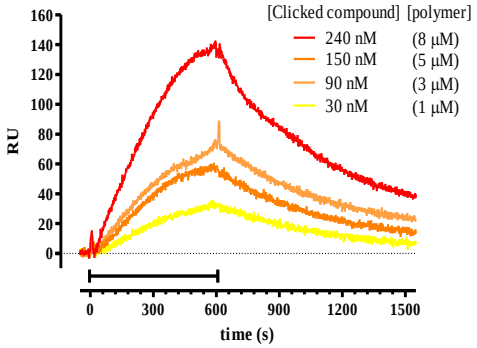

Figure 54: Concentration-dependent binding of PACA NPs 47 to $A\beta_{1\text{-}42}$ fibrils immobilized on the SPR sensor chip.

As for the liposome experiments, the resulting sensograms, after the corrections for the signal obtained with rhodaminated NPs, could not be fitted by a simple 1:1 interaction model (Langmuir equation) but required more complex interaction models. This is evident in the dissociation phase, which can't be fitted by a mono-exponential curve (as expected for simple interactions), indicating at least two binding components with two different rate constants, one faster and one slower. The fitting of these sensograms with a "two-site" model allowed to estimate the binding constants of the two putative components, highlighting the presence of a component representing about 60 % of the binding, characterized by a very low dissociation rate constants. The corresponding K_D value of the exposed clicked CUR derivative **4** was calculated in the low μM range (0.3 μM). It is important that the sensograms obtained with the different concentrations could not globally fit, suggesting that even the binding on this type of NPs to Aβ fibrils is complex and likely involves avidity effects[222].

3.5.3. Discussion

In this part of the work, CUR-decorated polymeric NPs were prepared and studied for their stability and binding affinity to $A\beta_{1-42}$ fibrils. For their preparation, we tried to functionalize some preformed nanodevice using a click reaction. Unfortunately it didn't work; we changed the strategy and obtained NPs **47** with CUR decoration and with good stability during both the storage or *in vitro* and *in vivo* experiments.

Considering all the results presented above, it is clear that (i) these polymeric NPs present really interesting features - such as dimension and stability - (ii) the polymerization process with the CUR moiety did not interfere with the amphiphilic properties of the copolymers and (iii) the presence of a fluorescent dye can be a really important feature for possible future *in vitro* experiments.

CE-LIF studies and SPR binding results show that the PACA NPs **47** are able to interact with Aβ fibrils. The CE-LIF method suggested that the NPs **47** are capable of eliminating Aβ peptides from the solution, forming some kinds of aggregates that are not soluble at all. This might mean that this NPs could improve the elimination of the early stage of aggregation of the Aβ peptide, decreasing the formation of toxic species. Other interesting information came out from the SPR experiments; as just presented, the CUR derivative **4** showed a clear binding to immobilized $A\beta_{1-42}$ fibrils, with an estimated K_D value of 7 μM. In particular, a significant amount of binding to fibrils dissociates very slowly, indicating a persistent interaction.

Interestingly, the affinity of the CUR derivative-exposed on NPs **47** for $A\beta_{1-42}$ fibrils (0.3 μM) was higher than the affinity of a corresponding compound not attached to NPs. We suggest, also for this type of NPs, the involvement of multivalent interactions; this is potentially very useful in the attempt to target these AD pathogenic markers for diagnostic and/or therapeutic purposes.

Conclusions

As presented above, the aim of all my work was the synthesis of different types of nanoparticles (NPs) with an improved binding ability to Aβ peptides in different forms. The strategy adopted was to design, in the first step, a satisfactory ligand for Aβ peptides with both right physic-chemical properties and a functional group for chemoselective ligation. Looking at previously reported works, it is well known that there are a lot of natural small molecules that can interact with the species responsible for Alzheimer's Disease (AD) (Table 1). Among them, we decided to use curcumin (CUR) as molecule of reference and as starting material. As presented above, it is recognised by a lot of scientist that CUR has a huge field of applications, but its stability, solubility, bioavailability, safety and tolerability is still lacking. Considering all the literature, we noticed that the mixture of natural curcuminoid products is insoluble in water and its stability is unique. It is stable at acidic and high (> 11.7) pH, but unstable at neutral and quite basic pH. It is rapidly degraded within 30 min of placement in phosphate buffer systems of pH = 7.2. In comparison, CUR is more stable in cell culture medium containing 10 % fetal calf serum and in human blood, < 20% of CUR being degraded within 1 h and approximately 50% by 8 h.

Another distinctive aspect of CUR is the fact that in water environment it exists in an equilibrium of enolic and β diketonic forms. In solution CUR exists primarily in its enolic form and this is important for the radical-scavenging ability and for its Aβ-binding activities. As a matter of facts, it is important to lock the enol form of CUR, avoiding the presence of the equilibrium, and increasing the quantity of molecules that can interact with different forms of amyloid peptides.

There are also other three prominent features are important for the inhibition of amyloid aggregation: the presence of two aromatic end groups, the substitution pattern of these aromatics, and the length and flexibility of the linker region. In particular, two aromatic

rings need to be coplanar and the linker between them must be rigid and restricted between 8 and 16 Å. The modifications that don't influence these parameters could improve the ability of CUR against Aβ. In 2008, Narlawar *et al.*[167] replaced the 1,3-dicarbonyl moiety with isosteric heterocycles to lock its conformation into an enol-type arrangement.

Thinking about this information, we synthesized a new series of compounds, replacing the 1,3-dicarbonyl moiety with a pyrazole ring not only for the reasons reported above, but mainly for improving water solubility and stability at physiological pH, while preserving the best features in the interaction with Aβ-peptides.

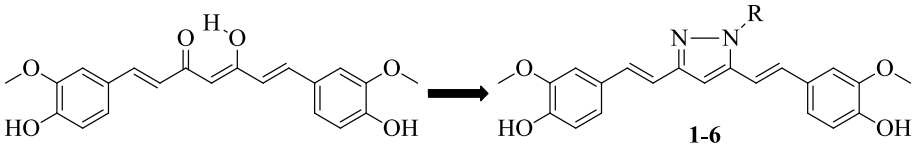

1-6

Figure 55: General structure of compounds 1-6.

All the synthesized CUR derivatives have an improved solubility (in particular in compound **3** that has a solubility greater than 1 mM in PBS, pH = 7.4), very high stability in all the type of organic or water mediums. We also obtained another important goal linked to their ability of interaction with Aβ. In fact, all the data presented above demonstrate that our derivatives retain CUR's ability to interfere with Aβ in all the different forms. From the NMR data, we demonstrated that the blocked CUR's enol-tautomer is implicated in the interaction with the $A\beta_{1-40}$ and $A\beta_{1-42}$ oligomers and no substitution on the pyrazole ring modify this property.

As a matter of facts, other experiments revealed that our compounds are able to modify the Aβ aptitude to form fibrils and fiber, obtaining some aggregates that are not related to these detrimental structures in AD patient's brains. We also found the ability of staining the Aβ plaque in *ex vivo* models without being involved in aspecific binding to tissue preparations. All these characteristics are important for future applications in both therapy and diagnosis of Aβ related disease.

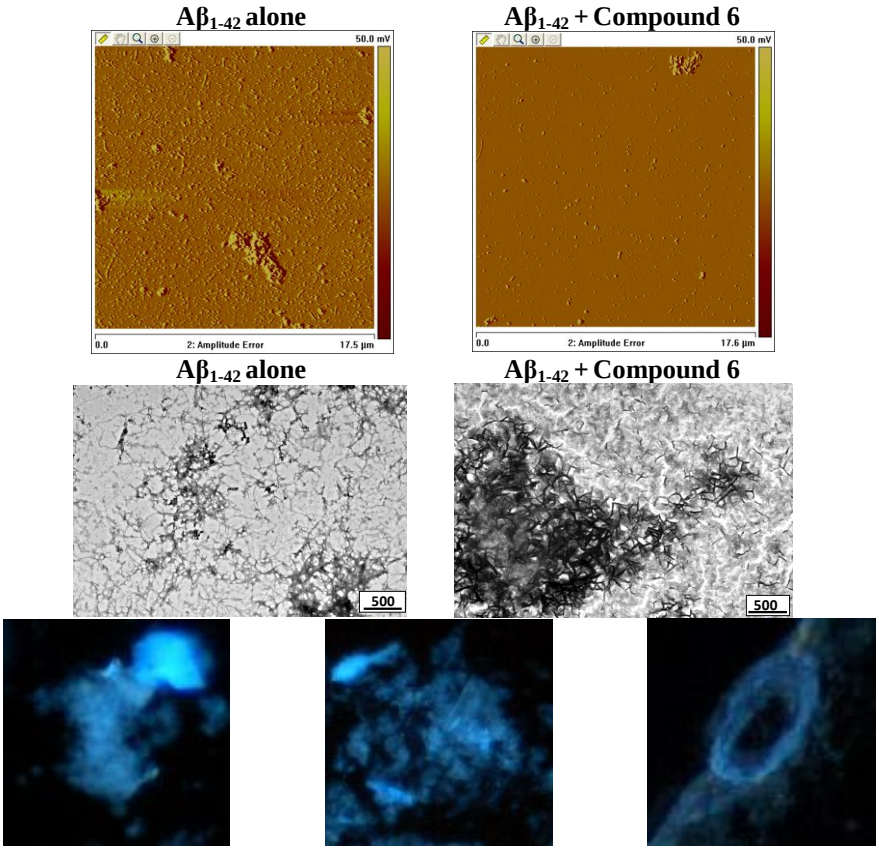

Figure 56: Examples of *in vitro* and *ex vivo* results obtained for compound 6; first row AFM experiment, second row TEM one, third row Tg CRND8 sections staining.

Another possibility for the application of the beneficial effects of CUR could be its attachment - in a stable way and active structural conformation - on the surface of biocompatible/biodegradable and stealth nanoparticles. Such attachment (on the surface of nanoparticles), might help to increase the drug bioavailability. Perhaps, it will further increase the binding affinity of CUR for Aβ peptides, because of the multivalency effect.

For this reasons, we set-up the decoration of three different types of NPs, in particular liposomes, solid lipid nanoparticles (SLN) and polymeric ones.

During the work, we synthesized different monomers for the linkage of a CUR derivative (**4**) with an alkyne moiety. For the lipid based NPs, we designed and obtained synthetic lipid as azido-functionalized monomers, with two fatty acid chain and a polyethylene glycol (PEG) chain as hydrophilic head. To obtain this compound we set up a successful, efficient, easy and direct procedure for the monofunctionalization of commercial PEG,

exploiting inexpensive silica gel as a solid support. After this we connected the hydrophobic and hydrophilic part of the anchor. We took advantage of the 1,3 Huisgen dipolar cycloaddition, to be sure that the linkage between them had the correct behaviour in water environment.
After these two preliminary synthesises, we moved on to the preparation and the decoration of three different type of NPs.

With regards to the lipid based NPs, we adopted the strategy of inserting the synthetic lipid inside the different structures of the nanodevices, before the linkage with the Aβ ligand. We made this decision to be sure that the CUR derivative was outside the lipidic region. In fact, it has an amphipatic behaviour and it may easily enter into the fatty layer.
Different preparations of liposomes and SLN were obtained with the synthetic lipid-PEG-N_3 **35** closely inserted inside the NPs. We functionalized and decorated them with the CUR derivative **4**, obtaining the desired nanostructures in very good yields, for both liposomes and SLNs. As presented above, the best results were obtained with liposomes. In fact, CUR decorated liposomes were prepared *via* a click chemistry method at room temperature, preserving the size distribution and the integrity of the NPs. This result is very important, since there is the possibility of using this method to drive important drugs to specific site of action, putting them inside liposomes that can be functionalized for targeting. The technique used herein for the formation of NPs was successful for preparing nanosized liposomes with an appropriate stability for the storage and for being used for *in vivo* applications (the same results were also obtained for SLNs). Taking into account the binding properties of the decorated liposomes **39**, we had demonstrated that they showed a clear binding to immobilized $A\beta_{1-42}$ fibrils. The estimated affinity (2-10 nM) was higher than the corresponding compound not attached to liposomes' one. We suggest the involvement of multivalent interactions; in particular, different molecules of CUR derivative on the same liposome could contribute to the binding to the immobilized $A\beta_{1-42}$ fibrils. This increased affinity resulted in the decrease of the dissociation rate constants and approached those of a pseudo-irreversible binding.

After these results, we moved to the functionalization of polymeric NPs - in particular nanodevices based on the poly-alchyl-cyanoacrylate (PACA) monomers. We tried the

same approach used for the lipid based NPs, but this did not allow us to obtained the desired structures. To overcome this problem, we shifted to the synthesis of the monomer before the formulation of the nanodispersion; this was possible thanks to the long hydrophilic PEG chain, that allowed the arrangement of the CUR derivative in the aqueous environment. After this first step, we were able to *co*-polymerize the monomer with the building blocks of the PACA NPs and to nanoprecipitate the resulting material, in order to obtain the desired decorated nanostructures. This technique was successful to prepare nanosized polymeric particles with an homogeneous population, as showed by the low polydispersity indices of the dispersions and the very high stability both for *in vivo* applications and storage. Following these results, we evaluate their Aβ binding ability with different *in vitro* techniques, in particular SPR and CE-LIF. The outcomes obtained from them suggested that also this type of NPs reveals some kinds of aspecific interactions with different $A\beta_{1\text{-}42}$ species. Using the SPR data, we were able to evaluate the binding ability of these NPs against $A\beta_{1\text{-}42}$ fibrils, revealing that also with them there are a sort of multivalent interaction, even if the calculated K_D (0.3 μM) is three times of magnitude higher than the one obtained for liposomes. This discrepancy may be caused by the different composition and/or structure of the NPs, but also for the very dissimilarity in the hydrophilic PEG chain. All this parameters can modify the ability of compounds or nanodevices to interact with the $A\beta_{1\text{-}42}$ species.

In conclusion, we judged that these data indicate that the decoration of different type of NPs with this CUR derivative provides them with a specific and high affinity binding for $A\beta_{1\text{-}42}$ fibrils. This is potentially very useful in the attempt to target these AD pathogenic markers for diagnostic and/or therapeutic purposes.

Supporting information

5.1. Chemical Synthesis

5.1.1. General comments

All commercial chemicals were purchased from Sigma-Aldrich. All chemicals were used without further purification, while all required anhydrous solvents were dried with molecular sieves, for at least 24 h prior to use. Rhodamine B alcohol and was synthesized as described elsewhere. Thin layer chromatography (TLC) was performed on silica gel 60 F_{254} plates (Merck) with detection using UV light when possible, or by charring with a solution of $(NH_4)_6Mo_7O_{24}$ (21 g), $Ce(SO_4)_2$ (1 g), concentrated H_2SO_4 (31 mL) in water (500 mL) or with an ethanol solution of ninhydrin or with Dragendorff' spray reagent.[279] Flash column chromatography was performed on silica gel 230-400 mesh (Merck). ^{1}H and ^{13}C NMR spectra were recorded at 25 °C unless otherwise stated, with a Varian Mercury 400 MHz instrument. Chemical shift assignments, reported in ppm, are referenced to the corresponding solvent peaks. MS were recorded on a QTRAP system with ESI source while HRMS were registered on a QSTAR elite system with a nanospray ion source.

5.1.1.1. *Chemical synthesis figure list*

5.1.2. Typical reaction conditions

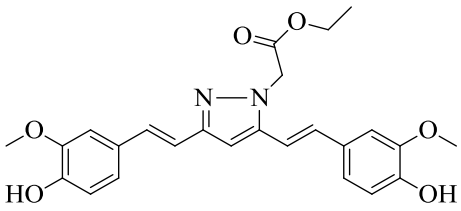

Figure S1: Chemical structure of compound 1.

ethyl 2-(3,5-bis((E)-4-hydroxy-3-methoxystyryl)-1H-pyrazol-1-yl)acetate (1): To a solution of Curcumin (1 g, 2.7 mmol, 1 eq) in Toluene dry (28 mL) was added ethyl 2-hydrazinylacetate hydrochloride (0.839 g, 5.4 mmol, 2 eq), triethylamine (0.753 mL, 5.4 mmol, 2 eq), TFA (0.1 mL, 1.3 mmol, 0.5 eq) and held at reflux for 2.5 hours. The reaction

was monitored by TLC. The reaction mixture was then cooled to ambient temperature, diluted with CH_2Cl_2 and washed with HCl $5\%_{(aq)}$ twice. The organic phase was dried with Na_2SO_4 and evaporated in vacuum to afford the crude product which was further purified by flash column chromatographic (CH_2Cl_2/isopropanol 98/2) to afford the desired product as yellow solid (1.058 g, 87%). ^{1}H NMR (400 MHz, DMSO d_6) δ ppm 7.22 – 6.70 (m, 11H, C*H* Ar and conjugated double bond), 5.16 (s, 2H CH_2C=O), 4.13 (q, J = 7.05 Hz, 2H, OCH_2CH$_3$), 3.82 – 3.77 (m, 6H, OCH_3), 1.19 (t, J = 7.12 Hz, 3H, OCH$_2$$CH_3$). ^{13}C NMR (100 MHz, DMSO d_6) δ 168.32 (C=O), 150.02, 147.86, 147.27, 146.68, 143.35 (5 CqAr), 132.25, 129.79 (2 CHAr), 128.49, 128.06 (2 CqAr), 120.81, 120.01, 117.75, 115.57, 111.66, 110.24, 109.58, 98.63 (8 CHAr and conjugated double bond), 61.11 (CH_2), 55.76, 55.59 (2 CH_3), 50.30 (CH_2), 14.09 (CH_3). MS (ESI) calcd for $[M + H]^+$ 451.48; found $[M + H]^+$ 451.60.

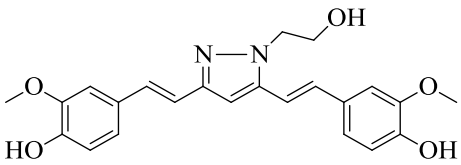

Figure S2: Chemical structure of compound 2.

4,4'-((1E,1'E)-(1-(2-hydroxyethyl)-1H-pyrazole-3,5-diyl)bis(ethene-2,1-diyl))bis(2-methoxyphenol) (2): To a solution of 1 (0.605 g, 1.34 mmol, 1 eq) in THF dry (20 mL) at 0°C was added dropwise $LiAlH_4$ 1M in THF(5.4 mL, 5.37 mmol, 4 eq). The temperature was raised to r.t. and the reaction was monitored by TLC. After the disappearance of the starting material the reaction mixture was cooled to 0 °C and the following solutions were added in the order indicated: H_2O (0.21 mL), $NaOH_{(aq.)}$ 4 M (0.26 mL), H_2O (0.65 mL), Na_2SO_4 (1.52 g). The reaction mixture was then filtrated in and the solvent was evaporated in vacuum. The crude product was further purified by flash column chromatographic (CH_2Cl_2/ ethanol 98/2) to afford the final product as a bright yellow powder (0.38 g, 70%). The ^{1}H-NMR and ^{13}C-NMR agree with the characterization reported by Narlawar *et al*..[167]

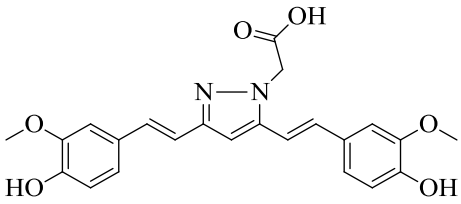

Figure S3: Chemical structure of compound 3.

2-(3,5-bis((E)-4-hydroxy-3-methoxystyryl)-1H-pyrazol-1-yl)acetic acid (3): Compound 1 (3g, 6,66 mmol, 1 eq) was dissolved in a methanolic solution of KOH 1.8M (70 mL). The solution was left under magnetic stirring at r. t. over night. The reaction was monitored by TLC. The solvent was evaporated in vacuum and purified by flash column chromatographic (eluent ethyl acetate/methanol gradient from 9/1 to 7/3) to afford the final product (2.813 g, quant.). ^{1}H NMR (400 MHz, CD_3OD) δ ppm 7.23 – 6.72 (m, 11H, C*H* Ar and conjugated double bond), 4.93 (s, 2H, *CH*$_2$C=O), 3.85 – 3.79 (m, 6H, OC*H*$_3$). ^{13}C NMR (100 MHz, DMSO) δ 170.17 (C=O), 147.85, 147.16, 146.58, 142.80 (4 CqAr), 131.54, 129.13 (2 CHAr), 128.62, 128.17 (2 CqAr), 120.61, 119.87, 118.08, 115.58, 112.31, 110.08, 109.53, 98.38 (8 CHAr and conjugated double bond), 55.74, 55.58 (2 CH_3), 51.58 (CH_2). MS (ESI) calcd for $[M + H]^+$ 423.43; found $[M + H]^+$ 423.4.

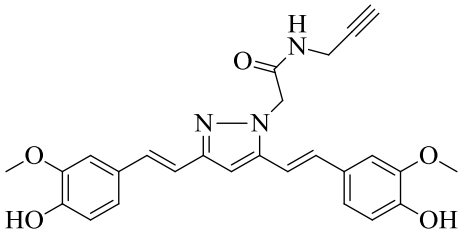

Figure S4: Chemical structure of compound 4.

2-(3,5-bis((E)-4-hydroxy-3-methoxystyryl)-1H-pyrazol-1-yl)-N-(prop-2-yn-1-yl)acetamide (4): HOBt (0.017 g, 0.123 mmol, 1.23 eq) and TBTU (0.039 g, 0.12 mmol, 1.2 eq) were added to a solution of the compound 3 (0.042 g, 0.1 mmol, 1 eq) in DMF dry (1mL). The reaction mixture was left in the dark, at r.t., under magnetic stirring for 15 minutes. Propargylamine (0.013mL, 0.2 mmol, 2 eq) and triethylamine (0.07 mL, 0.5 mmol, 5 eq) were added and the reaction was left in the dark, at r.t., under magnetic stirring over night. The reaction was monitored by TLC. The solvent was evaporated in vacuum. The crude product was diluted with CH_2Cl_2 and washed three times with water.

The organic phase was dried with Na_2SO_4 and evaporated in vacuum to afford the crude product which was further purified by flash column chromatographic (eluent petroleum ether/ethyl acetate gradient from 3/7 to ethyl acetate) to afford the desired product as a powder (0.031 g, 68%). ^{1}H NMR (400 MHz, CD_3OD) δ ppm 7.38 – 6.73 (m, 11H, C*H* Ar and conjugated double bond), 5.12 (s, 2H *CH*$_2$C=O), 4.04 (s, 2H, *CH*$_2$NH), 3.96 – 3.83 (m, 6H, OC*H*$_3$), 2.63 (s, 1H, *CH*). ^{13}C (100 MHz, $CDCl_3$) δ ppm 169.31 (C=O) 152.55, 149.33, 148.03, 145.63 (4Cq Ar), 135.08, 132.22 (2 CHAr), 130.75, 130.13 (2 CqAr), 122.07, 121.40, 118.27, 116.46, 112.40, 111.08, 110.70, 100.52 (8 CHAr and conjugated double bond),80.27 (Cq), 72.42 (CH), 56.64, 56.55(2 CH_3), 52.66 (CH_2), 29.71(CH_2). MS (ESI) calcd for $[M + H]^+$ 456.49; found $[M + H]^+$ 460.4.

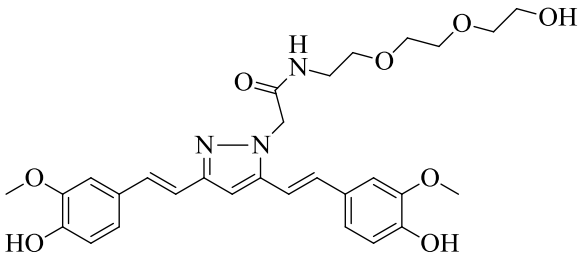

Figure S5: Chemical structure of compound 5.

2-(3,5-bis((E)-4-hydroxy-3-methoxystyryl)-1H-pyrazol-1-yl)-N-(2-(2-(2-hydroxyethoxy)ethoxy)ethyl)acetamide (5): HOBt (0.04 g, 0.291 mmol, 1.23 eq) and TBTU (0.091 g, 0.285 mmol, 1.2 eq) were added to a solution of the compound 3 (0.1 g, 0.237 mmol, 1 eq) in DMF dry (1.05 mL). The reaction mixture was left in the dark, at r.t., under magnetic stirring for 15 minutes. 2-(2-(2-aminoethoxy)ethoxy)ethanol 9 (0.071 g, 0.474 mmol, 2 eq) and triethylamine (0.2mL, 01.435 mmol, 6 eq) were added as a solution in DMF dry (0.5mL) and the reaction was left in the dark, at r.t., under magnetic stirring over night. The reaction was monitored by TLC. The solvent was evaporated in vacuum. The crude product was purified by flash column chromatographic (eluent petroleum ether/ethyl acetate gradient from 1/4 to ethyl acetate/ethanol 9/1) to afford the desired product (0.048 g, 37%). ^{1}H NMR (600 MHz, D_2O) δ ppm 7.27 – 7.07 (m, 6H C*H* Ar and conjugated double bond), 6.96 – 6.90 (m, 3H C*H* Ar and conjugated double bond), 6.85 – 6.78 (m, 2H C*H* Ar and conjugated double bond), 3.93 – 3.87 (m, 6H, OC*H*$_3$), 3.61 – 3.58 (m, 2H, CH_2CH_2OH), 3.57 – 3.53 (m, 2H, OC*H*$_2$$CH_2$OH), 3.52 – 3.49 (m, 2H, OC*H*$_2$$CH_2$N), 3.46 – 3.40 (m, 6H, C*H*$_2$O, OCH_2CH_2N). ^{13}C NMR (100 MHz, MeOD) δ

169.70 (C=O), 149.22, 148.52, 147.88, 145.58, 142.70 (5 CqAr), 134.99, 132.18 (2 CHAr), 130.53, 129.97 (2 CqAr), 121.99, 121.32, 118.07, 116.34, 112.22, 110.73, 110.28, 100.26 (8 CHAr and conjugated double bond), 73.44, 71.31, 71.20, 70.47, 70.37 (5 CH_2), 56.45, 56.35 (2 CH_3), 52.62, 40.39 (2 CH_2). MS (ESI) calcd for $[M + H]^+$ 554.60; found $[M + H]^+$ 554.70.

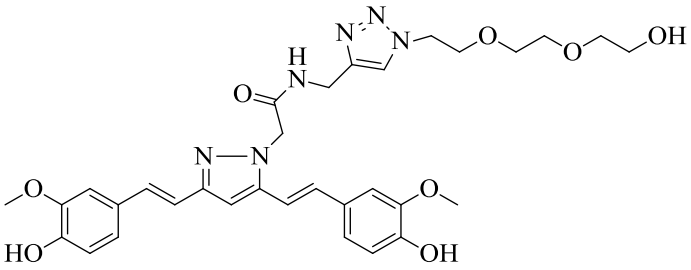

Figure S6: Chemical structure of compound 6.

2-(3,5-bis((E)-4-hydroxy-3-methoxystyryl)-1H-pyrazol-1-yl)-N-((1-(2-(2-(2-hydroxyethoxy)ethoxy)ethyl)-1H-1,2,3-triazol-4-yl)methyl)acetamide (6): $CuSO_4 \cdot 5H_2O$ (0.057 mg, 0.228 mmol, 1.2 eq) was dissolved in water (2 mL) and sodium ascorbate (0.057 g, 0.285 mmol, 1.5 eq) was added. . The reaction was stirred until the formation of an orange suspension. This freshly prepared catalyst was added to a solution of compond **4** (0.086 g, 0.19 mmol, 1 eq) and 2-(2-(2-azidoethoxy)ethoxy)ethanol **8** (0.252 g, 0.91 mmol, 1.2 eq) in THF (12 mL), stirring at r.t. until the formation of a light blue precipitate, which was removed by filtration. The crude product was purified by flash column chromatographic (eluent gradient from ethyl acetate to ethyl acetate/methanol 9/1) to afford the desired product (0.103 g, 72%). ^{1}H NMR (400 MHz, CD_3OD) δ ppm 7.83 (s, 1H, *H* triazole), 7.16 – 6.72 (m, 11H C*H* Ar and conjugated double bond), 4.97 (s, 2H, CH_2C=O), 4.47 (s, 2H, NHCH_2), 4.38 (t, *J* = 4.99 Hz, 2H, NCH_2CH_2O), 3.91 – 3.86 (m, 6H, OCH_3), 3.75 (t, *J* = 4.93, 2H, NCH$_2CH_2$O), 3.64 – 3.57 (m, 2H, OCH$_2$CH_2OH), 3.55 – 3.49 (m, 4H, OCH_2CH$_2$OH, OCH_2CH_2O), 3.48 – 3.43 (m, 2H, CH_2O). ^{13}C NMR (100 MHz, MeOD) δ 169.65 (C=O), 152.46, 149.30, 149.23, 147.98, 145.81, 145.55 (6 CqAr), 134.92, 132.19 (2 CHAr), 130.59, 129.96 (2 CqAr), 125.11, 122.03, 121.35, 118.14, 116.36, 112.28, 110.71, 110.35, 100.33 (9 CHAr and conjugated double bond), 73.62, 71.39, 71.34, 70.22, 62.20 (5 CH_2), 56.49, 56.39 (2 CH_3), 51.28, 35.78 (2 CH_2).MS (ESI) calcd for $[M + H]^+$ 635.28; found $[M + H]^+$ 635.5.

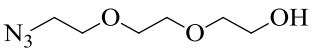

Figure S7: Chemical structure of 2-(2-(2-azidoethoxy)ethoxy)ethanol.

2-(2-(2-azidoethoxy)ethoxy)ethanol: this compound was sinthesyze according to the procedure of Schneekloth *et al.*.[280]

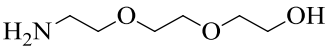

Figure S8: Chemical structure of 2-(2-(2-aminoethoxy)ethoxy)ethanol.

2-(2-(2-aminoethoxy)ethoxy)ethanol: 2-(2-(2-azidoethoxy)ethoxy)ethanol (200 mg, 1.14 mmol, 1 eq) was dissolved in methanol and Pd Lindlar on charcoal was added to the solution. The black suspension was stirred under hydrogen atmosphere over night at r.t. The resulting mixture was filtered through a nylon membrane filter 0.45 μm to obtain the analytically pure 2-(2-(2-aminoethoxy)ethoxy)ethanol in a quantitative yield. The ^{1}H-NMR and ^{13}C-NMR agree with the characterization reported by Sato *et al.*.[281]

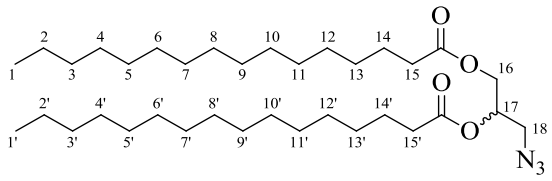

Figure S9: Chemical structure of 24.

3-deoxy-3-azido-1,2-dipalmitoyl-*sn*-glycerol (24): The 3-azido-1,2-diol-propane **26** was synthesized according to the procedure of Kazemi *et al.*.[282] Lithium tetrafluoroborate (0.190 g, 2 mmol, 0.2 eq) and sodium azide (1.30 g, 20 mmol, 2 eq) were added to a solution of 2-oxiranylmethanol (0.660 mL, 10 mmol, 1 eq) in 30 mL of *t*-butanol/H_2O (30:1). The reaction mixture was stirred under reflux for 2 h. The solvent was removed and the crude product was purified by chromatography on short column of silica-gel to eliminate salts. This purified azido alcohol, as a very unstable compound, was used in the next step without further characterization. Palmitoyl chloride (6.55 mL, 21.6 mmol, 2.4 eq) was added dropwise under argon to a solution of 1 (1.05 g, 9 mmol, 1 eq) and dry pyridine (2.9 mL, 36 mmol, 4 eq) in dry CH_2Cl_2 (50 mL). The resulting solution was stirred until

disappearance of starting material. The reaction mixture was diluted with CH_2Cl_2 and washed with an aqueous solution of HCl (5 %) and the aqueous layer was extracted with CH_2Cl_2 three times. The combined organic layer was dried with Na_2SO_4 and evaporated. The crude was purified by flash chromatography (eluent petroleum ether/AcOEt 99/1) to afford the title compound **2** (4.45 g, 7.5 mmol, 75 % over the two steps) as white wax. ^{1}H NMR (400 MHz, $CDCl_3$) δ ppm 5.21 – 5.14 (m, 1H, 17), 4.29 (dd, *J* = 11.9, 4.4 Hz, 1H, 16a), 4.14 (dd, *J* = 11.9, 5.6 Hz, 1H, 16b), 3.46 (m, 2H, 18), 2.38 – 2.28 (m, 4H, 15,15'), 1.68 – 1.56 (m, 4H, 14,14'), 1.25 (bs, 48H, 2-13, 2'-13'), 0.88 (t, *J* = 6.6 Hz, 6H, 1,1'); ^{13}C (100 MHz, $CDCl_3$) δ ppm 173.40, 173.03 (2 C=O), 70.08 (CH), 62.49, 51.07, 34.39, 34.24, 32.16, 29.93, 29.89, 29.85, 29.70, 29.60, 29.49, 29.33, 29.29, 25.08, 25.03, 22.92 (16 CH2), 14.34(CH3); MS (ESI) calcd for $[M + H]^+$ 594.93; found $[M + H]^+$ 594.89.

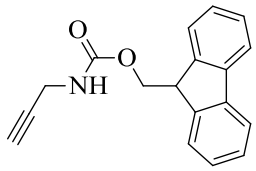

Figure S10: Chemical structure of 33.

(9H-fluoren-9-yl)methyl prop-2-yn-1-ylcarbamate (33): Commercial propargylamine (0.277 mL, 4.34 mmol, 1 eq) was dissolved in dioxane (17 mL) and a 0.8 M aqueous solution of Na_2CO_3 (14 mL) was added. A solution of FmocCl (1.343 g, 5.2 mmol, 1.2 eq) in dioxane (17 mL) was freshly prepared and added dropwise to the amine solution. The reaction was stirred for 1 h, until the disappearance of the starting material. The mixture was diluted with ethyl acetate and washed with H_2O three times. The organic layer was dried with Na_2SO_4 and concentrated. The crude solid was recrystallized from EtOAc to afford compound 6 (0.780 g, 2.81 mmol, 65 %) as white powder. The ^{1}H-NMR and ^{13}C-NMR agree with the characterization reported by Horne *et al.*.[283]

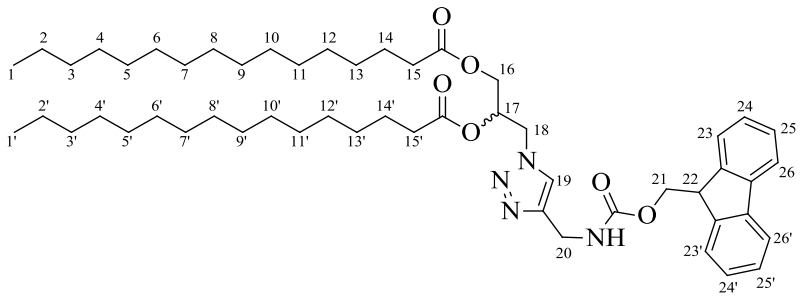

Figure S11: Chemical structure of 34.

3-deoxy-1,2-dipalmitoyl-3-(4'-(9H-fluoren-9''-yl)methoxy-methylcarbamoyl-1H-1',2',3'-triazol-1'-yl)-*sn*-glycerol (34): $CuSO_4 \cdot 5\ H_2O$ (0.227 g, 0.91 mmol, 1.2 eq) was dissolved in H_2O (4 mL) and sodium ascorbate (0.226 g, 1.14 mmol, 1.5 eq) was added. The solution was stirred until the formation of an orange suspension. This freshly prepared catalyst was added to a solution of compound **24** (0.450 g, 0.76 mmol, 1 eq) and compound **33** (0.252 g, 0.91 mmol, 1.2 eq) in THF (12 mL), stirring at R.T. until the formation of a light blue precipitate, which was removed by filtration. The filtrate was diluted with ethyl acetate and washed with water three times. The combined organic layer was anhydrificated with Na_2SO_4 and evaporated under reduced pressure. The crude product was purified by flash chromatography (eluent petroleum ether/ethyl acetate gradient from 9/1 to 1/1) to afford the compound **3** (0.578 mg, 0.66 mmol, 87%) as light yellow oil. ^{1}H NMR (400 MHz, $CDCl_3$) δ ppm 7.75 (d, *J* = 7.5 Hz, 2H, 26,26'), 7.60 – 7.54 (m, 3H, 19,23,23'), 7.39 (t, *J* = 7.4 Hz, 2H, 25,25'), 7.29 (t, *J* = 7.4 Hz, 2H, 24,24'), 5.55 – 5.48 (m, 1H, N*H*), 5.42 – 5.32 (m, 1H, 17), 4.63 – 4.52 (m, 2H, 18), 4.49 – 4.43 (m, 2H, 17), 4.41 – 4.35 (m, 2H, 21), 4.30 (dd, *J* = 12.1, 4.4 Hz, 1H, 16a), 4.24 – 4.13 (m, 1H, 22), 4.05 (dd, *J* = 12.1, 5.2 Hz, 1H, 16b), 2.37 – 2.24 (m, 4H, 15,15'), 1.66 – 1.48 (m, 4H, 14,14'), 1.36 – 1.17 (m, 48H, 2-13, 2'-13'), 0.87 (t, *J* = 6.8 Hz, 6H, 1,1'); ^{13}C NMR (100 MHz, $CDCl_3$) δ ppm 173.37, 172.79, 156.62 (3 C=O), 145.46, 144.01, 141.51 (3 CqAr), 127.94, 127.27, 125.29, 123.24, 120.23 (5 CHAr), 69.51 (CH), 67.16, 62.19, 50.31 (3 CH_2), 47.35 (CH), 36.61, 34.24, 32.17, 29.95, 29.92, 29.88, 29.73, 29.62, 29.53, 29.50, 29.37, 29.27, 25.08, 24.97, 22.95 (15 CH_2), 14.40 (CH_3); MS calcd for $[M + H]^+$ 872.27; found $[M + H]^+$ 872.24.

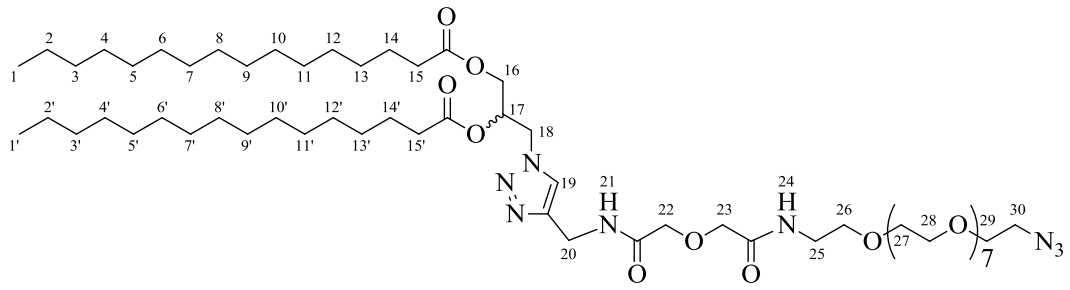

Figure S12: Chemical structure of 35.

3-deoxy-1,2-dipalmitoyl-3-(4'-methyl (O-(2-azidoethyl)-heptaethylenglycol-2-yl)-ethylcarbamoylmethoxy ethylcarbamoyl-1H-1',2',3'-triazol-1'-yl)-*sn*-glycerol (35) [Lipid-PEG-N_3]:

Compound **34** (0.250 g, 0.29 mmol, 1.1 eq) was dissolved in dry DMF (3 mL) and piperidine (26 μL, 10 μL/0.11 mmol) was added. The reaction was stirred until the complete disappearance of the starting material. The reaction mixture was evaporated under high vacuum to afford the analytically pure compound **22**. This compound was dissolved in CH_2Cl_2 (5 mL) and was added dropwise to a solution of O-(2-azidoethyl)-O'-(N-diglycolyl-2-aminoethyl)heptaethyleneglycol (0.145 g, 0.26 mmol, 1 eq), TBTU (0.109 g, 0.34 mmol, 1.3 eq) and DIPEA (60 μL, 0.34 mmol, 1.3 eq) in CH_2Cl_2 after 20 min of stirring. The reaction mixture was stirred for 3 days until the disappearance of the starting polyethyleneglycol compound. The reaction solution was evaporated under reduced pressure and the crude product was purified by flash chromatography (eluent ethyl acetate/methanol 95/5) do afford the compound **35** (0.285 g, 0.24 mmol, 92 %), as white solid. ^{1}H-NMR (400 MHz, $CDCl_3$) δ ppm 7.91 – 7.84 (m, 1H, 21), 7.60 (s, 1H, 19), 7.48 – 7.40 (m, 1H, 24), 5.34 – 5.27 (m, 1H, 17), 4.53 – 4.44 (m, 4H, 18,20), 4.25 (dd, *J* = 12.1, 4.0 Hz, 1H, 16a), 4.02 – 3.94 (m, 5H, 16b,22,23), 3.65 – 3.53 (m, 32H, 26,27,28,29), 3.47 – 3.38 (m, 2H, 25), 3.36 – 3.29 (m, 2H, 30), 2.30 – 2.19 (m, 4H, 15,15'), 1.60 – 1.45 (m, 4H, 14,14'), 1.30 – 1.13 (m, 48H, 2-13, 2'-13'), 0.81 (t, *J* = 6.6 Hz, 6H, 1,1'); ^{13}C NMR (100 MHz, $CDCl_3$) δ ppm 173.28, 172.73, 169.15, 168.92 (4 C=O), 145.07 (CqAr), 123.82 (CHAr), 71.05, 70.96, 70.78, 70.61, 70.19, 69.94 (6 CH_2), 69.49 (CH), 62.16, 50.81, 50.24, 38.98, 34.36, 34.15, 32.10, 29.88, 29.84, 29.81, 29.67, 29.54, 29.46, 29.45, 29.30, 29.21, 25.01, 24.91, 22.87 (19 CH_2), 14.33 (CH_3); HRMS calcd for $[M + Na]^+$ 1207.8139; found $[M + Na]^+$ 1207.8204.

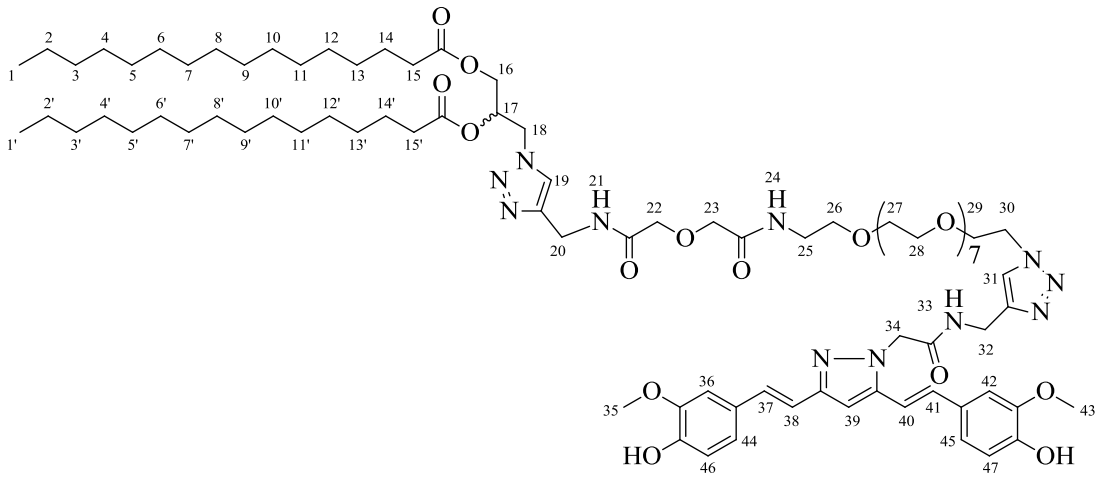

Figure S13: Chemical structure of 36.

3-deoxy-1,2-dipalmitoyl-3-(4'-(O-(2-(4''-(2-(3''',5'''-di(4-hydroxy-3-metoxystyryl)-1H-pyrazol-1'''-yl)-ethylcarbamoyl)-methyl-1H-1'',2'',3''-triazol-1''-yl-ethyl)-heptaethylenglycol-2-yl)-ethylcarbamoylmethoxyethylcarbamoyl-methyl-1H-1',2',3'-triazol-1'-yl)-sn-glycerol (36): For this synthesis two different procedures were followed:

Procedure A: $CuSO_4 \cdot 5\ H_2O$ (0.007 g, 27.5 μmol, 1.2 eq) was dissolved in H_2O (0.6 mL) and sodium ascorbate (0.007 g, 34.4 μmol, 1.5 eq) was added. The solution was stirred until the formation of an orange suspension. This freshly prepared catalyst was added to a solution of compound **35** (0.027 g, 23 μmol, 1 eq) and compound **4** (0.013 g, 27.5 μmol, 1.2 eq) in THF (1.8 mL). The mixture was stirred at r.t. until the formation of a light blue precipitate, which was removed by filtration. The filtrate was evaporated under reduced pressure. The crude product was purified by flash chromatography (eluent ethyl acetate /methanol 85/15) to afford the compound **36** (0.025 g, 15.2 μmol, 87%) as brown wax. ^{1}H-NMR (400 MHz, $CDCl_3$) δ ppm 8.03 - 7.91 (m, 1H, 21), 7.75 - 7.60 (m, 2H, 19,31), 7.50 – 7.43 (m, 1H, 24), 7.19 – 7.06 (m, 1H, 33), 7.08 – 6.81 (m, 9H, 36,37,39,41,42,44,45,46,47), 6.73 – 6.61 (m, 2H, 38,40), 5.41 – 5.30 (m, 1H, 17), 4.91 (s, 2H, 34), 4.60 – 4.46 (m, 6H, 20,32,18), 4.41 – 4.33 (m, 2H, 30), 4.29 (dd, *J* = 11.5, 3.5 Hz, 1H, 16a), 4.06 – 3.97 (m, 5H, 16b,22,23), 3.96 – 3.84 (m, 6H, 35,43), 3.71 – 3.79 (m, 2H, 29), 3.65 – 3.50 (m, 30H, 28,27,28), 3.49 – 3.43 (m, 2H, 25), 3.42 – 3.34 (m, 2H, 30), 2.35 – 2.23 (m, 4H, 15,15'), 1.67 – 1.52 (m, 4H, 14,14'), 1.35 – 1.15 (m, 48H, 2-13,2'-13'), 0.86 (t, *J* = 6.2 Hz, 6H, 1,1'); ^{13}C NMR (100 MHz, $CDCl_3$) δ ppm 173.41, 172.86, 169.32, 169.12, 167.84 (5 C=O), 147.33, 147.16, 146.98, 146.16 (4 CqAr), 134.21, 131.09 (2

CHAr), 129.62, 128.67 (2 CqAr), 121.31, 120.89, 117.87, 115.20, 114.94, 111.15, 108.93, 108.36 (8 CHAr and CH conjugated C=C), 70.97, 70.93, 70.60, 70.25, 69.96 (5 CH_2), 69.52 (CH), 69.45 (CH_2), 68.51 (CH), 68.23, 62.21 (2 CH_2), 56.29, 56.09 (2 CH), 50.40, 39.05, 35.15, 34.20, 32.14, 29.92, 29.88, 29.72, 29.59, 29.50, 29.35, 29.26, 25.05, 24.95, 22.92 (15 CH_2), 19.03, 14.37 (2 CH_3); MS calcd for $[M + Na]^+$ 1666.99; found $[M + Na]^+$ 1667.14.

Procedure B: CUR-alkyne derivative **4** (7 mg, 15.18 µmole, 1.2 eq), Lipid-peg-N_3 **35** (15 mg, 12.6 µmol, 1 eq), CuBr (3.63 mg, 25.3 µmol, 2 eq) and PMDTA (21.1 µl, 101.2 µmole, 8 eq) were dissolved in 700 µl Acetonitrile (AcCN). Sodium ascorbate in H_2O (10 mg, 50.6 µmole, 2 eq) was added and the reaction mixture was sealed and kept at room temperature. TLC and HPLC analysis of the reaction mixture showed that 10 min after sodium ascorbate addition 9 was completely reacted and 10 was selectively produced. The reaction mixture was vortexed to remove a light blue precipitate formed during the reaction and the reaction mixture was subjected to purification. AcCN was removed under reduced pressure and the oily product was re-dissolved in $CHCl_3$. The chloroform phase was acidified with 5% aq. HCl and extracted three times with 0.05% aq. NaCl. The organic phase was dried over Na_2SO_4 and was further purified using a 10 mL silica gel column using $CHCl_3$/MeOH (9:1) as eluent to afford 10 (19.15 mg, 11.64 µmol, 92%). ^1H and ^{13}C-NMR analysis had the same profile as in procedure A. MS calcd for $[M + H]^+$ 1645.01; found $[M + H]^+$: 1645.48.

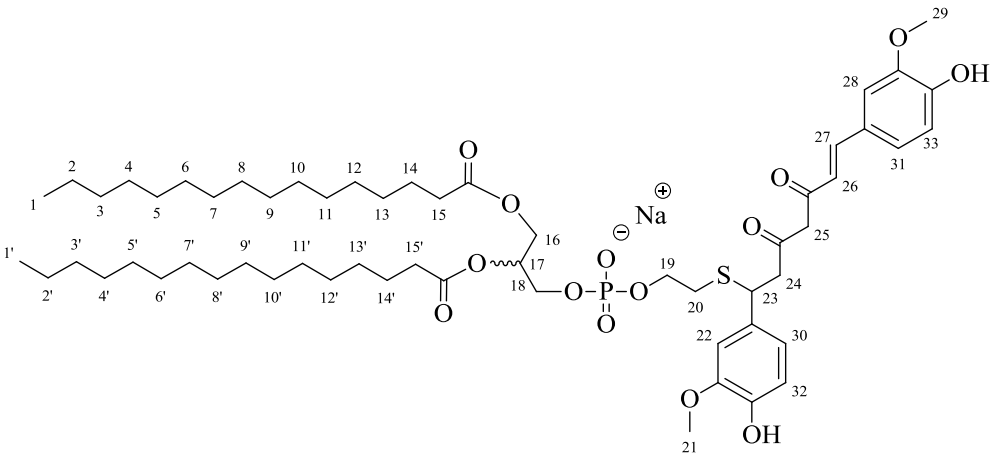

Figure S14: Chemical structure of 37.

1,2-dipalmitoyl-3-(2-(1,7-bis(4-hydroxy-3-methoxyphenyl)-3,5-dioxohept-6-enylthio)ethylphospho)-*sn*-glycerol [DPS-curcumin] (37): Curcumin (0.129 g, 0.35 mmol, 3 eq) was dissolved in CH_2Cl_2 and DIPEA (1.76 mmol, 0.3 mL, 15 eq). The mixture is flushed with N_2 at r.t. for 10 min and 1,2-dipalmitoyl-*sn*-glycero-3-phosphothioethanol (sodium salt) [DPSH] (0.085 g, 0.12 mmol, 1 eq) dissolved in N_2 degassed CH_2Cl_2 is added slowly within 2 hours. The mixture is further reacted overnight under continuous N_2 atmosphere at r.t.. The reaction mixture is subjected to purification using a 20 mL silica gel column prewashed with 100 mL $CHCl_3$. The silica was washed with additional 20 mL $CHCl_3$ followed by 20 mL of each of the following $CHCl_3$/MeOH mixtures: 40/1, 30/1, 20/1, 15/1, 12.5/1, 10/1, 7.5/1, 5/1, 4/1, 3/1, MeOH. Fractions 5/1 and 4/1 were combined and concentrated under reduced pressure to afford 11 (96.74 mg, 0.088 mmol, 75 %). ^{1}H NMR (400 MHz, MeOD) δ ppm 7.47-6.55 (m, 8H, 22,26,27,28,30,31,32,33), 5.22-5.12 (m, 1H, 17), 4.6-4.53 (m, 1H, 23), 4.38 (dd, 1H, 16a), 4.30-4.11 (m, 3H, 16b, 25), 4.04-3.92 (m, 4H, 18, 19), 3.90-3.82 (m, 6H, 21,29), 2.93-2.7 (m, 3H, 20, 24a), 2.6-2.49 (m, 1H, 24b), 2.3-2.2 (m, 4H, 15, 15´), 1.67-1.5 (m, 4H, 14´, 14´´), 1.40-1.20 (m, 48H, 2-13, 2´-13´), 0,90 (t, 6H, 1, 1´), OH signal not detected; ESI-MS: $[M + Na]^+$ calc. 1121.57 $[M + Na]^+$ found: 1121.88.

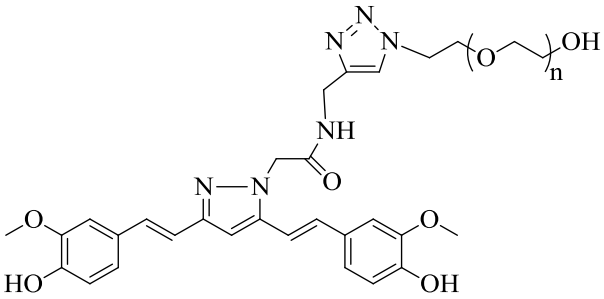

Figure S15: Chemical structure of 44.

Cur-PEG$_{2000}$ conjugate (44): $CuSO_4 \cdot 5\ H_2O$ (0.011 g, 44 μmol, 1.2 eq) was dissolved in H_2O (1 mL) and sodium ascorbate (0.011 g, 55.5 μmol, 1.5 eq) was added. The solution was stirred until the formation of an orange suspension. This freshly prepared catalyst was added to a solution of compound **4** (0.027 g, 44 μmol, 1.2 eq) and compound **43** (0.075 g, 37 μmol, 1 eq) - synthesized as presented by Nicolas *et al.*[273] - in THF (3 mL). The mixture was stirred at r.t. until the formation of a light blue precipitate, which was removed by

filtration. The filtrate was evaporated to remove organic solvent under reduced pressure. A solution of EDTA 1 M (1 mL) was then added to the aqueous residue and it was dialyzed extensively. The purification afforded the compound **44** (0.080 g, 32 μmol, 86%) as brown wax. ^{1}H NMR (300 MHz, $CD_3(C=O)CD_3$) δ ppm 7.83 (s, 1H, *H* triazole), 7.16 – 6.72 (m, 11H C*H* Ar and conjugated double bond), 4.97 (s, 2H, CH_2C=O), 4.47 (s, 2H, NHCH_2), 4.38 (bt, 2H, NCH_2CH_2O), 3.91 – 3.86 (m, 6H, OCH_3), 3.62–3.45 (m, 188H, OCH_2CH_2O).

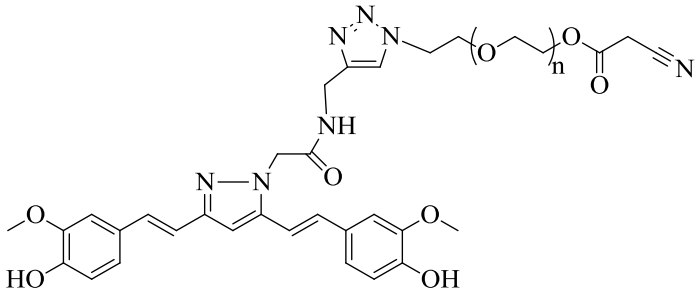

Figure S16: Chemical structure of 45.

Cur-PEG$_{2000}$-CA (45): In a 25 mL round bottom flask containing Cur-PEG$_{2000}$ **44** (0.0654 g, 26.3 μmol, 1 eq), cyanoacetic acid (0.00027 g, 31.6 μmol, 1.2 eq) and CH_2Cl_2/AcOEt (2:1, 1 mL) were introduced dropwise by a syringe, a solution of DCC (0.0065 g, 31.6 μmol, 1.2 eq) and DMAP (catalytic amount) in CH_2Cl_2/AcOEt (2:1, 0.5 mL). The reaction medium was stirred during 24 h at room temperature under argon atmosphere. The solid was filtered off and the solvent was removed under reduced pressure. The solid was then purified by precipitation from cold Et_2O, filtered and dried under vacuum overnight to give a fine, white powder: 0.050 g (74 %). ^{1}H NMR (300 MHz, $CD_3(C=O)CD_3$) δ ppm 7.83 (s, 1H, *H* triazole), 7.16 – 6.72 (m, 11H C*H* Ar and conjugated double bond), 4.97 (s, 2H, CH_2C=O), 4.47 (s, 2H, NHCH_2), 4.32 (bt, 2H, COOCH_2CH_2), 4.38 (bt, 2H, NCH_2CH_2O), 3.91 – 3.86 (m, 6H, OCH_3), 3.62–3.45 (m, 188H, OCH_2CH_2O).

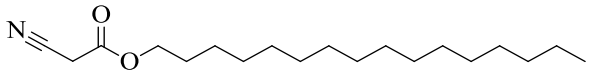

Figure S17: Chemical structure of HDCA.

Hexadecyl cyanoacetate (HDCA): HDCA was synthesized as follows. In a 250 mL round bottom flask containing hexadecane-1-ol (10.65 g, 44 mmol), cyanoacetic acid (7.48 g, 88 mmol), EtOAc (5 mL) and CH_2Cl_2 (50 mL) were introduced dropwise by a syringe over ca. 20 min, a solution of DCC (9.98 g, 48.4 mmol) and DMAP (120 mg, 0.82 mmol) in DCM (50 mL). The reaction medium was stirred during 24 h at ambient temperature under argon atmosphere. The solid was filtered off and the solvents were removed under reduced pressure. The solid was then purified by flash chromatography (SiO2, hexane/EtOAc; 5:1; v:v) to give a fine, white powder: 12.9 g (95 %). ^{1}H NMR (300 MHz, $CDCl_3$) δ ppm 4.20 (t, *J* = 6.8 Hz, 2H, COOC*H*$_2$CH$_2$), 3.45 (s, 2H, CNC*H*$_2$), 1.67 (m, *J* = 13.6, 6.8 Hz, 2H, COOCH$_2$C*H*$_2$), 1.14–1.50 (m, 26H, C*H*$_2$), 0.88 (t, *J* = 7.0 Hz, 3H, CH$_2$C*H*$_3$).

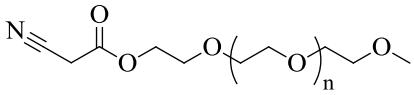

Figure S18: Chemical structure of MePEGCA.

Methoxypoly(ethylene glycol) cyanoacetate (MePEGCA): MePEGCA was synthesized as follows. In a 100 mL round bottom flask containing poly(ethylene glycol) monomethyl ether (11.0 g, 5.5 mmol), cyanoacetic acid (0.955 g, 11.0 mmol) and CH_2Cl_2 (30 mL) were introduced dropwise by a syringe over ca. 20 min, a solution of DCC (2.27 g, 11.0 mmol) and DMAP (60 mg, 0.41 mmol) in CH_2Cl_2 (10 mL). The reaction medium was stirred during 24 h at room temperature under argon atmosphere. The solid was filtered off and the solvent was removed under reduced pressure. The solid was then purified by recrystallization from isopropanol, filtered and dried under vacuum overnight to give a fine, white powder: 10.7 g (94 %). ^{1}H NMR (300 MHz, $CDCl_3$) δ ppm 4.32 (t, 2H, *J* = 4.5 Hz, COOC*H*$_2$CH$_2$), 3.25–3.92 (m, 172H, OC*H*$_2$C*H*$_2$O), 3.53 (s, 2H, CNC*H*$_2$), 3.34 (s, 3H, OC*H*$_3$).

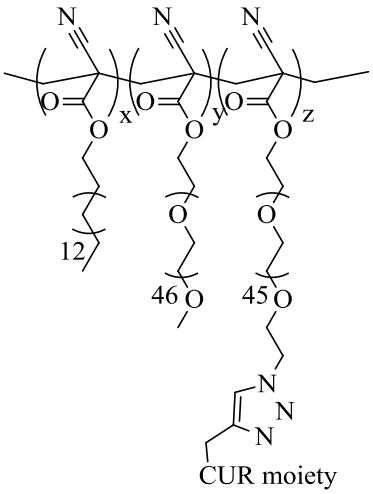

Figure S19: Chemical structure of 46.

Poly[hexadecyl cyanoacrylate-*co*-CurPEG$_{2000}$cyanoacrylate-*co*-methoxypoly (ethylene glycol) cyanoacrylate] (P(HDCA-*co*-CurPEGCA-*co*-MePEGCA)) copolymer (46): In a 25 mL round bottom flask containing MePEGCA (0.258 g, 123.8 μmol, 9 eq), HDCA (0.170 g, 550.4 μmol), Cur-PEG$_{2000}$-CA **45** (0.035 g, 13.8 μmol, 10 mol.% in the initial PEGylated cyanoacetate mixture), EtOH (1.42 mL) and CH_2Cl_2 (2.84 mL) under magnetic stirring, was sequentially introduced formaldehyde (0.345 mL, 4.63 mmol) and pyrrolidine (14.5 μL, 0.176 mmol). The mixture was allowed to stir during 24 h at room temperature and was then concentrated under reduced pressure. The residue was taken into CH_2Cl_2 and washed multiple times with water. The resulting organic layer was dried over $MgSO_4$, filtered and concentrated under reduced pressure and dried under vacuum to give a brown, waxy solid. Quantification of CurPEG$_{2000}$CA in the copolymers was not undertaken due to its very low percentage, which would have led to strong inaccuracies.

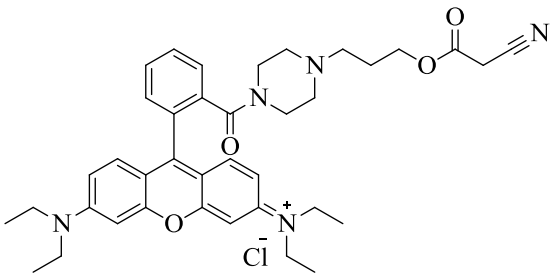

Figure S20: Chemical structure of RCA.

Rhodamine B cyanoacetate (RCA): The Rhodamine B cyanoacetate monomer was synthesized as follows. In a round bottom flask, Rhodamine B alcohol (0.450 g, 0.74 mmol, 1 eq) and cyanoacetic acid (0.127 mg, 1.49 mmol, 2 eq) were dissolved in a mixture of CH_2Cl_2 (10 mL) and EtOAc (1 mL). The resulting solution was bubbled for 30 min with N_2 while cooling down to 0 °C in an ice/water bath. To this solution was added dropwise over 20 min at 0 °C under N_2 a solution of DCC (0.169 g, 0.82 mmol, 1.1 eq) and DMAP (cat. amount) in CH_2Cl_2 (10 mL). The reaction mixture was allowed to warm to room temperature and then stirred for 24 h. The resulting solution was filtered off to remove insoluble dicyclohexylurea and the precipitate was rinsed with dichloromethane until only a faint purple coloration was observed. The mother liquors were concentrated, redissolved in a minimum amount of CH_2Cl_2 and precipitated in a large volume of cold diethyl ether. The precipitate was filtered and dried under high vacuum to give the pure product as purple crystals: 0.33 mg (70 % yield). ^{1}H NMR (300 MHz, $CDCl_3$) δ ppm 7.60–7.78 (m, 2H, HAr), 7.29 (d, 1H, *J* = 7.6 Hz, HAr), 7.18 (d, 2H, *J* = 9.2 Hz, HAr), 6.98 (d, 2H, *J* = 6.98 Hz, HAr), 6.72 (s, 2H, HAr), 4.25 (t, 2H, *J* = 6.0 Hz, C*H*$_2$CN), 3.72 (s, 2H, C*H*$_2$OCO), 3.70 (bs, 4H, C*H*$_2$NC=O), 3.61 (q, 8H, *J* = 7.0 Hz, CH_3CH_2N), 3.27 (bs, 4H, $NCH_2CH_2NCH_2$), 3.20 (t, 2H, $NCH_2(CH_2)_2O$), 2.17 (t, 2H, *J* = 6.2 Hz, $CH_2CH_2CH_2$), 1.31 (t, 12H, *J* = 7.0 Hz, CH_3CH_2N). ESI-MS: $[M + H]^+$ calc. 636.35; $[M + H]^+$ found: 635.5.

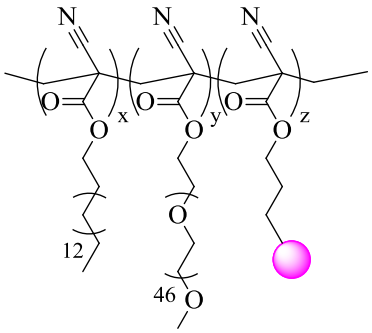

Figure S21: Chemical structure of P(HDCA-*co*-RCA-*co*-MePEGCA).

Poly[hexadecyl cyanoacrylate-*co*-rhodamine B cyanoacrylate-*co*-methoxypoly (ethylene glycol) cyanoacrylate] (P(HDCA-*co*-RCA-*co*-MePEGCA)) fluorescent copolymer: A typical synthesis of P(HDCA-*co*-RCA-*co*-MePEGCA) fluorescent copolymer was as follows. In a 50 mL round bottom flask containing MePEGCA (0.4 g, 0.19 mmol), HDCA (0.26 g, 0.84 mmol), RCA (29.72 mg, 11 μmol, 1.10 mol.% in the

initial cyanoacetate mixture), EtOH (5 mL) and DCM (10 mL) under magnetic stirring, was sequentially introduced dropwise by a syringe over ca. 20 min, formaldehyde (0.4 mL, 5.3 mmol) and pyrrolidine (20 µL, 0.24 mmol). The mixture was allowed to stir during 24 h at room temperature and was then concentrated under reduced pressure. The residue was taken into CH_2Cl_2 and washed multiple times with water. The resulting organic layer was dried over $MgSO_4$, filtered and concentrated under reduced pressure and dried under vacuum to give a purple, waxy solid. Quantification of RCA in the copolymers was not undertaken due to its very low percentage, which would have led to strong inaccuracies.

5.1.3. Identification and Quantification of 36 in liposomal dispersion 39

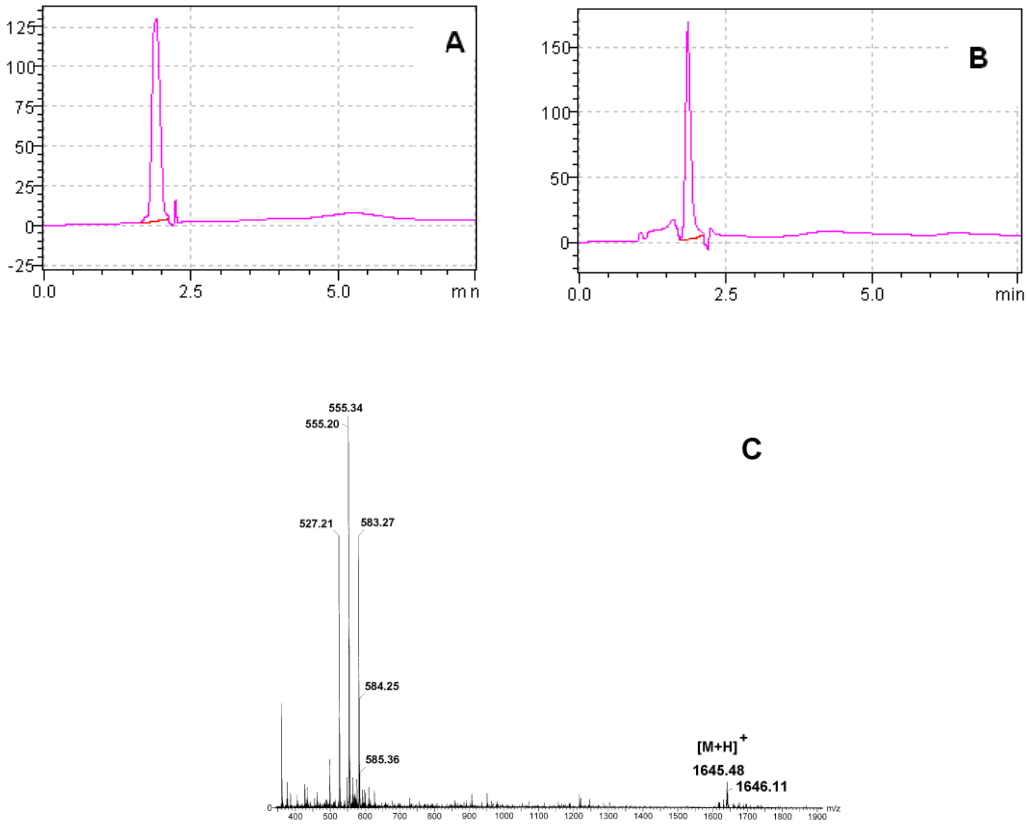

Figure S22: A) HPLC-UV analysis of compound 36 dissolved in $CHCl_3$; column: Lichrosphere 100 RP-18 (5 µm column:); mobile phase: $CHCl_3$/MeOH (9:1) + 0.08% TFA (isocratic); flow rate: 1 mL/min; detection at 330 nm. B) HPLC-UV analysis of freeze-dried liposomal dispersion 39 dissolved in $CHCl_3$; HPLC condition as in (A). C) ESI-MS of compound 36.

Identification of **36** in liposomal dispersion **39** was achieved both by ESI-MS of the liposomal dispersion **39** and ESI-MS analysis of the purified by HPLC liposomal dispersion **39** (Figure S22 B).

Quantification of **36** in final liposomal dispersion **39** after liposomal click reaction is achieved by HPLC analysis of a specific quantity of freeze-dried liposomal dispersion and integration of the corresponding peak. The area of the peaks of known quantities of synthesized in organic media compound **36** are compared to the corresponding area of the freeze-dried liposomal dispersions in which compound **36** has been incorporated in their lipid (Figure S22).

5.2. Peptide synthesis and purification.

$A\beta_{1-40}$, and $A\beta_{1-42}$ were prepared by solid-phase peptide synthesis on a 433A synthesizer (Applied Biosystems) using Fmoc-protected L-amino acid derivatives, NOVASYN-TGA resin on a 0.1 mM scale.[284] Peptides were cleaved from the resin as previously described[285] and purified by reverse phase HPLC on a semi-preparative C4 column (Waters) using water:acetonitrile gradient elution. Peptide identity was confirmed by MALDI-TOF analysis (model Reflex III, Bruker). Peptide purity was always above 95%.

5.3. NMR spectroscopy binding studies.

NMR experiments were recorded on a Bruker 600-MHz Advance equipped with a Bruker CryoProbe and a *z*-axis gradient coil. A batch of $A\beta_{1-42}$ was selected that contained pre-amyloidogenic seeds highly toxic to N2a cells. Immediately before use, lyophilized $A\beta_{1-42}$ was dissolved in 10 mM NaOD in D_2O at a concentration of 80 μM, then diluted 1:1 with 10 mM phosphate buffer saline, pH = 7.4 containing 150 mM NaCl (PBS) and one of the tested compounds. Compounds **2**, **3**, **4**, **5** and **6** were dissolved in 10 mM NaOD in D_2O and then diluted in PBS, pH = 7.4, sonicated for 1 h and added to the peptide solution. The pH of each sample was verified with a Microelectrode (Mettler Toledo) for 5 mm NMR tubes and adjusted with NaOD or DCl. All pH values were corrected for isotope effect. For STD, a train of Gaussian-shaped pulses each of 50 ms was employed to saturate selectively

the protein envelope; the total saturation time of the protein envelope was adjusted by the number of shaped pulses and was varied between 3 s and 0.3 s.

5.4. Electron Microscopy (EM).

$A\beta_{1-42}$ was dissolved at the final concentration of 110 μM, as previously described, in the presence or in the absence of a twofold concentration of test compounds. After five days of incubation at 37 °C, samples were diluted to 5 μM and 10 μL of peptide solution was dropped onto copper formvar carbon-coated 400-mesh EM grids (AGAR Scientific, Stansted, UK) and removed after 5 minutes. Samples were then stained with a saturated solution of uranyl acetate in water for 5 minutes. EM was done with a Zeiss Libra 120 transmission electron microscope operating at 120 kV equipped with a Proscan Slow Scan CCD camera (Carl Zeiss SMT, Oberkochen, Germany). In parallel the compounds alone were analyzed at the same experimental conditions.

5.5. Atomic Force Microscopy (AFM).

Peptide samples were diluted to the final concentration of 5 μM with 10 mM HCl and 60 μL of sample were immediately spotted onto a freshly cleaved muscovite mica disk (Veeco/Digital Instruments, Mannheim, Germany) and incubated for 5 minutes. The disk was then washed with copious amounts of milliQ water and dried under a gentle nitrogen stream. Samples were mounted onto a Multimode AFM with a NanoScope V system (Veeco/Digital Instruments, Mannheim, Germany) operating in Tapping Mode using standard phosphorus-doped silicon probes (Veeco, Mannheim, Germany).

5.6. Sections Staining.

Brains from Tg CRND8 mice encoding a double mutant form of amyloid precursor protein 695 (KM670/671NL+V717F) under the control of the PrP gene promoter were dissected and immediately frozen at -80°C until use. To investigate the binding of the compounds to amyloid plaques, cryostatic 20 μm sections obtained from fresh tissue and mounted on gelatin coated microscope slides that were covered with a solution of

EtOH:water 50:50 (v/v) containing the different test compounds. After 30 min of incubation the section were washed two times with PBS 10 mM. Thereafter, the sections were incubated sequentially in EtOH 70 %, EtOH 96% and xylene before the application of the coverslip. Samples were observed with an OlympusBX51 microscope with filter UV(Ex 330-385 nm / Em > 420) and FITC (Ex 450-480 nm / Em > 515); pictures were obtained with an Olympus Camedia C-5060 Digital Compact Camera in wide field and fluorescent observation. Thioflavin T staining (6 μM) was used as reference compound.

5.7. Preparation of polymeric nanoparticles

Nanoparticles were prepared by the nanoprecipitation technique.6 In practice, the copolymer (50% of CUR derivatized *co*-polymer + 50% Rhodamine labelled *co*-polymer) (20 mg) was dissolved in acetone (2 mL), and the copolymer solution was added dropwise to an aqueous solution 0.5 % (w/v) of Pluronic F68 (4 mL) under vigorous mechanical stirring. A purple suspension was observed almost instantaneously. Acetone was then evaporated under reduced pressure and nanoparticles were purified by ultracentrifugation (150 000 *g*, 1 h, 4 °C, Beckman Coulter, Inc.). The supernatant was discarded and the pellet was resuspended in the appropriated volume of water to yield a stable nanoparticles suspension of 5 mg/mL.

5.8. Nanoparticles characterization.

The nanoparticles diameter (D_z) was measured by Dynamic Light Scattering (DLS) with a Nano ZS from Malvern (173° scattering angle) at 25 °C. DLS measurements were used to monitor the nanoparticles stability as a function of time incubated in the buffer employed for capillary electrophoresis experiments, at 4 and 37°C.

5.9. Capillary electrophoresis.

CE was performed on PA 800 instrument (Beckman Coulter, Roissy, France) using uncoated silica capillaries (Phymep, Paris) with an internal diameter of 50 μm and 50 cm total length (40 cm effective length was employed for the separation). All buffers were

prepared with deionised water and were filtered through a 0.22 µm membrane (VWR) before use. Before analysis, the capillaries were preconditioned by the following rinsing sequence: 0.1 M NaOH for 5 min, 1 M NaOH for 5 min and then deionised water for 5 min. The in-between-runs rinsing cycles were carried out by pumping sequentially through the capillary: water for 5 min, 50 mM SDS for 2 min (to inhibit the aggregation and subsequent peptide adsorption on the capillary wall[286]), and 0.1 M NaOH for 5 min. The samples were introduced into the capillary by hydrodynamic injection under 3.4 kPa. The capillary was thermostated at 25 °C and the samples were maintained at 37°C by the storage sample module of the PA 800 apparatus. The separations were carried out at 16 kV with positive polarity at the inlet using 80 mM phosphate buffer pH 7.4. The electrolyte was renewed after each run. The peptides were detected by a Laser-Induced Fluorescence (LIF) detection system equipped with 3.5 mW argon-ion laser with a wavelength excitation of 488 nm, the emission being collected through a 520 nm band-pass filter or by Diode-Array Detector (DAD) at 190 nm. Peak areas were estimated using the 32 Karat™ software (Beckman Coulter).

5.9.1. Peptide samples preparation and storage.

Lyophilized HiLyte Fluor™ labelled $A\beta_{1-42}$ peptide was dissolved in 0.16% (m/V) ammonium hydroxide aqueous solution to reach a concentration of 2 $mg.mL^{-1}$. The fluorescent peptide solutions were then divided into aliquots individually stored at -20°C which were thawed just prior to analysis.

5.9.2. Capillary electrophoresis experiments.

To study the interaction between the monomeric form of the $A\beta_{1-42}$ peptide and the nanoparticles, aliquots of HiLyte Fluor™ labelled $A\beta_{1-42}$ peptide stock solutions were diluted in 20 mM phosphate buffer (NaH_2PO_4) at pH 7.4 containing a 20 µM P(HDCA-*co*-CurPEGCA-*co*-MePEGCA) nanoparticles suspension to obtain final peptide concentrations of 5 µM. The samples were then incubated at 37 °C and analyzed by capillary electrophoresis every 80 min. These experiments allow determining the evolution of % monomer peak as a function of time of incubation. % monomer peak is calculated as

the ratio between the absolute peak of the monomer observed at t=0 to the one observed at each incubation time.

Bibliography

(1) *Alzheimer's Disease*; Springer-Verlag: Berlin, 2008; Vol. 2.

(2) Brookmeyer, R.; Corrada, M. M.; Curriero, F. C.; Kawas, C. *Archives of Neurology* **2002**, *59*, 1764.

(3) Brookmeyer, R.; Gray, S.; Kawas, C. *American Journal of Public Health* **1998**, *88*, 1337.

(4) Ferri, C. P.; Prince, M.; Brayne, C.; Brodaty, H.; Fratiglioni, L.; Ganguli, M.; Hall, K.; Hasegawa, K.; Hendrie, H.; Huang, Y. Q.; Jorm, A.; Mathers, C.; Menezes, P. R.; Rimmer, E.; Scazufca, M.; Alzheimers Dis, I. *Lancet* **2005**, *366*, 2112.

(5) Walsh, D. M.; Selkoe, D. J. *Journal of Neurochemistry* **2007**, 1172.

(6) Takashima, A. *Journal of Alzheimer's Disease* **2009**, *17*, 729.

(7) Citron, M. *Nature Reviews* **2004**, *5*, 677.

(8) Jianga, H.-C. H. a. Z.-F. *Journal of Alzheimer's Disease* **2009**, *16*, 15.

(9) Wikipedia; Wikipedia: 2010; Vol. 2010.

(10) Carlo, M. D. *Eur. Biophys. J.* **2010**, *39*, 877.

(11) *Amyloid Proteins: The Beta Sheet Conformation and Disease*; WILEY-VCH Verlag: Weinheim, 2005; Vol. 2.

(12) Querfurth, H. W.; LaFerla, F. M. *The New England Journal of Medicine* **2010**, *362*, 329.

(13) Amijee, H.; Scopes, D. I. C. *Journal of Alzheimer's Disease* **2009**, *17*, 33.

(14) Kayed, R.; Head, E.; Thompson, J. L.; McIntire, T. M.; Milton, S. C.; Cotman, C. W.; Glabe, C. G. *Science* **2003**, *300*, 486.

(15) Cleary, J. P.; Walsh, D. M.; Hofmeister, J. J.; Shankar, G. M.; Kuskowski, M. A.; Selkoe, D. J.; Ashe, K. H. *Nature Neuroscience* **2005**, *8*, 79.

(16) Demuro, A.; Mina, E.; Kayed, R.; Milton, S. C.; Parker, I.; Glabe, C. G. *Journal of Biological Chemistry* **2005**, *280*, 17294.

(17) Pawar, A. P.; DuBay, K. F.; Zurdo, J.; Chiti, F.; Vendruscolo, M.; Dobson, C. M. *Journal of Molecular Biology* **2005**, *350*, 379.

(18) Danielsson, J.; Jarvet, J.; Damberg, P.; Graslund, A. *Febs Journal* **2005**, *272*, 3938.

(19) Riek, R.; Guntert, P.; Dobeli, H.; Wipf, B.; Wuthrich, K. *European Journal of Biochemistry* **2001**, *268*, 5930.

(20) Danielsson, J.; Andersson, A.; Jarvet, J.; Graslund, A. *Magnetic Resonance in Chemistry* **2006**, *44*, S114.

(21) Walsh, D. M.; Klyubin, I.; Fadeeva, J. V.; Rowan, M. J.; Selkoe, D. J. *Biochemical Society Transactions* **2002**, *30*, 552.

(22) Shen, L.; Ji, H. F.; Zhang, H. Y. *Journal of Physical Chemistry B* **2008**, *112*, 3164.

(23) Lee, J. P.; Stimson, E. R.; Ghilardi, J. R.; Mantyh, P. W.; Lu, Y. A.; Felix, A. M.; Llanos, W.; Behbin, A.; Cummings, M.; Vancriekinge, M.; Timms, W.; Maggio, J. E. *Biochemistry* **1995**, *34*, 5191.

(24) Zhang, S.; Iwata, K.; Lachenmann, M. J.; Peng, J. W.; Li, S.; Stimson, E. R.; Lu, Y.; Felix, A. M.; Maggio, J. E.; Lee, J. P. *Journal of Structural Biology* **2000**, *130*, 130.

(25) Jarvet, J.; Damberg, P.; Bodell, K.; Eriksson, L. E. G.; Graslund, A. *Journal of the American Chemical Society* **2000**, *122*, 4261.

(26) Barrow, C. J.; Zagorski, M. G. *Science* **1991**, *253*, 179.

(27) Sticht, H.; Bayer, P.; Willbold, D.; Dames, S.; Hilbich, C.; Beyreuther, K.; Frank, R. W.; Rosch, P. *European Journal of Biochemistry* **1995**, *233*, 293.

(28) Kohno, T.; Kobayashi, K.; Maeda, T.; Sato, K.; Takashima, A. *Biochemistry* **1996**, *35*, 16094.

(29) Tomaselli, S.; Esposito, V.; Vangone, P.; van Nuland, N. A. J.; Bonvin, A.; Guerrini, R.; Tancredi, T.; Temussi, P. A.; Picone, D. *Chembiochem* **2006**, *7*, 257.

(30) Barghorn, S.; Nimmrich, V.; Striebinger, A.; Krantz, C.; Keller, P.; Janson, B.; Bahr, M.; Schmidt, M.; Bitner, R. S.; Harlan, J.; Barlow, E.; Ebert, U.; Hillen, H. *Journal of Neurochemistry* **2005**, *95*, 834.

(31) Lesne, S.; Koh, M. T.; Kotilinek, L.; Kayed, R.; Glabe, C. G.; Yang, A.; Gallagher, M.; Ashe, K. H. *Nature* **2006**, *440*, 352.

(32) Sabate, R.; Estelrich, J. *Journal of Physical Chemistry B* **2005**, *109*, 11027.

(33) Chiti, F.; Dobson, C. M. *Annual Review of Biochemistry* **2006**, *75*, 333.

(34) Laurents, D. V.; Gorman, P. M.; Guo, M.; Rico, M.; Chakrabartty, A.; Bruix, M. *Journal of Biological Chemistry* **2005**, *280*, 3675.

(35) Blackley, H. K. L.; Sanders, G. H. W.; Davies, M. C.; Roberts, C. J.; Tendler, S. J. B.; Wilkinson, M. J. *Journal of Molecular Biology* **2000**, *298*, 833.

(36) Petkova, A. T.; Yau, W. M.; Tycko, R. *Biochemistry* **2006**, *45*, 498.

(37) Tycko, R. *Current Opinion in Structural Biology* **2004**, *14*, 96.

(38) Balbach, J. J.; Ishii, Y.; Antzutkin, O. N.; Leapman, R. D.; Rizzo, N. W.; Dyda, F.; Reed, J.; Tycko, R. *Biochemistry* **2000**, *39*, 13748.

(39) Antzutkin, O. N.; Balbach, J. J.; Tycko, R. *Biophysical Journal* **2003**, *84*, 3326.

(40) Petkova, A. T.; Leapman, R. D.; Guo, Z. H.; Yau, W. M.; Mattson, M. P.; Tycko, R. *Science* **2005**, *307*, 262.

(41) Kuwata, K.; Matumoto, T.; Cheng, H.; Nagayama, K.; James, T. L.; Roder, H. *Proceedings of the National Academy of Sciences of the United States of America* **2003**, *100*, 14790.

(42) Kheterpal, I.; Zhou, S.; Cook, K. D.; Wetzel, R. *Proceedings of the National Academy of Sciences of the United States of America* **2000**, *97*, 13597.

(43) Williams, A. D.; Portelius, E.; Kheterpal, I.; Guo, J. T.; Cook, K. D.; Xu, Y.; Wetzel, R. *Journal of Molecular Biology* **2004**, *335*, 833.

(44) Jayasinghe, S. A.; Langen, R. *Journal of Biological Chemistry* **2004**, *279*, 48420.

(45) Fraser, P. E.; Nguyen, J. T.; Inouye, H.; Surewicz, W. K.; Selkoe, D. J.; Podlisny, M. B.; Kirschner, D. A. *Biochemistry* **1992**, *31*, 10716.

(46) Dong, J.; Atwood, C. S.; Anderson, V. E.; Siedlak, S. L.; Smith, M. A.; Perry, G.; Carey, P. R. *Biochemistry* **2003**, *42*, 2768.

(47) Margittai, M.; Langen, R. *Proceedings of the National Academy of Sciences of the United States of America* **2004**, *101*, 10278.

(48) Serag, A. A.; Altenbach, C.; Gingery, M.; Hubbell, W. L.; Yeates, T. O. *Nature Structural Biology* **2002**, *9*, 734.

(49) Sunde, M.; Blake, C. C. F. *Quarterly Reviews of Biophysics* **1998**, *31*, 1.

(50) Oyler, N. A.; Tycko, R. *Journal of the American Chemical Society* **2004**, *126*, 4478.

(51) Qin, X. R.; Abe, H.; Nakanishi, H. *Biochemical and Biophysical Research Communications* **2002**, *297*, 1011.

(52) Yu, J. X.; Bakhos, L.; Chang, L.; Holterman, M. J.; Klein, W. L.; Venton, D. L. *Journal of Molecular Neuroscience* **2002**, *19*, 51.

(53) Camilleri, P.; Haskins, N. J.; Howlett, D. R. *Febs Letters* **1994**, *341*, 256.

(54) Danielsson, J.; Jarvet, J.; Damberg, P.; Graslund, A. *Biochemistry* **2004**, *43*, 6261.

(55) Mandal, P. K.; Pettegrew, J. W. *Neurochemical Research* **2004**, *29*, 447.

(56) Lambert, M. P.; Barlow, A. K.; Chromy, B. A.; Edwards, C.; Freed, R.; Liosatos, M.; Morgan, T. E.; Rozovsky, I.; Trommer, B.; Viola, K. L.; Wals, P.; Zhang, C.; Finch, C. E.; Krafft, G. A.; Klein, W. L. *Proceedings of the National Academy of Sciences of the United States of America* **1998**, *95*, 6448.

(57) McLaurin, J.; Chakrabartty, A. *Journal of Biological Chemistry* **1996**, *271*, 26482.

(58) ChooSmith, L. P.; Surewicz, W. K. *Febs Letters* **1997**, *402*, 95.

(59) McLaurin, J.; Franklin, T.; Fraser, P. E.; Chakrabartty, A. *Journal of Biological Chemistry* **1998**, *273*, 4506.

(60) Martins, I. C.; Kuperstein, I.; Wilkinson, H.; Maes, E.; Vanbrabant, M.; Jonckheere, W.; Van Gelder, P.; Hartmann, D.; D'Hooge, R.; De Strooper, B.; Schymkowitz, J.; Rousseau, F. *Embo Journal* **2008**, *27*, 224.

(61) Matsuzaki, K.; Horikiri, C. *Biochemistry* **1999**, *38*, 4137.

(62) Ariga, T.; Kobayashi, K.; Hasegawa, A.; Kiso, M.; Ishida, H.; Miyatake, T. *Archives of Biochemistry and Biophysics* **2001**, *388*, 225.

(63) Gazit, E. *Faseb Journal* **2002**, *16*, 77.

(64) Tjernberg, L. O.; Naslund, J.; Lindqvist, F.; Johansson, J.; Karlstrom, A. R.; Thyberg, J.; Terenius, L.; Nordstedt, C. *Journal of Biological Chemistry* **1996**, *271*, 8545.

(65) Findeis, M. A.; Musso, G. M.; Arico-Muendel, C. C.; Benjamin, H. W.; Hundal, A. M.; Lee, J. J.; Chin, J.; Kelley, M.; Wakefield, J.; Hayward, N. J.; Molineaux, S. M. *Biochemistry* **1999**, *38*, 6791.

(66) Soto, C.; Sigurdsson, E. M.; Morelli, L.; Kumar, R. A.; Castano, E. M.; Frangione, B. *Nature Medicine* **1998**, *4*, 822.

(67) Cairo, C. W.; Strzelec, A.; Murphy, R. M.; Kiessling, L. L. *Biochemistry* **2002**, *41*, 8620.

(68) Chalifour, R. J.; McLaughlin, R. W.; Lavoie, L.; Morissette, C.; Tremblay, N.; Boule, M.; Sarazin, P.; Stea, D.; Lacombe, D.; Tremblay, P.; Gervais, F. *Journal of Biological Chemistry* **2003**, *278*, 34874.

(69) Austen, B. M.; Paleologou, K. E.; Ali, S. A. E.; Qureshi, M. M.; Allsop, D.; El-Agnaf, O. M. A. *Biochemistry* **2008**, *47*, 1984.

(70) Chafekar, S. M.; Malda, H.; Merkx, M.; Meijer, E. W.; Viertl, D.; Lashuel, H. A.; Baas, F.; Scheper, W. *Chembiochem* **2007**, *8*, 1857.

(71) Zhang, G. B.; Leibowitz, M. J.; Sinko, P. J.; Stein, S. *Bioconjugate Chemistry* **2003**, *14*, 86.

(72) Fulop, L.; Zarandi, M.; Datki, Z.; Soos, K.; Penke, B. *Biochemical and Biophysical Research Communications* **2004**, *324*, 64.

(73) Bond, J. P.; Deverin, S. P.; Inouye, H.; El-Agnaf, O. M. A.; Teeter, M. M.; Kirschner, D. A. *Journal of Structural Biology* **2003**, *141*, 156.

(74) Liu, R. T.; McAllister, C.; Lyubchenko, Y.; Sierks, M. R. *Journal of Neuroscience Research* **2004**, *75*, 162.

(75) Etienne, M. A.; Aucoin, J. P.; Fu, Y. W.; McCarley, R. L.; Hammer, R. P. *Journal of the American Chemical Society* **2006**, *128*, 3522.

(76) Gordon, D. J.; Sciarretta, K. L.; Meredith, S. C. *Biochemistry* **2001**, *40*, 8237.

(77) Hughes, E.; Burke, R. M.; Doig, A. J. *Journal of Biological Chemistry* **2000**, *275*, 25109.

(78) Gordon, D. J.; Meredith, S. C. *Biochemistry* **2003**, *42*, 475.

(79) Sabate, R.; Estelrich, J. *Langmuir* **2005**, *21*, 6944.

(80) Bush, A. I. *Neurobiology of Aging* **2002**, *23*, 1031.

(81) Taniguchi, S.; Suzuki, N.; Masuda, M.; Hisanaga, S.; Iwatsubo, T.; Goedert, M.; Hasegawa, M. *Journal of Biological Chemistry* **2005**, *280*, 7614.

(82) Pollack, S. J.; Sadler, I. I. J.; Hawtin, S. R.; Tailor, V. J.; Shearman, M. S. *Neuroscience Letters* **1995**, *197*, 211.

(83) Lorenzo, A.; Yankner, B. A. *Proceedings of the National Academy of Sciences of the United States of America* **1994**, *91*, 12243.

(84) Necula, M.; Kayed, R.; Milton, S.; Glabe, C. G. *Journal of Biological Chemistry* **2007**, *282*, 10311.

(85) Xie, Y. L.; Deng, S. M.; Chen, Z. Z.; Yan, S. D.; Landry, D. W. *Bioorganic & Medicinal Chemistry Letters* **2006**, *16*, 4657.

(86) Porat, Y.; Abramowitz, A.; Gazit, E. *Chemical Biology & Drug Design* **2006**, *67*, 27.

(87) Ono, K.; Hasegawa, K.; Naiki, H.; Yamada, M. *Journal of Neuroscience Research* **2004**, *75*, 742.

(88) Lim, G. P.; Chu, T.; Yang, F. S.; Beech, W.; Frautschy, S. A.; Cole, G. M. *Journal of Neuroscience* **2001**, *21*, 8370.

(89) Yang, F. S.; Lim, G. P.; Begum, A. N.; Ubeda, O. J.; Simmons, M. R.; Ambegaokar, S. S.; Chen, P. P.; Kayed, R.; Glabe, C. G.; Frautschy, S. A.; Cole, G. M. *Journal of Biological Chemistry* **2005**, *280*, 5892.

(90) Lashuel, H. A.; Hartley, D. M.; Balakhaneh, D.; Aggarwal, A.; Teichberg, S.; Callaway, D. J. E. *Journal of Biological Chemistry* **2002**, *277*, 42881.

(91) Howlett, D.; Cutler, P.; Heales, S.; Camilleri, P. *Febs Letters* **1997**, *417*, 249.

(92) Lim, G. P.; Calon, F.; Morihara, T.; Yang, F. S.; Teter, B.; Ubeda, O.; Salem, N.; Frautschy, S. A.; Cole, G. M. *Journal of Neuroscience* **2005**, *25*, 3032.

(93) Ono, K.; Hasegawa, K.; Naiki, H.; Yamada, M. *Biochimica Et Biophysica Acta-Molecular Basis of Disease* **2004**, *1690*, 193.

(94) Ono, K.; Hirohata, M.; Yamada, M. *Biochemical and Biophysical Research Communications* **2005**, *336*, 444.

(95) Ono, K.; Yoshiike, Y.; Takashima, A.; Hasegawa, K.; Naiki, H.; Yamada, M. *Experimental Neurology* **2004**, *189*, 380.

(96) Ono, K.; Hirohata, M.; Yamada, M. *Biochemical and Biophysical Research Communications* **2006**, *341*, 1046.

(97) Ono, K.; Hasegawa, K.; Naiki, H.; Yamada, M. *Biochemical and Biophysical Research Communications* **2005**, *330*, 111.

(98) Hirohata, M.; Ono, K.; Naiki, H.; Yamada, M. *Neuropharmacology* **2005**, *49*, 1088.

(99) Thomas, T.; Nadackal, T. G.; Thomas, K. *Neuroreport* **2001**, *12*, 3263.

(100) in 't Veld, B. A.; Ruitenberg, A.; Hofman, A.; Launer, L. J.; van Duijn, C. M.; Stijnen, T.; Breteler, M. M. B.; Stricker, B. H. C. *New England Journal of Medicine* **2001**, *345*, 1515.

(101) Lim, G. P.; Yang, F.; Chu, T.; Chen, P.; Beech, W.; Teter, B.; Tran, T.; Ubeda, O.; Ashe, K. H.; Frautschy, S. A.; Cole, G. M. *Journal of Neuroscience* **2000**, *20*, 5709.

(102) Lim, G. P.; Yang, F.; Chu, T.; Gahtan, E.; Ubeda, O.; Beech, W.; Overmier, J. B.; Hsiao-Ashe, K.; Frautschy, S. A.; Cole, G. M. *Neurobiology of Aging* **2001**, *22*, 983.

(103) Ono, K.; Hasegawa, K.; Naiki, H.; Yamada, M. *Neurochemistry International* **2006**, *48*, 275.

(104) Sano, M.; Ernesto, C.; Thomas, R. G.; Klauber, M. R.; Schafer, K.; Grundman, M.; Woodbury, P.; Growdon, J.; Cotman, D. W.; Pfeiffer, E.; Schneider, L. S.; Thal, L. J. *New England Journal of Medicine* **1997**, *336*, 1216.

(105) Ono, K.; Hasegawa, K.; Yamada, M.; Naiki, H. *Biological Psychiatry* **2002**, *52*, 880.

(106) Ono, K.; Hasegawa, K. U.; Yoshiike, Y.; Takashima, A.; Yamada, M.; Naiki, H. *Journal of Neurochemistry* **2002**, *81*, 434.

(107) Zeng, H.; Zhang, Y. B.; Peng, L. J.; Shao, H. Y.; Menon, N. K.; Yang, J.; Salomon, A. R.; Freidland, R. P.; Zagorski, M. G. *Biological Psychiatry* **2001**, *49*, 248.

(108) Li, J.; Zhu, M.; Manning-Bog, A. B.; Di Monte, D. A.; Fink, A. L. *Faseb Journal* **2004**, *18*, 962.

(109) Inanami, O.; Watanabe, Y.; Syuto, B.; Nakano, M.; Tsuji, M.; Kuwabara, M. *Free Radical Research* **1998**, *29*, 359.

(110) Shutenko, Z.; Henry, Y.; Pinard, E.; Seylaz, J.; Potier, P.; Berthet, F.; Girard, P.; Sercombe, R. *Biochemical Pharmacology* **1999**, *57*, 199.

(111) Bastianetto, S.; Zheng, W. H.; Quirion, R. *British Journal of Pharmacology* **2000**, *131*, 711.

(112) Virgili, M.; Contestabile, A. *Neuroscience Letters* **2000**, *281*, 123.

(113) Choi, Y. T.; Jung, C. H.; Lee, S. R.; Bae, J. H.; Baek, W. K.; Suh, M. H.; Park, J.; Park, C. W.; Suh, S. I. *Life Sciences* **2001**, *70*, 603.

(114) Levites, Y.; Weinreb, O.; Maor, G.; Youdim, M. B. H.; Mandel, S. *Journal of Neurochemistry* **2001**, *78*, 1073.

(115) Hirohata, M.; Hasegawa, K.; Tsutsumi-Yasuhara, S.; Ohhashi, Y.; Ookoshi, T.; Ono, K.; Yamada, M.; Naiki, H. *Biochemistry* **2007**, *46*, 1888.

(116) Abd El Mohsen, M. M.; Kuhnle, G.; Rechner, A. R.; Schroeter, H.; Rose, S.; Jenner, P.; Rice-Evans, C. A. *Free Radical Biology and Medicine* **2002**, *33*, 1693.

(117) Matthews, R. T.; Yang, L. C.; Browne, S.; Baik, M.; Beal, M. F. *Proceedings of the National Academy of Sciences of the United States of America* **1998**, *95*, 8892.

(118) Frautschy, S. A.; Hu, W.; Kim, P.; Miller, S. A.; Chu, T.; Harris-White, M. E.; Cole, G. M. *Neurobiology of Aging* **2001**, *22*, 993.

(119) Garcia-Alloza, M.; Borrelli, L. A.; Rozkalne, A.; Hyman, B. T.; Bacskai, B. J. *Journal of Neurochemistry* **2007**, *102*, 1095.

(120) Begum, A. N.; Jones, M. R.; Lim, G. P.; Morihara, T.; Kim, P.; Heath, D. D.; Rock, C. L.; Pruitt, M. A.; Yang, F. S.; Hudspeth, B.; Hu, S. X.; Faull, K. F.; Teter, B.; Cole, G. M.; Frautschy, S. A. *Journal of Pharmacology and Experimental Therapeutics* **2008**, *326*, 196.

(121) Ono, K.; Yoshiike, Y.; Takashima, A.; Hasegawa, K.; Naiki, H.; Yamada, M. *Journal of Neurochemistry* **2003**, *87*, 172.

(122) De Felice, F. G.; Houzel, J. C.; Garcia-Abreu, J.; Louzada, P. R. F.; Afonso, R. C.; Meirelles, M. N. L.; Lent, R.; Neto, V. M.; Ferreira, S. T. *Faseb Journal* **2001**, *15*, 1297.

(123) Suganuma, M.; Okabe, S.; Oniyama, M.; Tada, Y.; Ito, H.; Fujiki, H. *Carcinogenesis* **1998**, *19*, 1771.

(124) Farr, S. A.; Poon, H. F.; Dogrukol-Ak, D.; Drake, J.; Banks, W. A.; Eyerman, E.; Butterfield, D. A.; Morley, J. E. *Journal of Neurochemistry* **2003**, *84*, 1173.

(125) Tomiyama, T.; Asano, S.; Suwa, Y.; Morita, T.; Kataoka, K.; Mori, H.; Endo, N. *Biochemical and Biophysical Research Communications* **1994**, *204*, 76.

(126) Tomiyama, T.; Shoji, A.; Kataoka, K.; Suwa, Y.; Asano, S.; Kaneko, H.; Endo, N. *Journal of Biological Chemistry* **1996**, *271*, 6839.

(127) Kisilevsky, R.; Lemieux, L. J.; Fraser, P. E.; Kong, X. Q.; Hultin, P. G.; Szarek, W. A. *Nature Medicine* **1995**, *1*, 143.

(128) Pappolla, M.; Bozner, P.; Soto, C.; Shao, H. Y.; Robakis, N. K.; Zagorski, M.; Frangione, B.; Ghiso, J. *Journal of Biological Chemistry* **1998**, *273*, 7185.

(129) Forloni, G.; Colombo, L.; Girola, L.; Tagliavini, F.; Salmona, M. *Febs Letters* **2001**, *487*, 404.

(130) Youdim, K. A.; Qaiser, M. Z.; Begley, D. J.; Rice-Evans, C. A.; Abbott, N. J. *Free Radical Biology and Medicine* **2004**, *36*, 592.

(131) Mindermann, T.; Zimmerli, W.; Gratzl, O. *Antimicrobial Agents and Chemotherapy* **1998**, *42*, 2626.

(132) Sam, E.; Sarre, S.; Michotte, Y.; Verbeke, N. *European Journal of Pharmacology* **1997**, *329*, 9.

(133) Kelloff, G. J.; Crowell, J. A.; Hawk, E. T.; Steele, V. E.; Lubet, R. A.; Boone, C. W.; Covey, J. M.; Doody, L. A.; Omenn, G. S.; Greenwald, P.; Hong, W. K.; Parkinson, D. R.; Bagheri, D.; Baxter, G. T.; Blunden, M.; Doeltz, M. K.; Eisenhauer, K. M.; Johnson, K.; Knapp, G. G.; Longfellow, D. G.; Malone, W. F.; Nayfield, S. G.; Seifried, H. E.; Swall, L. M.; Sigman, C. C. *Journal of Cellular Biochemistry* **1996**, 54.

(134) Chandra, V.; Ganguli, M.; Ratcliff, G.; Pandav, R.; Sharma, S.; Gilby, J.; Belle, S.; Ryan, C.; Baker, C.; Seaberg, E.; Dekosky, S.; Nath, L. *Aging-Clinical and Experimental Research* **1994**, *6*, 307.

(135) Zhao, B. L.; Li, X. J.; He, R. G.; Cheng, S. J.; Xin, W. J. *Cell Biophysics* **1989**, *14*, 175.

(136) Reinke, A. A.; Gestwicki, J. E. *Chem Biol Drug Des* **2007**, *70*, 206.

(137) Gururangan, S.; Friedman, H. S. *Neuroimaging Clinics of North America* **2002**, *12*, 583.

(138) Brightma.Mw; Reese, T. S. *Journal of Cell Biology* **1969**, *40*, 648.

(139) Abraham, M. H.; Chadha, H. S.; Mitchell, R. C. *Journal of Pharmaceutical Sciences* **1994**, *83*, 1257.

(140) Hardy, J.; Selkoe, D. J. *Science* **2002**, *297*, 353.

(141) Bell, R. D.; Zlokovic, B. V. *Acta Neuropathologica* **2009**, *118*, 103.

(142) Donahue, J. E.; Johanson, C. E.; Apolipoprotein, E. *Journal of Neuropathology and Experimental Neurology* **2008**, *67*, 634.

(143) Ito, S.; Ohtsuki, S.; Terasaki, T. *Neuroscience Research* **2006**, *56*, 246.

(144) Matsuoka, Y.; Saito, M.; LaFrancois, J.; Gaynor, K.; Olm, V.; Wang, L. L.; Casey, E.; Lu, Y. F.; Shiratori, C.; Lemere, C.; Duff, K. *Journal of Neuroscience* **2003**, *23*, 29.

(145) Sagare, A.; Deane, R.; Bell, R. D.; Johnson, B.; Hamm, K.; Pendu, R.; Marky, A.; Lenting, P. J.; Wu, Z. H.; Zarcone, T.; Goate, A.; Mayo, K.; Perlmutter, D.; Coma, M.; Zhong, Z. H.; Zlokovic, B. V. *Nature Medicine* **2007**, *13*, 1029.

(146) Selkoe, D. J. *Neuron* **2001**, *32*, 177.

(147) Zlokovic, B. V. *Journal of Neurochemistry* **2004**, *89*, 807.

(148) Holtzman, D. M. *Journal of Molecular Neuroscience* **2001**, *17*, 147.

(149) Jiang, Q.; Lee, C. Y. D.; Mandrekar, S.; Wilkinson, B.; Cramer, P.; Zelcer, N.; Mann, K.; Lamb, B.; Willson, T. M.; Collins, J. L.; Richardson, J. C.; Smith, J. D.; Comery, T. A.; Riddell, D.; Holtzman, D. M.; Tontonoz, P.; Landreth, G. E. *Neuron* **2008**, *58*, 681.

(150) Solomon, B. *Current Opinion in Investigational Drugs* **2007**, *8*, 519.

(151) Farlow, M. R.; Cummings, J. L. *American Journal of Medicine* **2007**, *120*, 388.

(152) Doraiswamy, P. M. *Cns Drugs* **2002**, *16*, 811.

(153) Tariot, P. N.; Farlow, M. R.; Grossberg, G. T.; Graham, S. M.; McDonald, S.; Gergel, I.; Memantine Study, G. *Jama-Journal of the American Medical Association* **2004**, *291*, 317.

(154) Oken, B. S.; Storzbach, D. M.; Kaye, J. A. *Archives of Neurology* **1998**, *55*, 1409.

(155) Henderson, V. W. *Neuroscience* **2006**, *138*, 1031.

(156) Aisen, P. S.; Gauthier, S.; Vellas, B.; Briand, R.; Saurnier, D.; Laurin, J.; Garceau, D. *Current Alzheimer Research* **2007**, *4*, 473.

(157) Bilikiewicz, A.; Gaus, W. *Journal of Alzheimers Disease* **2004**, *6*, 17.

(158) Roney, C.; Kulkarni, P.; Arora, V.; Antich, P.; Bonte, F.; Wu, A.; Mallikarjuana, N. N.; Manochar, S.; Liang, H.-F.; Kulkarni, A. R.; Sung, H.-W.; Sairam, M.; Aminabhavi, T. M. *Journal of Controlled Release* **2005**, *108*, 193.

(159) Uner, M. *Pharmazie* **2006**, *61*, 375.

(160) Moghimi, S. M.; Hunter, A. C.; Murray, J. C. *Pharmacological Reviews* **2001**, *53*, 283.

(161) Kreuter, J. *Advanced Drug Delivery Reviews* **2001**, *47*, 65.

(162) Rolland, O.; Turrin, C. O.; Caminade, A. M.; Majoral, J. P. *New Journal of Chemistry* **2009**, *33*, 1809.

(163) Denora, N.; Trapani, A.; Laquintana, V.; Lopedota, A.; Trapani, G. *Current Topics in Medicinal Chemistry* **2009**, *2009*, 182.

(164) LI, H.; DUAN, X. *Nanoscience* **2006**, *11*, 207.

(165) Shen, L.; Ji, H. F. *Spectrochimica Acta Part a-Molecular and Biomolecular Spectroscopy* **2007**, *67*, 619.

(166) Yanagisawa, D.; Shirai, N.; Amatsubo, T.; Taguchi, H.; Hirao, K.; Urushitani, M.; Morikawa, S.; Inubushi, T.; Kato, M.; Kato, F.; Morino, K.; Kimura, H.; Nakano, I.; Yoshida, C.; Okada, T.; Sano, M.; Wada, Y.; Wada, K.; Yamamoto, A.; Tooyama, I. *Biomaterials* **2010**, *31*, 4179.

(167) Narlawar, R.; Pickhardt, M.; Leuchtenberger, S.; Baumann, K.; Krause, S.; Dyrks, T.; Weggen, S.; Mandelkow, E.; Schmidt, B. *Chemmedchem* **2008**, *3*, 165.

(168) Ringman, J. M.; Frautschy, S. A.; Cole, G. M.; Masterman, D. L.; Cummings, J. L. *Current Alzheimer Research* **2005**, *2*, 131.

(169) Aggarwal, B. B.; Kumar, A.; Bharti, A. C. *Anticancer Research* **2003**, *23*, 363.

(170) Vlietinck, A. J.; De Bruyne, T.; Apers, S.; Pieters, L. A. *Planta Medica* **1998**, *64*, 97.

(171) Egan, M. E.; Pearson, M.; Weiner, S. A.; Rajendran, V.; Rubin, D.; Glockner-Pagel, J.; Canny, S.; Du, K.; Lukacs, G. L.; Caplan, M. J. *Science* **2004**, *304*, 600.

(172) Tohgi, H.; Abe, T.; Yamazaki, K.; Murata, T.; Ishizaki, E.; Isobe, C. *Neuroscience Letters* **1999**, *269*, 52.

(173) Pratico, D.; Clark, C. M.; Lee, V. M. Y.; Trojanowski, J. Q.; Rokach, J.; FitzGerald, G. A. *Annals of Neurology* **2000**, *48*, 809.

(174) Engelhart, M. J.; Geerlings, M. I.; Ruitenberg, A.; van Swieten, J. C.; Holman, A.; Witteman, J. C. M.; Breteler, M. M. B. *Jama-Journal of the American Medical Association* **2002**, *287*, 3223.

(175) Akiyama, H.; Barger, S.; Barnum, S.; Bradt, B.; Bauer, J.; Cole, G. M.; Cooper, N. R.; Eikelenboom, P.; Emmerling, M.; Fiebich, B. L.; Finch, C. E.; Frautschy, S.; Griffin, W. S. T.; Hampel, H.; Hull, M.; Landreth, G.; Lue, L. F.; Mrak, R.; Mackenzie, I. R.; McGeer, P. L.; O'Banion, M. K.; Pachter, J.; Pasinetti, G.; Plata-Salaman, C.; Rogers, J.; Rydel, R.; Shen, Y.; Streit, W.; Strohmeyer, R.; Tooyoma, I.; Van Muiswinkel, F. L.; Veerhuis, R.; Walker, D.; Webster, S.; Wegrzyniak, B.; Wenk, G.; Wyss-Coray, T.; Neuroinflammation Working, G. *Neurobiology of Aging* **2000**, *21*, 383.

(176) Ammon, H. P. T.; Safayhi, H.; Mack, T.; Sabieraj, J. *Journal of Ethnopharmacology* **1993**, *38*, 113.

(177) Xu, Y. X.; Pindolia, K. R.; Janakiraman, N.; Chapman, R. A.; Gautam, S. C. *Hematopathology and Molecular Hematology* **1998**, *11*, 49.

(178) Pan, M. H.; Lin-Shiau, S. Y.; Lin, J. K. *Biochemical Pharmacology* **2000**, *60*, 1665.

(179) Puglielli, L.; Ellis, B. C.; Ingano, L. A. M.; Kovacs, D. M. *Journal of Molecular Neuroscience* **2004**, *24*, 93.

(180) Soni, K. B.; Kuttan, R. *Indian Journal of Physiology and Pharmacology* **1992**, *36*, 273.

(181) Bernabe-Pineda, M.; Ramirez-Silva, M. T.; Romero-Romo, M.; Gonzadlez-Vergara, E.; Rojas-Hernandez, A. *Spectrochimica Acta Part a-Molecular and Biomolecular Spectroscopy* **2004**, *60*, 1091.

(182) Wang, Y. J.; Pan, M. H.; Cheng, A. L.; Lin, L. I.; Ho, Y. S.; Hsieh, C. Y.; Lin, J. K. *Journal of Pharmaceutical and Biomedical Analysis* **1997**, *15*, 1867.

(183) Tonnesen, H. H.; Karlsen, J. *Zeitschrift Fur Lebensmittel-Untersuchung Und-Forschung* **1985**, *180*, 132.

(184) Tonnesen, H. H.; Karlsen, J. *Zeitschrift Fur Lebensmittel-Untersuchung Und-Forschung* **1985**, *180*, 402.

(185) Meyer, B.; Peters, T. *Angewandte Chemie-International Edition* **2003**, *42*, 864.

(186) Biet, T.; Peters, T. *Angewandte Chemie-International Edition* **2001**, *40*, 4189.

(187) Berteau, O.; Sandstrom, C.; Bielicki, J.; Anson, D. S.; Kenne, L. *Journal of the American Chemical Society* **2003**, *125*, 15296.

(188) Yuan, Y.; Wen, X.; Sanders, D. A. R.; Pinto, B. M. *Biochemistry* **2005**, *44*, 14080.

(189) Brecker, L.; Straganz, G. D.; Tyl, C. E.; Steiner, W.; Nidetzky, B. *Journal of Molecular Catalysis B-Enzymatic* **2006**, *42*, 85.

(190) Yuan, Y.; Bleile, D. W.; Wen, X.; Sanders, D. A. R.; Itoh, K.; Liu, H. W.; Pinto, B. M. *Journal of the American Chemical Society* **2008**, *130*, 3157.

(191) Airoldi, C.; Colombo, L.; Manzoni, C.; Sironi, E.; Natalello, A.; Doglia, S. M.; Forloni, G.; Tagliavini, F.; Del Favero, E.; Cantu, L.; Nicotra, F.; Salmona, M. *Organic & Biomolecular Chemistry* **2011**, *9*, 463.

(192) Cardoso, I.; Merlini, G.; Saraiva, M. J. *Faseb Journal* **2003**, *17*, 803.

(193) Dreborg, S.; Akerblom, E. B. *Critical Reviews in Therapeutic Drug Carrier Systems* **1990**, *6*, 315.

(194) Zalipsky, S. *Advanced Drug Delivery Reviews* **1995**, *16*, 157.

(195) Zalipsky, S. *Bioconjugate Chemistry* **1995**, *6*, 150.

(196) Luxon, B. A.; Grace, M.; Brassard, D.; Bordens, R. *Clinical Therapeutics* **2002**, *24*, 1363.

(197) Ortega-Munoz, M.; Lopez-Jaramillo, J.; Hernandez-Mateo, F.; Santoyo-Gonzalez, F. *Advanced Synthesis & Catalysis* **2006**, *348*, 2410.

(198) Guo, Z. M.; Lei, A. W.; Liang, X. M.; Xu, Q. *Chemical Communications* **2006**, 4512.

(199) Hancock, W. S.; Battersby, J. E. *Analytical Biochemistry* **1976**, *71*, 260.

(200) Ressler, C.; Banerjee, S. N. *Journal of Organic Chemistry* **1976**, *41*, 1336.

(201) Montet, X.; Funovics, M.; Montet-Abou, K.; Weissleder, R.; Josephson, L. *J Med Chem* **2006**, *49*, 6087.

(202) Hong, S.; Leroueil, P. R.; Majoros, I. J.; Orr, B. G.; Baker, J. R., Jr.; Banaszak Holl, M. M. *Chem Biol* **2007**, *14*, 107.

(203) Tassa, C.; Duffner, J. L.; Lewis, T. A.; Weissleder, R.; Schreiber, S. L.; Koehler, A. N.; Shaw, S. Y. *Bioconjug Chem* **2010**, *21*, 14.

(204) Antimisiaris, S. G.; Kallinteri, P.; Fatouros, D. In *Pharmaceutical Manufacturing Handbook. Production and Processes*; Gad, S. C., Ed.; John Wiley & Sons: 2008, p 443.

(205) Needham, D.; McIntosh, T. J.; Lasic, D. D. *Biochimica Et Biophysica Acta* **1992**, *1108*, 40.

(206) de Gennes, P. G. *Macromolecules* **1980**, *13*, 1069.

(207) Blume, G.; Cevc, G. *Biochimica et Biophysica Acta (BBA) - Biomembranes* **1993**, *1146*, 157.

(208) Vert, M.; Domurado, D. *Journal of Biomaterials Science-Polymer Edition* **2000**, *11*, 1307.

(209) Johnstone, S. A.; Masin, D.; Mayer, L.; Bally, M. B. *Biochimica Et Biophysica Acta-Biomembranes* **2001**, *1513*, 25.

(210) Allen, C.; Dos Santos, N.; Gallagher, R.; Chiu, G. N. C.; Shu, Y.; Li, W. M.; Johnstone, S. A.; Janoff, A. S.; Mayer, L. D.; Webb, M. S.; Bally, M. B. *Bioscience Reports* **2002**, *22*, 225.

(211) Said Hassane, F.; Frisch, B.; Schuber, F. *Bioconjug Chem* **2006**, *17*, 849.

(212) Cavalli, S.; Tipton, A. R.; Overhand, M.; Kros, A. *Chem Commun (Camb)* **2006**, 3193.

(213) Hein, C. D.; Liu, X. M.; Wang, D. *Pharm Res* **2008**, *25*, 2216.

(214) Frisch, B.; Hassane, F. S.; Schuber, F. *Methods Mol Biol* **2010**, *605*, 267.

(215) Usta, M.; Wortelboer, H. M.; Vervoort, J.; Boersma, M. G.; Rietjens, I. M.; van Bladeren, P. J.; Cnubben, N. H. *Chem Res Toxicol* **2007**, *20*, 1895.

(216) Kokkona, M.; Kallinteri, P.; Fatouros, D.; Antimisiaris, S. G. *Eur J Pharm Sci* **2000**, *9*, 245.

(217) Taniguchi, A.; Sohma, Y.; Hirayama, Y.; Mukai, H.; Kimura, T.; Hayashi, Y.; Matsuzaki, K.; Kiso, Y. *Chembiochem* **2009**, *10*, 710.

(218) Beeg, M.; Stravalaci, M.; Bastone, A.; Salmona, M.; Gobbi, M. *Anal Biochem* **2010**, *in press*.

(219) Balducci, C.; Beeg, M.; Stravalaci, M.; Bastone, A.; Sclip, A.; Biasini, E.; Tapella, L.; Colombo, L.; Manzoni, C.; Borsello, T.; Chiesa, R.; Gobbi, M.; Salmona, M.; Forloni, G. *Proc Natl Acad Sci U S A* **2010**, *107*, 2295.

(220) Dahlgren, K. N.; Manelli, A. M.; Stine, W. B., Jr.; Baker, L. K.; Krafft, G. A.; LaDu, M. J. *J Biol Chem* **2002**, *277*, 32046.

(221) Bravman, T.; Bronner, V.; Lavie, K.; Notcovich, A.; Papalia, G. A.; Myszka, D. G. *Anal Biochem* **2006**, *358*, 281.

(222) Gobbi, M.; Re, F.; Canovi, M.; Beeg, M.; Gregori, M.; Sesana, S.; Sonnino, S.; Brogioli, D.; Musicanti, C.; Gasco, P.; Salmona, M.; Masserini, M. E. *Biomaterials* **2010**, *31*, 6519.

(223) Lallana, E.; Fernandez-Megia, E.; Riguera, R. *J Am Chem Soc* **2009**, *131*, 5748.

(224) Yanagisawa, D.; Shirai, N.; Amatsubo, T.; Taguchi, H.; Hirao, K.; Urushitani, M.; Morikawa, S.; Inubushi, T.; Kato, M.; Kato, F.; Morino, K.; Kimura, H.; Nakano, I.; Yoshida, C.; Okada, T.; Sano, M.; Wada, Y.; Wada, K. N.; Yamamoto, A.; Tooyama, I. *Biomaterials* **2010**, *31*, 4179.

(225) Muller, R. H.; Lucks, J. S. *European Patent No. EP 0605497* **1996**.

(226) Shahgaldian, P.; Da Silva, E.; Coleman, A. W.; Rather, B.; Zaworotko, M. J. *International Journal of Pharmaceutics* **2003**, *253*, 23.

(227) Dubes, A.; Parrot-Lopez, H.; Abdelwahed, W.; Degobert, G.; Fessi, H.; Shahgaldian, P.; Coleman, A. W. *European Journal of Pharmaceutics and Biopharmaceutics* **2003**, *55*, 279.

(228) Muller, R. H.; Mehnert, W.; Lucks, J. S.; Schwarz, C.; Zurmuhlen, A.; Weyhers, H.; Freitas, C.; Ruhl, D. *European Journal of Pharmaceutics and Biopharmaceutics* **1995**, *41*, 62.

(229) Muller, R. H.; Mader, K.; Gohla, S. *European Journal of Pharmaceutics and Biopharmaceutics* **2000**, *50*, 161.

(230) Mehnert, W.; Mader, K. *Advanced Drug Delivery Reviews* **2001**, *47*, 165.

(231) Schwarz, C.; Mehnert, W.; Lucks, J. S.; Muller, R. H. *Journal of Controlled Release* **1994**, *30*, 83.

(232) Muller, R. H.; Weyhers, H.; zurMuhlen, A.; Dingler, A.; Mehnert, W. *Pharmazeutische Industrie* **1997**, *59*, 423.

(233) Mehnert, W.; zurMuhlen, A.; Dingler, A.; Weyhers, H. *Pharmazeutische Industrie* **1997**, *59*, 511.

(234) Muller, R. H.; Dingler, A.; Weyhers, H.; zurMuhlen, A.; Mehnert, W. *Pharmazeutische Industrie* **1997**, *59*, 614.

(235) Westesen, K.; Bunjes, H.; Koch, M. H. J. *Journal of Controlled Release* **1997**, *48*, 223.

(236) Siekmann, B.; Westesen, K. *Colloids and Surfaces B: Biointerfaces* **1994**, *3*, 159.

(237) Westesen, K. *Colloid and Polymer Science* **2000**, *278*, 608.

(238) Gohla, S. H.; Dingler, A. *Pharmazie* **2001**, *56*, 61.

(239) Lockman, P. R.; Oyewumi, M. O.; Koziara, J. M.; Roder, K. E.; Mumper, R. J.; Allen, D. D. *Journal of Controlled Release* **2003**, *93*, 271.

(240) Diederichs, J. E.; Muller, R. H. *Pharmazeutische Industrie* **1994**, *56*, 267.

(241) Fundaro, A.; Cavalli, R.; Bargoni, A.; Vighetto, D.; Zara, G. P.; Gasco, M. R. *Pharmacological Research* **2000**, *42*, 337.

(242) Yang, S.; Zhu, J.; Lu, Y.; Liang, B.; Yang, C. *Pharmaceutical Research* **1999**, *16*, 751.

(243) Tabatt, K.; Sameti, M.; Olbrich, C.; Muller, R. H.; Lehr, C. M. *European Journal of Pharmaceutics and Biopharmaceutics* **2004**, *57*, 155.

(244) Gasco, M. R. *US Patent No. 5250236* **1993**.

(245) Cavalli, R.; Marengo, E.; Rodriguez, L.; Gasco, M. R. *European Journal of Pharmaceutics and Biopharmaceutics* **1996**, *42*, 110.

(246) Cortesi, R.; Esposito, E.; Luca, G.; Nastruzzi, C. *Biomaterials* **2002**, *23*, 2283.

(247) Cavalli, R.; Caputo, O.; Marengo, E.; Pattarino, F.; Gasco, M. R. *Pharmazie* **1998**, *53*, 392.

(248) Igartua, M.; Saulnier, P.; Heurtault, B.; Pech, B.; Proust, J. E.; Pedraz, J. L.; Benoit, J. P. *International Journal of Pharmaceutics* **2002**, *233*, 149.

(249) Couvreur, P.; Kante, B.; Roland, M.; Guiot, P.; Bauduin, P.; Speiser, P. *Journal of Pharmacy and Pharmacology* **1979**, *31*, 331.

(250) Vauthier, C.; Dubernet, C.; Fattal, E.; Pinto-Alphandary, H.; Couvreur, P. *Advanced Drug Delivery Reviews* **2003**, *55*, 519.

(251) Garcia-Garcia, E.; Andrieux, K.; Gil, S.; Couvreur, P. *International Journal of Pharmaceutics* **2005**, *298*, 274.

(252) Couvreur, P.; Vauthier, C. *Pharmaceutical Research* **2006**, *23*, 1417.

(253) Couvreur, P.; Gref, R.; Andrieux, K.; Malvy, C. *Progress in Solid State Chemistry* **2006**, *34*, 231.

(254) Vauthier, C.; Labarre, D.; Ponchel, G. *Journal of Drug Targeting* **2007**, *15*, 641.

(255) Yang, S. C.; Ge, H. X.; Hu, Y.; Jiang, X. Q.; Yang, C. Z. *Colloid and Polymer Science* **2000**, *278*, 285.

(256) Seijo, B.; Fattal, E.; Roblottreupel, L.; Couvreur, P. *International Journal of Pharmaceutics* **1990**, *62*, 1.

(257) Limouzin, C.; Caviggia, A.; Ganachaud, F.; Hemery, P. *Macromolecules* **2003**, *36*, 667.

(258) Brigger, I.; Armand-Lefevre, L.; Chaminade, P.; Besnard, M.; Rigaldie, Y.; Largeteau, A.; Andremont, A.; Grislain, L.; Demazeau, G.; Couvreur, P. *Pharmaceutical Research* **2003**, *20*, 674.

(259) Altinbas, N.; Fehmer, C.; Terheiden, A.; Shukla, A.; Rehage, H.; Mayer, C. *Journal of Microencapsulation* **2006**, *23*, 567.

(260) Hillaireau, H.; Le Doan, T.; Chacun, H.; Janin, J.; Couvreur, P. *International Journal of Pharmaceutics* **2007**, *331*, 148.

(261) Chauvierre, C.; Leclerc, L.; Labarre, D.; Appel, M.; Marden, M. C.; Couvreur, P.; Vauthier, C. *International Journal of Pharmaceutics* **2007**, *338*, 327.

(262) Bertholon, I.; Lesieur, S.; Labarre, D.; Besnard, M.; Vauthier, C. *Macromolecules* **2006**, *39*, 3559.

(263) Bertholon, I.; Vauthier, C.; Labarre, D. *Pharmaceutical Research* **2006**, *23*, 1313.

(264) Bravo-Osuna, I.; Ponchel, G.; Vauthier, C. *European Journal of Pharmaceutical Sciences* **2007**, *30*, 143.

(265) Veronese, F. M. *Biomaterials* **2001**, *22*, 405.

(266) Oowaki, H.; Matsuda, S.; Sakai, N.; Ohta, T.; Iwata, H.; Sadato, A.; Taki, W.; Hashimoto, N.; Yoshito, I. *Biomaterials* **2000**, *21*, 1039.

(267) Reece, T. B.; Maxey, T. S.; Kron, I. L. *The American Journal of Surgery* **2001**, *182*, S40.

(268) Marcovich, R.; Williams, A. L.; Rubin, M. A.; Wolf, J. S. *Urology* **2001**, *57*, 806.

(269) Pollak, J. S.; White, J. R. I. *Journal of Vascular and Interventional Radiology* **2001**, *12*, 907.

(270) Peracchia, M. T.; Desmaele, D.; Couvreur, P.; dAngelo, J. *Macromolecules* **1997**, *30*, 846.

(271) Stella, B.; Arpicco, S.; Peracchia, M. T.; Desmaele, D.; Hoebeke, J.; Renoir, M.; D'Angelo, J.; Cattel, L.; Couvreur, P. *Journal of Pharmaceutical Sciences* **2000**, *89*, 1452.

(272) Stella, B.; Marsaud, V.; Arpicco, S.; Geraud, G.; Cattel, L.; Couvreur, P.; Renoir, J. M. *Journal of Drug Targeting* **2007**, *15*, 146.

(273) Nicolas, J.; Bensaid, F.; Desmaele, D.; Grogna, M.; Detrembleur, C.; Andrieux, K.; Couvreur, P. *Macromolecules* **2008**, *41*, 8418.

(274) Brambilla, D.; Nicolas, J.; Le Droumaguet, B.; Andrieux, K.; Marsaud, V.; Couraud, P. O.; Couvreur, P. *Chemical Communications* **2010**, *46*, 2602.

(275) Sabella, S.; Quaglia, M.; Lanni, C.; Racchi, M.; Govoni, S.; Caccialanza, G.; Calligaro, A.; Bellotti, V.; De Lorenzi, E. *ELECTROPHORESIS* **2004**, *25*, 3186.

(276) Colombo, R.; Carotti, A.; Catto, M.; Racchi, M.; Lanni, C.; Verga, L.; Caccialanza, G.; De Lorenzi, E. *ELECTROPHORESIS* **2009**, *30*, 1418.

(277) Kato, M.; Kinoshita, H.; Enokita, M.; Hori, Y.; Hashimoto, T.; Iwatsubo, T.; Toyo'oka, T. *Analytical Chemistry* **2007**, *79*, 4887.

(278) Brambilla, D.; Verpillot, R.; Taverna, M.; De Kimpe, L.; Le Droumaguet, B.; Nicolas, J.; Canovi, M.; Gobbi, M.; Mantegazza, F.; Salmona, M.; Nicolas, V. r.; Scheper, W.; Couvreur, P.; Andrieux, K. *Analytical Chemistry* **2010**, *82*, 10083.

(279) Thoma, K.; Rombach, R.; Ullmann, E. *Scientia Pharmaceutica* **1964**, *32*, 216.

(280) Schneekloth, A. R.; Pucheault, M.; Tae, H. S.; Crews, C. M. *Bioorganic & Medicinal Chemistry Letters* **2008**, *18*, 5904.

(281) Sato, H.; Hayashi, E.; Yamada, N.; Yatagai, M.; Takahara, Y. *Bioconjugate Chemistry* **2001**, *12*, 701.

(282) Kazemi, F.; Kiasat, A. R.; Ebrahimi, S. *Synthetic Communications* **2003**, *33*, 999.

(283) Horne, W. S.; Stout, C. D.; Ghadiri, M. R. *Journal of the American Chemical Society* **2003**, *125*, 9372.

(284) Di Fede, G.; Catania, M.; Morbin, M.; Rossi, G.; Suardi, S.; Mazzoleni, G.; Merlin, M.; Giovagnoli, A. R.; Prioni, S.; Erbetta, A.; Falcone, C.; Gobbi, M.; Colombo,

L.; Bastone, A.; Beeg, M.; Manzoni, C.; Francescucci, B.; Spagnoli, A.; Cantu, L.; Del Favero, E.; Levy, E.; Salmona, M.; Tagliavini, F. *Science* **2009**, *323*, 1473.

(285) Salmona, M.; Morbin, M.; Massignan, T.; Colombo, L.; Mazzoleni, G.; Capobianco, R.; Diomede, L.; Thaler, F.; Mollica, L.; Musco, G.; Kourie, J. J.; Bugiani, O.; Sharma, D.; Inouye, H.; Kirschner, D. A.; Forloni, G.; Tagliavini, F. *Journal of Biological Chemistry* **2003**, *278*, 48146.

(286) Han, Y.; He, C.; Cao, M.; Huang, X.; Wang, Y.; Li, Z. *Langmuir* **2009**, *26*, 1583.